PNNL-26226, Rev. 1

Pacific Northwest
NATIONAL LABORATORY

Potential Impacts of Accelerated Climate Change

Second Annual Report of Work for NRC Agreement Number NRC-HQ-60-14-D-0025

July 2019

LR Leung
R Prasad

U.S. DEPARTMENT OF ENERGY

PACIFIC NORTHWEST NATIONAL LABORATORY
operated by
BATTELLE
for the
UNITED STATES DEPARTMENT OF ENERGY
under Contract DE-AC05-76RL01830

Printed in the United States of America

Available to DOE and DOE contractors from the
Office of Scientific and Technical Information,
P.O. Box 62, Oak Ridge, TN 37831-0062;
ph: (865) 576-8401
fax: (865) 576-5728
email: reports@adonis.osti.gov

Available to the public from the National Technical Information Service
5301 Shawnee Rd., Alexandria, VA 22312
ph: (800) 553-NTIS (6847)
email: orders@ntis.gov <http://www.ntis.gov/about/form.aspx>
Online ordering: http://www.ntis.gov


This document was printed on recycled paper.
(8/2010)

PNNL-26226, Rev. 1

Potential Impacts of Accelerated Climate Change

Second Annual Report of Work for NRC Agreement Number NRC-HQ-60-14-D-0025

July 2019

LR Leung
R Prasad

Prepared for the U.S. Nuclear Regulatory Commission
under an Interagency Agreement with the U.S. Department of Energy
Contract DE-AC05-76RL01830

Pacific Northwest National Laboratory
Richland, Washington 99352

Abstract

This study is part of the U.S. Nuclear Regulatory Commission's (NRC) Probabilistic Flood Hazard Assessment (PFHA) research plan that aims to develop regulatory tools and guidance to support and enhance the NRC's capacity to perform thorough and efficient reviews of license applications and license amendment requests. In Year 1, Pacific Northwest National Laboratory staff prepared an annual report that summarized recent scientific findings on climate change, with a particular focus on climatic elements that are relevant to NRC concerns on a regional level (i.e., increasing air and water temperatures, decreasing water availability, increasing frequency and intensity of storms and flooding, and sea-level rise). This report summarizes Year 2 activities, which focused on reviewing scientific findings regarding region-specific climatic extremes for the southeastern United States. According to the U.S. Global Change Research Program Third National Climate Assessment, the U.S. Southeast Region consists of 11 southeastern states, Puerto Rico, and the Virgin Islands. Except for Kentucky, Puerto Rico, and the Virgin Islands, all included states have operating nuclear power plants. Further, new nuclear power reactor permit and license applications have been submitted to the NRC in the recent past for sites located in several southeastern states. Therefore, having an improved understanding of potential climate changes and their hydrologic impacts in the Southeast Region is important to inform the PFHA research plan.

Climatic features relevant to the NRC for the Southeast Region include high temperature extremes, precipitation extremes, flooding, high winds associated with tropical cyclones and tornadoes, sea-level rise, and storm surge and associated inland inundation. Drawing primarily from the climate assessment reports and peer-reviewed literature, this Year 2 annual report summarizes the observed climate, its past changes, and its projected changes, as well as 21st century hydrologic impacts in the Southeast Region. Despite the relatively mild changes observed in the past and projected in the future for the mean climate of the Southeast Region, many aspects of climatic extremes such as extreme precipitation have exhibited changes in the last century. In addition, climate and hydrologic models project further changes in the future. Pacific Northwest National Laboratory staff presented updates summarizing these findings at the Second Annual PFHA Research Workshop, which took place from January 23 to 25, 2017, at NRC Headquarters in Rockville, Maryland.

Executive Summary

This study is part of the U.S. Nuclear Regulatory Commission's (NRC) Probabilistic Flood Hazard Assessment (PFHA) research plan that aims to develop regulatory tools and guidance to support and enhance the NRC's capacity to perform thorough and efficient reviews of license applications and license amendment requests. In Year 1, Pacific Northwest National Laboratory staff prepared an annual report that summarized recent scientific findings on climate change, focusing in particular on climatic elements that are relevant to NRC concerns broadly across the conterminous United States (i.e., increasing air and water temperatures, decreasing water availability, increasing frequency and intensity of storms and flooding, and sea-level rise). This report summarizes Year 2 activities, which focused on reviewing scientific findings regarding region-specific climatic extremes for the southeastern United States, with other U.S. regions to be discussed in future reports. According to the U.S. Global Change Research Program Third National Climate Assessment, the Southeast Region consists of 11 southeastern states, Puerto Rico, and the Virgin Islands. Except for Kentucky, Puerto Rico, and the Virgin Islands (hereafter, Southeast Region), all included states have operating nuclear power plants. Further, new nuclear power reactor permit and license applications have been submitted to the NRC in the recent past for sites located in several southeastern states. Therefore, having an improved understanding of potential climate changes and their hydrologic impacts in the Southeast Region is important to informing the PFHA research plan.

Climatic features relevant to the NRC for the Southeast Region include high temperature extremes, precipitation extremes, flooding, high winds associated with tropical cyclones and tornadoes, sea-level rise, and storm surge and associated inland inundation. Drawing primarily from climate assessment reports and peer-reviewed literature, this Year 2 annual report summarizes the observed climate, its past changes, and its projected changes, as well as 21st century hydrologic impacts in the Southeast Region. The Southeast Region experiences large interannual and interdecadal variability associated with large-scale modes of variability such as the El Niño-Southern Oscillation in the coupled atmosphere-ocean system. The observed long-term trends in seasonal and annual mean temperature and precipitation during the 20th century have been small relative to the large variability. Despite the relatively mild changes observed in the past and projected in the future for the mean climate of the Southeast Region, many aspects of climatic extremes have exhibited changes in the last century. In addition, climate and hydrologic models project further changes in the future. For example, the Southeast Region has experienced an 8 percent increase in 5-year extreme precipitation between 1986–2015 relative to 1901–1960. Based on a multimodel ensemble, the 20-year daily extreme precipitation is projected to increase by 12 and 21 percent in the mid- and late-21st century, respectively, under a higher emissions scenario. A recent study using convection-permitting simulations at 4 km grid spacing projected a fourfold increase in probability of exceedance for the present-day 99.95 percentile hourly precipitation comparing the late 20th and 21st centuries. A higher-resolution hurricane model projected an increase in the frequency of Category 4 and 5 tropical cyclones by up to five storms per decade in the North Atlantic and Gulf of Mexico, which is consistent with the projection of increased tropical cyclone intensity by global models. Analysis of the observed tornado count in the United States shows positive linear trends in the percentiles of the number of tornadoes per outbreak, particularly for the high percentile. As warming and the associated increase in atmospheric moisture enhance the convective available potential energy, the severe thunderstorm environment is projected to increase during spring between 5 and 15 percent in the central and southeastern United States; however, changes are less consistent across models for summer.

The rate of global mean sea-level rise almost doubled between 1993 and 2007 compared to the average over the 20th century. The southeastern U.S. coast experienced increases in sea surface height of up to 1.5 in. per decade between 1993 and 2014, with an increased frequency of nuisance tidal floods. With continued ocean thermal expansion and potentially more rapid melting of glaciers and ice sheets in the

future, the relative sea level along the southeastern U.S. coast is projected to rise by 3 to 6 ft by 2100 under an interagency intermediate 1 m global mean sea-level rise scenario. Driven mainly by sea-level rise, storm surge is projected to increase in the future. In addition, increases in tropical cyclone intensity characterized by the maximum winds also contribute 10 to 15 percent to the storm-surge increase. Nuisance tidal flooding is projected to be more frequent due to sea-level rise coupled with increased development in the last century encroaching on flood-prone areas.

Warming in the future could lead to changes in precipitation, runoff, and soil moisture in the Southeast Region. More specifically, increases in extreme precipitation will likely increase the frequency of floods. In general, previous studies in the climate change and hydrologic communities have examined mean changes rather than hydrologic extremes. The NRC currently uses extreme events such as the Probable Maximum Precipitation, Probable Maximum Flood, and Probable Maximum Storm Surge in permitting and licensing. The NRC is developing methods for perfoming PFHA under the PFHA Plan. Future studies should assess hydrologic changes in the Southeast Region at spatial and temporal scales more relevant to the NRC's needs. Advances in computing resources have enabled very high-resolution climate modeling at some modeling centers. Combining a limited number of very high-resolution climate projections with a large multimodel ensemble from the Coupled Model Intercomparison Project and large ensemble modeling that samples the internal variability of the climate system will allow better characterization of uncertainty in climate projections that are useful for the probabilistic framework of the PFHA Plan. However, such a framework should consider potential changes that may arise from tipping-point elements (e.g., rapid sea-level rise from ice sheet instability) and compound extreme events (e.g., heat and wildfires) that currently are not well understood or modeled.

Glossary

AMO	The Atlantic Multidecadal Oscillation is a mode of natural variability that affects the sea surface temperature of the North Atlantic Ocean on multidecadal timescales.
AMOC	The Atlantic meridional overturning circulation is a major component of the global thermohaline ocean circulation driven by the sinking of cold, dense water in the North Atlantic near Greenland.
Bermuda High	The Bermuda High is a semi-permanent, subtropical area of high pressure in the North Atlantic Ocean off the East Coast of North America that migrates east and west with varying central pressure. It is also known as the North Atlantic Subtropical High. When it is displaced westward, during the Northern Hemispheric summer and fall, the center is located in the western North Atlantic, near Bermuda. In the winter and early spring, it is primarily centered near the Azores in the eastern part of the North Atlantic so it is also known as the Azores High.
climate change	Changes in average weather conditions that persist over multiple decades or longer. Climate change encompasses both increases and decreases in temperature, as well as shifts in precipitation, changing risk of certain types of severe weather events, and changes to other features of the climate system.
climate variability	Natural changes in climate that fall within the observed range of extremes for a particular region, as measured by temperature, precipitation, and frequency of events. Drivers of climate variability include the El Niño-Southern Oscillation and other phenomena.
enhanced Fujita scale	An update of the original Fujita scale implemented in the United States on 1 February 2007. Similar to the Fujita scale, it rates the intensity of tornadoes based on the observed damage they cause.
extreme event	An extreme event is defined by its frequency of occurrence or return period. The definition of “extreme” is a statistical concept that varies depending on location, season, and length of the historical record. For example, 99.9 percent precipitation, which refers to the precipitation that has an annual probability of exceedance of 1/1000, or a return period of 1000 years, is one definition of extreme precipitation used in this report.
forcing	Factors that affect the Earth’s climate. For example, natural factors such as volcanoes and human factors such as the emission of heat-trapping gases and particles through fossil fuel composition.

greenhouse gases	Gases that absorb heat in the atmosphere near the Earth's surface, preventing it from escaping into space. If the atmospheric concentrations of these gases rise, the average temperature of the lower atmosphere will gradually increase, a phenomenon known as the greenhouse effect. Greenhouse gases included, for example, carbon dioxide, water vapor, and methane.
global climate models (GCMs)	Mathematical models that are used to numerically simulate the physics,chemistry, and biology that influence the climate system.
heat wave	A period of abnormally hot weather lasting days to weeks.
isostatic	Changes in the level of land relative to a fixed point in the Earth, possibly due to thermal buoyancy or tectonic effects; it implies no change in the volume of water in the oceans.
land cover	The physical characteristics of the land surface, such as crops, trees, or concrete.
land use	Activities taking place on land, such as growing food, cutting trees, or building cities.
mean higher high water	The average of the higher high water height of each tidal day observed over the National Tidal Datum Epoch. For stations with shorter series, comparison of simultaneous observations with a control tide station is made in order to derive the equivalent datum of the National Tidal Datum.
nuisance flooding	Nuisance flooding is defined to occur when the water level at a National Oceanic and Atmospheric Administration tide gauge exceeds the threshold for minor flooding impacts that has been established by the local Weather Forecast Office of the National Weather Service. The local Weather Forecast Office sets the threshold based on years of flood monitoring. Each location's nuisance flood threshold is reported as height above the mean higher high water level. Nuisance flood thresholds vary by location, and they depend on the surrounding landscape, topography, and infrastructure. In general, however, U.S. infrastructure is vulnerable when local water levels are 1–2 feet above the mean higher high water level.
proxy	A proxy is a way to indirectly measure or infer aspects of climate. For example, environmental proxies are used to infer the occurrence of severe storms to address issues related to observational records and direct modeling of the phenomena.

Representative Concentration Pathways (RCPs)	These are four greenhouse gas concentration (not emissions) trajectories adopted by the Intergovernmental Panel on Climate Change for its fifth Assessment Report (AR5) in 2014. It supersedes the Special Report on Emissions Scenarios (SRES) published in 2000. The four scenarios—RCP2.6, RCP4.5, RCP6, and RCP8.5—all of which are possible, are named after a possible range of radiative forcing values in the year 2100 relative to pre-industrial values (+2.6, +4.5, +6.0, and +8.5 Wm-2, respectively).
rapid intensification	Rapid intensification is defined as an event in which hurricane intensity increases by 25 knots or higher in 24 hours.
return period	A return period, also called a recurrence interval, is a measure of the likelihood of an event of a specified magnitude to occur. As the inverse of the annual probability of exceedance, it is the average time interval between events of a similar size or intensity.
Special Report on Emission Scenarios (SRES)	A set of emission scenarios from the Intergovernmental Panel on Climate Change Special Report on Emission Scenarios released in 2000 that describe a wide range of potential future socioeconomic conditions and resulting emissions. The emission scenarios are “baseline” scenarios that do not take into account any current or future measures to limit greenhouse gas emissions. The four scenarios, A1, B1, A2, and B2, are delineated by more focus on economic vs. environmental and globalization vs. regionalization.
tornado outbreak	A tornado outbreak is the occurrence of multiple tornadoes spawned by the same synoptic-scale weather system. The number of tornadoes required to qualify as an outbreak is at least 6 to 10.
tropical cyclone intensity	Tropical cyclone intensity is measured by the Saffir-Simpson hurricane wind scale. Category 4 and 5 hurricanes have sustained winds of 130 to 156 mph and 157 mph or higher, respectively.
wet bulb temperature	The wet bulb temperature is the temperature that a parcel of air would have if it were cooled to saturation by the evaporation of water into it. It is largely determined by both the air temperature and the amount of moisture in the air.

Acronyms and Abbreviations

AEP	annual exceedance probability
AMAP	Arctic Monitoring and Assessment Programme
AR4	(IPCC) Fourth Assessment Report
AMO	Atlantic Multidecadal Oscillation
AMOC	Atlantic Meridional Overturning Circulation
CAPE	convective available potential energy
CETA	Central and eastern tropical Atlantic
CMIP	Coupled Model Intercomparison Project
CMIP3	Coupled Model Intercomparison Project Phase 3
CMIP5	Coupled Model Intercomparison Project Phase 5
CSSR	Climate Science Special Report
DJF	December-January-February
DOE	U.S. Department of Energy
ECB	Engineering and Construction Bulletin
ET	evapotranspiration
FI	flood index
GCM	global climate model or general circulation model
GFDL	Geophysical Fluid Dynamics Laboratory
GHG	greenhouse gases
GISS	(NASA) Goddard Institute for Space Studies
GMSL	global mean sea level
HUC	Hydrologic Unit Code
IA	Integrated assessment
IAV	impacts, adaptation, and vulnerability
IGIM	Interagency Group on Integrative Modeling
IPCC	Intergovernmental Panel on Climate Change
JJA	June-July-August
LOCA	Localized Constructed Analogs
MAM	March-April-May
NARCCAP	North American Regional Climate Change Assessment Program
NASA	National Aeronautics and Space Administration
NASH	North Atlantic Subtropical High
NCA	National Climate Assessment
NCA3	Third National Climate Assessment
NCA4	Fourth National Climate Assessment
NCEI	National Centers for Environmental Information

NOAA	National Oceanic and Atmospheric Administration
NRC	U.S. Nuclear Regulatory Commission
NTC	number of tropical cyclones
PDI	Power Dissipation Index
PET	Potential evapotranspiration
PFHA	Probabilistic Flood Hazard Assessment
PI	potential intensity
PNNL	Pacific Northwest National Laboratory
PRISM	Precipitation Elevation Regression on Independent Slopes Model
PRMS	Precipitation-Runoff Modeling System
PGW	pseudo global warming
RCM	regional climate model
RCP	representative concentration pathways
RI	rapid intensification
RSL	regional sea level
SLR	sea-level rise
SRES	Special Report on Emissions Scenarios
SSH	sea surface height
STEnv	Severe thunderstorm environment
TC	tropical cyclone
USACE	U.S. Army Corps of Engineers
USGCRP	U.S. Global Change Research Program
USGS	U.S. Geological Survey
WaSSI	Water-Supply Stress Index

Contents

Figures

Tables

1.0 Introduction

This study is part of the U.S. Nuclear Regulatory Commission's (NRC) Probabilistic Flood Hazard Assessment (PFHA) research plan that aims to develop regulatory tools and guidance to support and enhance the NRC's capacity to perform thorough and efficient reviews of license applications and license amendment requests. In Year 1, Pacific Northwest National Laboratory (PNNL) staff prepared an annual report that summarized recent scientific findings on climate change, focusing in particular on climatic elements that are relevant to NRC concerns broadly across the conterminous United States (i.e., increasing air and water temperatures, decreasing water availability, increasing frequency and intensity of storms and flooding, and sea-level rise). This report summarizes Year 2 activities, which focused on reviewing scientific findings regarding region-specific climatic extremes for the southeastern United States, with other U.S. regions to be discussed in future reports.

The U.S. Global Change Research Program (USGCRP) Third National Climate Assessment (NCA) discussed the regional climate and historical trends and future changes in 10 climate regions (Melillo et al. 2014). The region of interest for the purpose of this report consists of 11 southeastern states, Puerto Rico, and the Virgin Islands (hereafter, Southeast Region) (Ingram et al. 2013; Figure 1.1). Except for Kentucky, Puerto Rico, and the Virgin Islands, all states within the Southeast Region have operating nuclear power plants (Figure 1.2). In the Fourth NCA, Puerto Rico and the Virgin Islands were split from the Southeast Region and now comprise the Caribbean region (USGCRP 2017). New nuclear power reactor site permit and license applications have been submitted to the NRC in the recent past for sites located in several Southeast Region states (i.e., Virginia, North Carolina, South Carolina, Tennessee, and Florida; Figure 1.3).

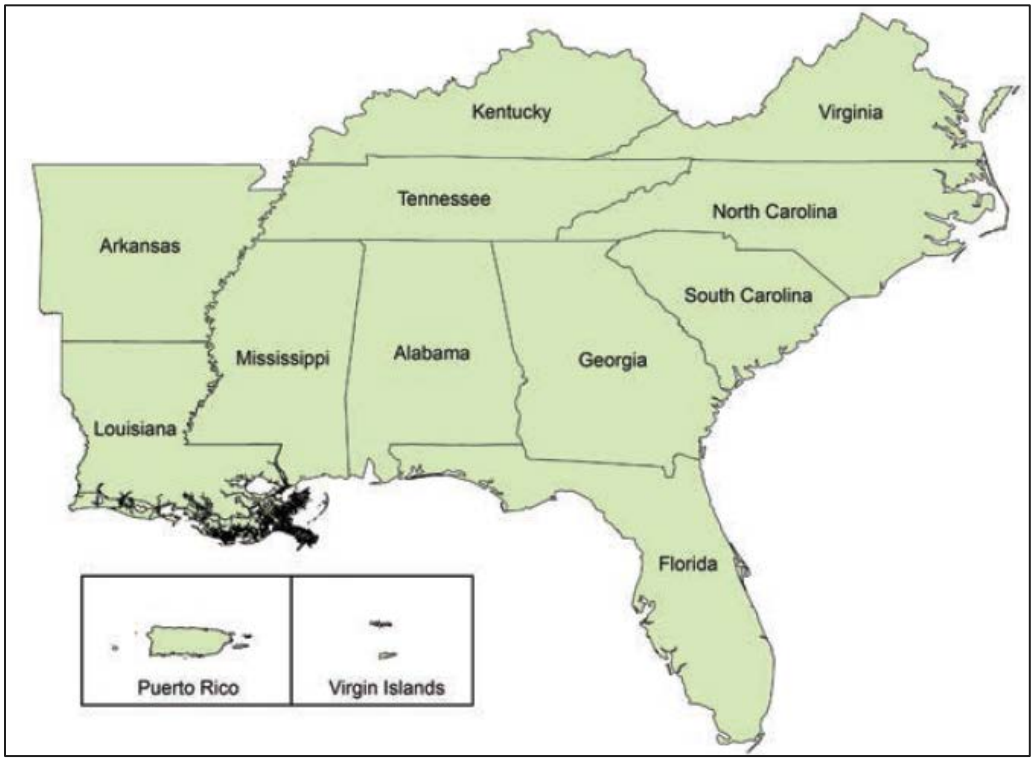

Figure 1.1. The 11 Southeastern States, Puerto Rico, and Virgin Islands Compose the Southeast Region for the USGCRP NCA3 (Ingram et al. 2013). In NCA4, Puerto Rico and Virgin Islands were split from the Southeast Region and comprise the Caribbean region (USGCRP 2017).

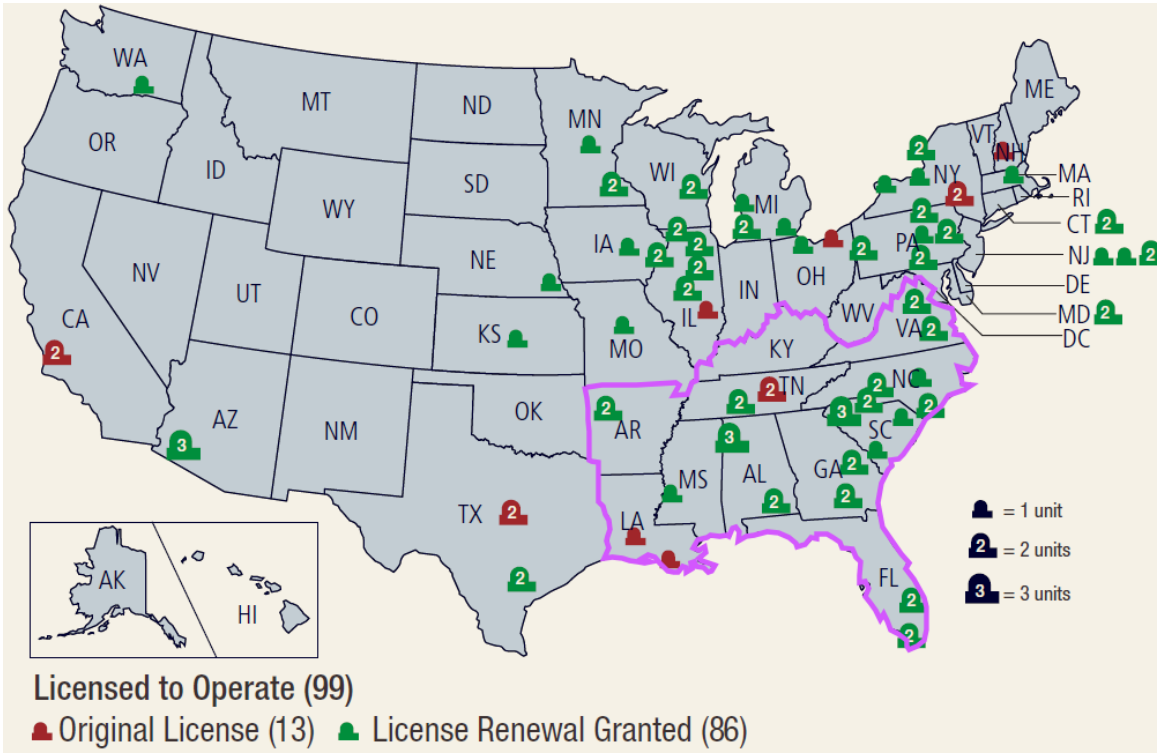

Figure 1.2. Operating Nuclear Power Reactors in the United States as of July 2018 (NRC 2018). The delineated area shows the Southeast Region.

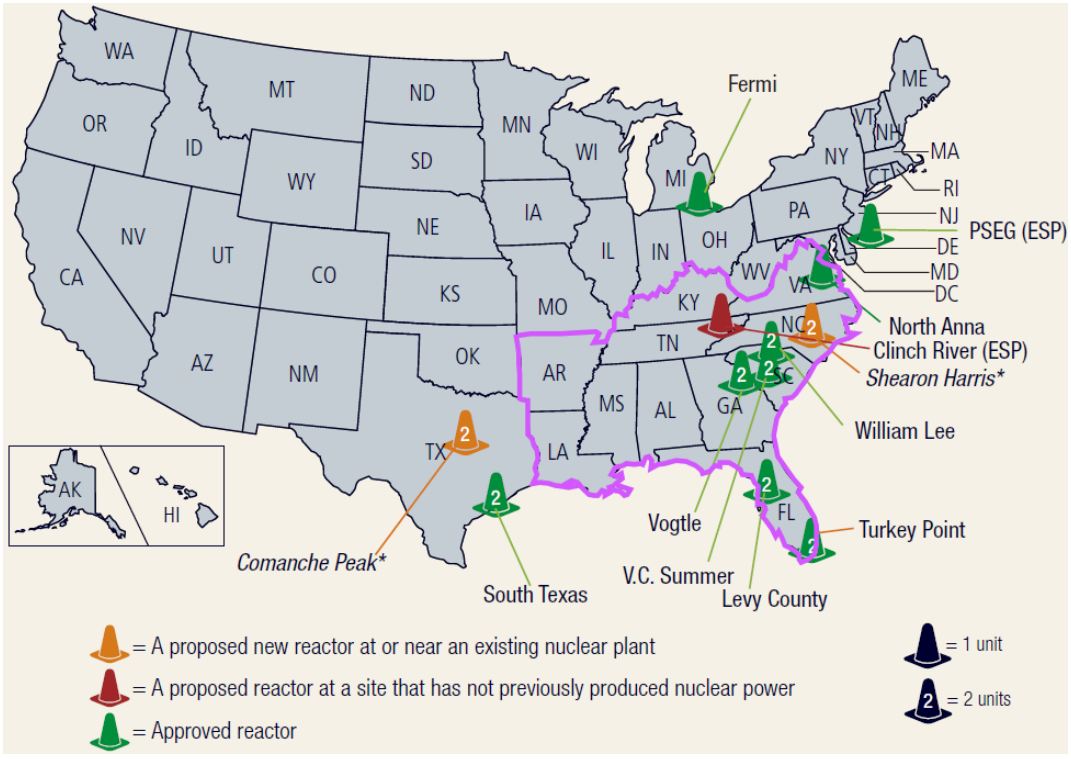

Figure 1.3. Proposed Nuclear Power Reactors in the United States as of July 2018 (NRC 2018). The delineated area shows the Southeast Region.

To support the NRC's (1) PFHA research plan in developing a risk-informed licensing framework for flood hazards and design standards, (2) environmental reviews at existing and proposed facilities, and (3) significance determination tools for evaluating potential flood hazards and their protection at plant facilities, this report summarizes key findings available in the broad climate research literature about observed regional climate trends and projected climate change, as well as observed and potential hydrologic impacts in the Southeast Region. The contents are drawn from published reports including the NCA Regional Technical Input Report Series for the Southeast United States (Ingram et al. 2013); the National Oceanic and Atmospheric Administration (NOAA) Technical Report NESDIS 142-2, Regional Climate Trends and Scenarios for the U.S. NCA Part 2: Climate of the Southeast U.S. (Kunkel et al. 2013a); the Fourth NCA (USGCRP 2017, 2018); papers published in peer-reviewed journals; NOAA websites; and other sources including information available from the Southeast Regional Climate Center website.

1.1 Climate Modeling Primer

Global climate models (GCM) are used to project climate changes in the future. The Intergovernmental Panel on Climate Change (IPCC) used results from an ensemble of GCMs developed by climate modeling centers around the world. The most recent IPCC Fifth Assessment Report (AR5) used GCM simulations of historical and future climate that are part of the Coupled Model Intercomparison Project Phase 5 (CMIP5) (Taylor et al. 2012). In CMIP5, GCMs were run at grid resolutions between 100 and 300 km, and model outputs can be accessed via websites serving as portals to the Earth System Grid Federation archive. The GCM simulations were initialized in 1850 and run through 2100 using historical forcings including concentrations of greenhouse gases (GHG) and aerosols, the history of land use and land cover between 1850 and 2005, and scenarios of future forcings for 2006–2100. These results also were used in the USGCRP Climate Science Special Report (CSSR) (USGCRP 2017) for the Fourth National Climate Assessment (NCA4).

This annual report discusses the climate change projections for the southeastern United States summarized in the NCA4 CSSR based on the CMIP5 GCMs. Because the CSSR discusses climate change broadly across the United States but does not provide more detailed information by region, this report also makes use of the comprehensive regional climate change information available from the Third National Climate Assessment (NCA3), as reported by Kunkel et al. (2013a) and Ingram et al. (2013) for the Southeast Region. In NCA3, climate change information was derived from climate projections produced by GCMs that participated in the Coupled Model Intercomparison Project Phase 3 (CMIP3) and used by the IPCC Fourth Assessment Report (AR4). The GCMs used in AR4 were generally earlier versions of the GCMs used in AR5 and were applied at a comparable range of horizontal grid resolutions. NCA3 also used higher-resolution climate projections from two downscaled products developed using statistical and dynamic downscaling methods applied to the CMIP3 GCM outputs. The statistical downscaled product includes daily temperature and precipitation at $^1/_8$-degree resolution for 1961–2100. The dynamical downscaled product is a collection of 11 regional climate projections generated by six regional climate models driven by four CMIP3 GCMs. These regional climate projections at a grid resolution of 50 km over North America are part of the North American Regional Climate Change Assessment Project (NARCCAP). They cover the historical period of 1979–2004 and a future period for the mid-century (2040–2070). The projected changes reported by Kunkel et al. (2013a) and Ingram et al. (2013) are for future periods relative to a reference period of 1971–1999.

To project the future climate, GCMs were forced by scenarios of concentrations of GHGs and aerosols and land use/land cover projected by integrated assessment models. The GCM projections used in CMIP3 and NCA3 were forced by the A2 and B1 emissions scenarios prepared by the IPCC Special Report on Emissions Scenarios (SRES) (IPCC 2000). The A2 and B1 scenarios correspond to the business-as-usual

and the emission mitigation scenarios with high and low emissions, respectively. Figure 1.4 shows the global GHG emissions and the global surface warming projected by the GCMs used in IPCC AR4. The GCM projections used in CMIP5 and NCA4 were driven by emission scenarios described by the Representative Concentration Pathways (RCP). Figure 1.5 shows a comparison of the SRES scenarios used in CMIP3 and NCA3 and the RCP scenarios used in CMIP5 and NCA4. The A2 and RCP8.5 scenarios produce comparable trajectories of radiative forcing relative to pre-industrial time that correspond to the business-as-usual scenario. Similarly, the B1 and RCP4.5 scenarios share similar trajectories of radiative forcing corresponding to emission mitigation. Knutti and Sedláček (2012) showed that the projected global temperature changes and spatial patterns of temperature change from the CMIP5 models are very similar to those projected by the CMIP3 models after accounting for the different underlying scenarios.

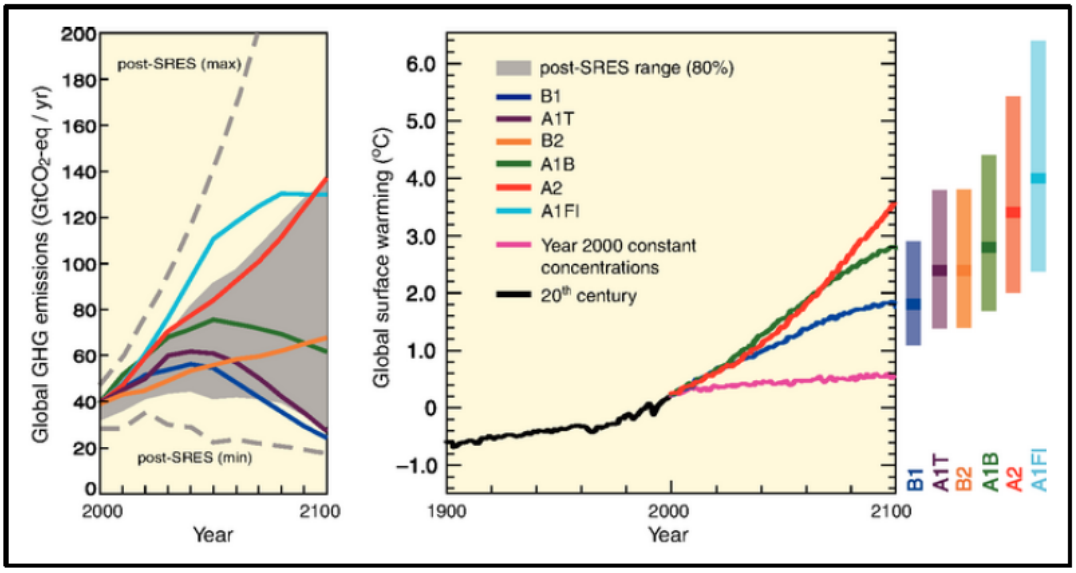

Figure 1.4. (Left) Global GHG Emissions (in $GtCO_2$-eq) in the Absence of Climate Policies for Six SRES Scenarios (colored lines: B1, A1T, B2, A1B, A2, A1F1) and the 80th Percentile Range (gray shaded area) and Full Range (dashed lines) of Recent Scenarios Published since SRES (post-SRES) and between 2000 and 2100. The emissions include CO_2, CH_4, N_2O, and F-gases (right). Multimodel global averaged surface warming for scenarios A2, A1B, and B1 are shown as continuations of the 20th century simulations. These projections also take into account short-lived GHGs and aerosols. The pink line is a projection in which atmospheric concentrations are held constant at the year 2000 level. The multimodel mean global averaged surface warming between 1900 and 2000 is shown in black. The color bars at the right indicate the best estimate (the solid line within each bar) and the likely range of global surface warming in 2090–2099. All temperatures are relative to the period 1980–1999. (Source: Kunkel et al. 2013a)

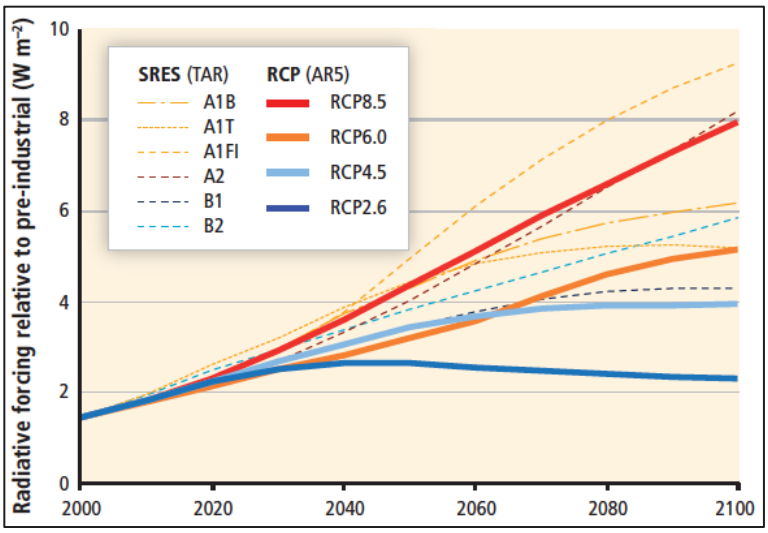

Figure 1.5. Comparison of the radiative forcing using the different SRES and RCP emissions scenarios in the 21st century. (Source: Burkett et al. 2014)

In summary, this report discusses future climate projections for the southeastern United States based on synthesis produced by NCA3 and NCA4, which used GCM outputs from CMIP3 and CMIP5 that contributed to IPCC AR3 and AR4, respectively. Figure 1.6 summarizes the relationships among the more recent international (IPCC) and national (NCA) assessments, the Coupled Model Intercomparison Projects (CMIPs) that designed and coordinated the GCM experiments that generated the model outputs adopted by the assessments, and the emission scenarios used by the GCMs.

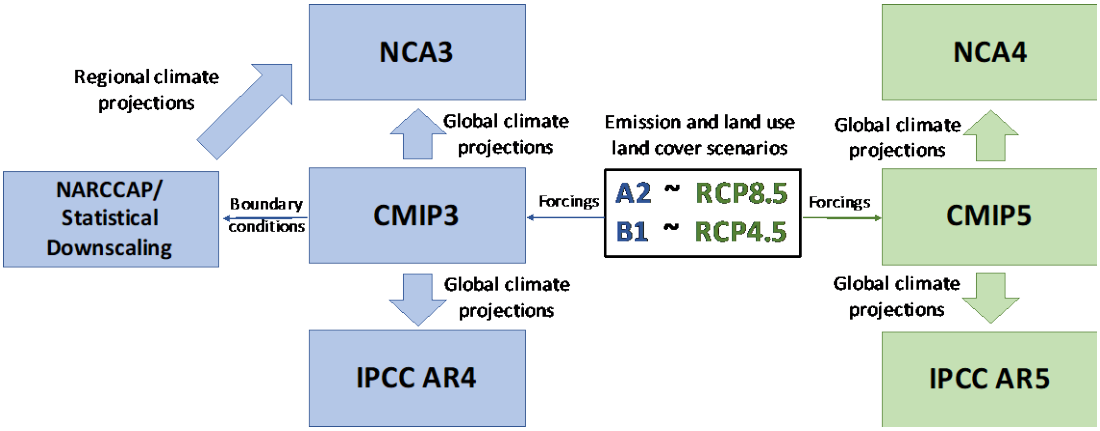

Figure 1.6. Relationships Among Assessments, , CMIPs, and Emission Scenarios. The climate change information used in this report is largely derived from the Third and Fourth National Climate Assessments (NCA3 and NCA4), which used GCM global climate projections from the Coupled Model Intercomparison Project Phase 3 and Phase 5 (CMIP3 and CMIP5) that also formed the basis of the climate information used in the IPCC Third and Fourth Assessment Reports (AR4 and AR5), respectively. The GCMs used in CMIP3 and CMIP5 were forced by emission and land use/land cover scenarios (A2 and B1) and (RCP8.5 and RCP4.5), respectively, generated by integrated assessment models. As shown in Figure 1.5, A2 and RCP8.5 produced comparable radiative forcings for the high emission scenarios, while B1 and RCP4.5 produced comparable radiative forcings for the low emission scenarios. In NCA3, regional climate projections produced by statistical and dynamical downscaling methods were used in addition to the CMIP3 global climate projections.

Because this report draws heavily on findings based on CMIP3 and CMIP5, it would be useful to understand how well these models simulate the historical climate of the United States and how they may differ in their simulation skills and projections for the future. As part of the *Journal of Climate* Special Collection on "North America in CMIP5 Models," Sheffield et al. (2013) evaluated the CMIP5 historical simulations, focusing on the continental and regional climatology of North America. They noted that the multimodel ensemble mean represents the observed spatial patterns of basic climate and hydrological variables quite well, but a large variability exists across models and regions; no single model stands out as being particularly better or worse across all analyses presented. They also found slight improvement in the CMIP5 multimodel ensemble relative to CMIP3 (Figure 1.7), and higher-resolution models tend to perform better for regional processes.

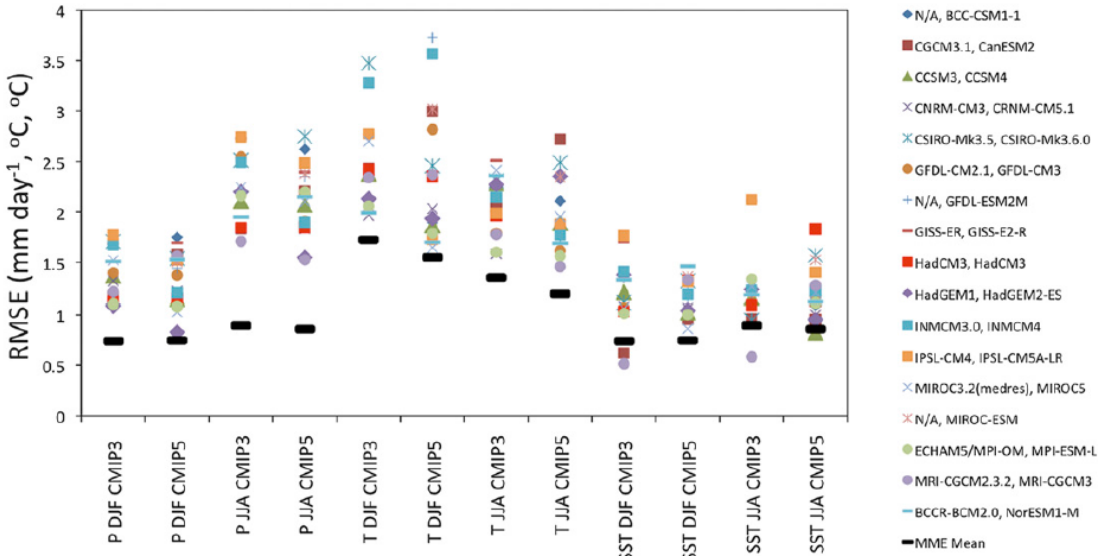

Figure 1.7. Comparison of CMIP5 and CMIP3 Model Performance for Seasonal (DJF and JJA) Precipitation (P), Surface Air Temperature (T), and Sea Surface Temperature. Results are shown as root-mean-square error values calculated for 1971–1999 relative to the Global Precipitation Climatology Project, Climatic Research Unit, and Hadley Centre Sea Ice and Sea Surface Temperature observational data sets. Precipitation and temperature root-mean-square error values are calculated over North America (1308–608W, 08–608N) and sea surface temperature root-mean-square error values are calculated over neighboring oceans (1708–358W, 108S–408N). The core set of CMIP5 models and their equivalent CMIP3 models where available (otherwise indicated by ''N/A'') are shown. The multimodel ensemble mean values are also shown. (Source: Sheffield et al. 2013)

At grid resolutions between 100 and 300 km, the GCMs used in CMIP3 and CMIP5 can resolve broad mountain ranges such as the Rockies and large-scale atmospheric circulation while subgrid-scale moist processes associated with clouds and convection are parameterized. Tropical cyclones and severe storms such as tornadoes are not resolved by the GCMs, so their changes are typically inferred from changes in the large-scale environments that are known to support their development. Regional models at a grid resolution of 50 km used in NARCCAP can better resolve smaller-scale topographic features and their influence on mesoscale flow and cloud and precipitation. Regional models at sub-kilometer grid resolutions can begin to explicitly resolve convection that plays key roles in severe weather and extreme precipitation, but so far very few studies were able to simulate historical and/or future climate using models such resolution.

As described by Ingram et al. (2013), the climate in the Southeast Region is generally mild and is locally influenced by latitude, topography, and distance from a coastline. Elevations in the region vary from sea level near the coasts to 3000 ft in the Ozark Mountains in Arkansas and to 6600 ft in the Appalachian Mountains. The climate of the Southeast Region is also influenced by the Bermuda/Azores High, a semi-permanent subtropical high-pressure system in the North Atlantic that migrates east and west depending on the season. The location of the Bermuda High has important influences on moisture transport from the Atlantic and Gulf of Mexico to the region during summer months and the tracks of hurricanes during the Atlantic hurricane season. In concert with the jet stream during cooler months, the Bermuda High also influences the development of severe thunderstorms, high winds, hail, ice storms, and tornadoes.

1.2 Contents of the Report

In this report, climatic and hydrologic features important for the Southeast Region are discussed in various chapters. Chapter 2 provides an overview of the regional temperature characteristics of the Southeast Region including observed history and projected future changes. Chapter 3 summarizes observed history and projected future changes in precipitation in the Southeast Region. The chapter also includes a summary of hydrologic impacts including flooding from projected future changes. Chapter 4 summarizes impacts of climate change on hurricane winds, sea-level rise, and storm surge in the Southeast Region. Chapter 5 summarizes impacts of climate change on tornadoes and small-scale convective storms in the Southeast Region. Chapter 6 summarizes recent U.S. agency activities related to climate change and its impacts. Finally, Chapter 7 provides citation information for the references cited in this report.

We note that the terminology used in the broad climate research community is not aligned with that used in the NRC permitting and licensing context. For example, Ingram et al. (2013, Figure 2.6) describe trends in “extreme” precipitation events in the Southeast Region using the 24-hour and 5-day, 0.2 annual probability of exceedance of precipitation events. In contrast, the NRC’s interest in extreme events span a much lower range of annual frequencies of exceedance—10^{-3} and lower (NRC 2015, 2016). The flood events of interest to the NRC may be generated by precipitation at a range of timescales—from 5 minutes to several days. Therefore, interpreting the research results performed in the climate community should be carefully evaluated for use in the NRC permitting and licensing context. As far as possible, this report endeavors to explicitly state the event time scales and the annual probabilities of exceedance or frequencies reported in the reviewed literature.

2.0 Temperature in the Southeast Region

This chapter summarizes the observed temperatures in the Southeast Region. The data were obtained from NOAA National Centers for Environmental Information (NCEI) and from published papers and reports in the broad climate research community. The chapter includes information related to historical trends in observed temperatures, and it summarizes the projected temperature in the Southeast Region from published papers and reports.

2.1 Observed Temperature Changes

- The Southeast Region is one of a few regions globally that did not exhibit long-term warming trends in the 20th century.
- The lack of warming, also known as the "warming hole," is partly related to interdecadal variability associated with the Atlantic Multidecadal Oscillation.
- Consistent with the "warming hole," no overall trends are observed in the number of extreme hot and cold events.

The NOAA NCEI summarizes the daily temperature in the form of maps to visualize the information. The NCEI currently uses an averaging period of 1981–2010[1] to create climatology maps (NCEI 2016b). The annual average minimum temperatures vary from the 60s (in degrees Fahrenheit) in the southern parts of the Southeast Region to the 30s and 40s progressively inland and with rising elevations within the region (Figure 2.1a).

The annual average maximum temperatures vary from the 80s in the southern parts of the region to the 50s and 60s °F progressively inland and with rising elevations within the region (Figure 2.1b). On average, January is the coolest month (average January temperatures vary from 50s in the south to the 20s inland and at higher elevations; Figure 2.1c) and July is the warmest month (average July temperatures vary from the 90s in the southern half of the region to the 80s in inland areas and the 70s at higher elevations; Figure 2.1d).

The Southeast Region is one of a few regions globally that did not exhibit long-term warming trends in the 20th century (Figure 2.2). This lack of warming in the Southeast Region and part of the Great Plains and Midwest is known as the "warming hole." Several mechanisms have been hypothesized to contribute to the warming hole, including increased cloudiness associated with enhanced moisture transport, increased aerosols that reduced shortwave radiation reaching the surface, irrigation that increased evaporative cooling, and decadal variability in the North Atlantic and tropical Pacific sea surface temperatures that influenced circulation patterns (Kunkel et al. 2013a). While some of the hypothesized mechanisms for the warming hole may have a larger influence in the summer, the lack of long-term warming trends in the Southeast Region is observed in all seasons as well as in the annual mean. Figure 2.3 shows the multidecadal spatial and temporal variability of the warming hole in the United States. Kumar et al. (2013) found that the lack of long-term warming trends in the southeastern and eastern United States is related to low-frequency multidecadal variability in the North Atlantic temperatures associated with the Atlantic Multidecadal Oscillation (AMO).

[1] The Third National Climate Assessment used the 1971–2000 normals.

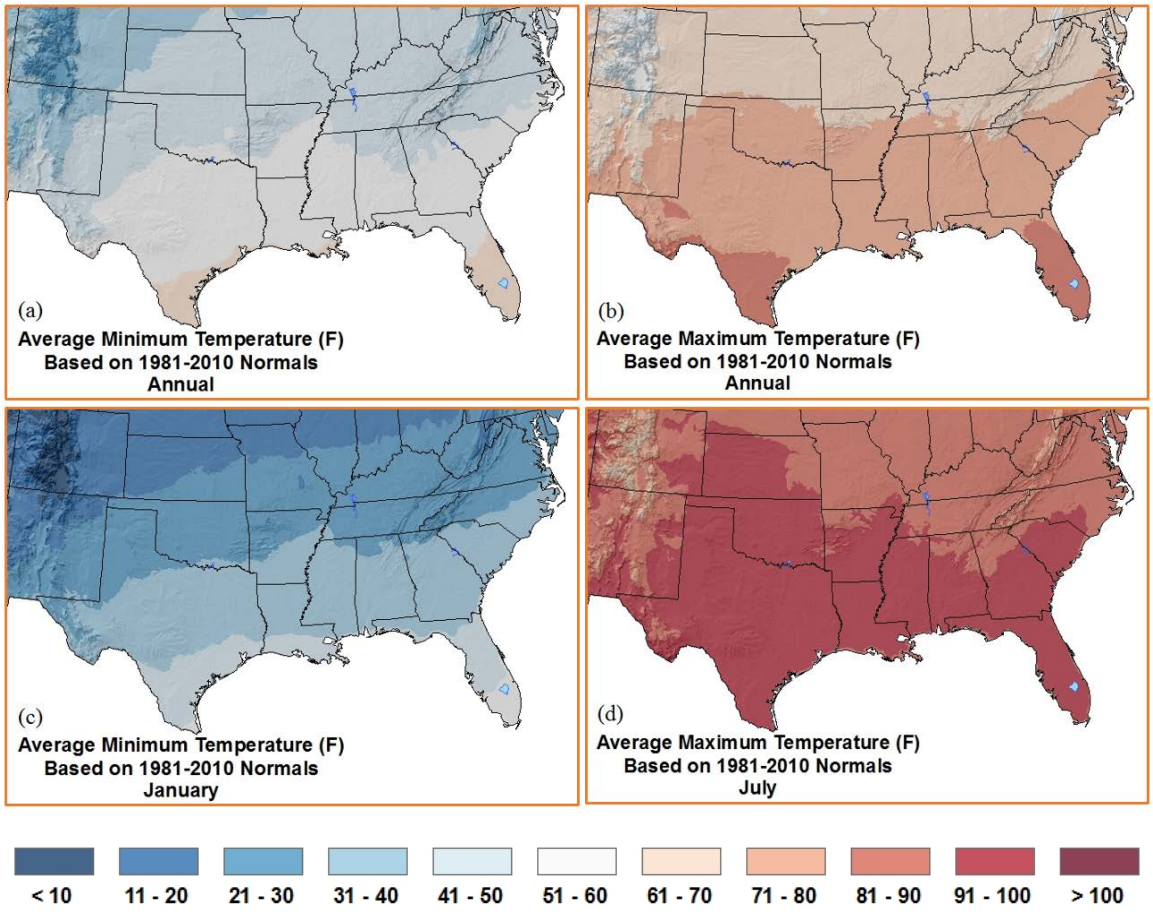

Figure 2.1. Average Minimum (a) and Maximum (b) Annual Temperatures and Average Minimum January (c) and Maximum July (d) Temperatures Based on the 1981–2010 Normals. (Source: NOAA NCEI 2016b)

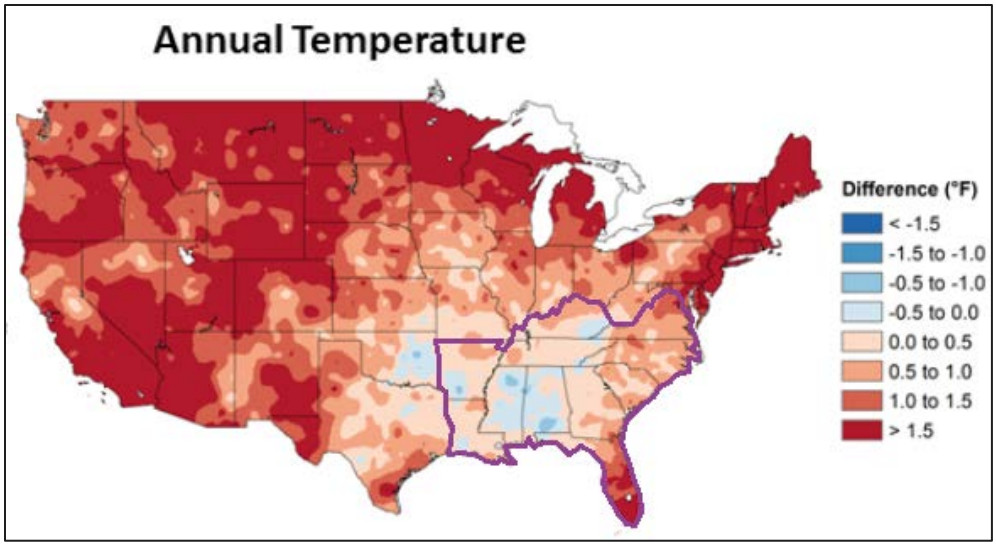

Figure 2.2. Observed Changes in Annual Temperature (°F). Changes are the difference between the average for present day (1986–2015) and the average for the first half of the last century (1901–1960). (Source: USGCRP 2017)

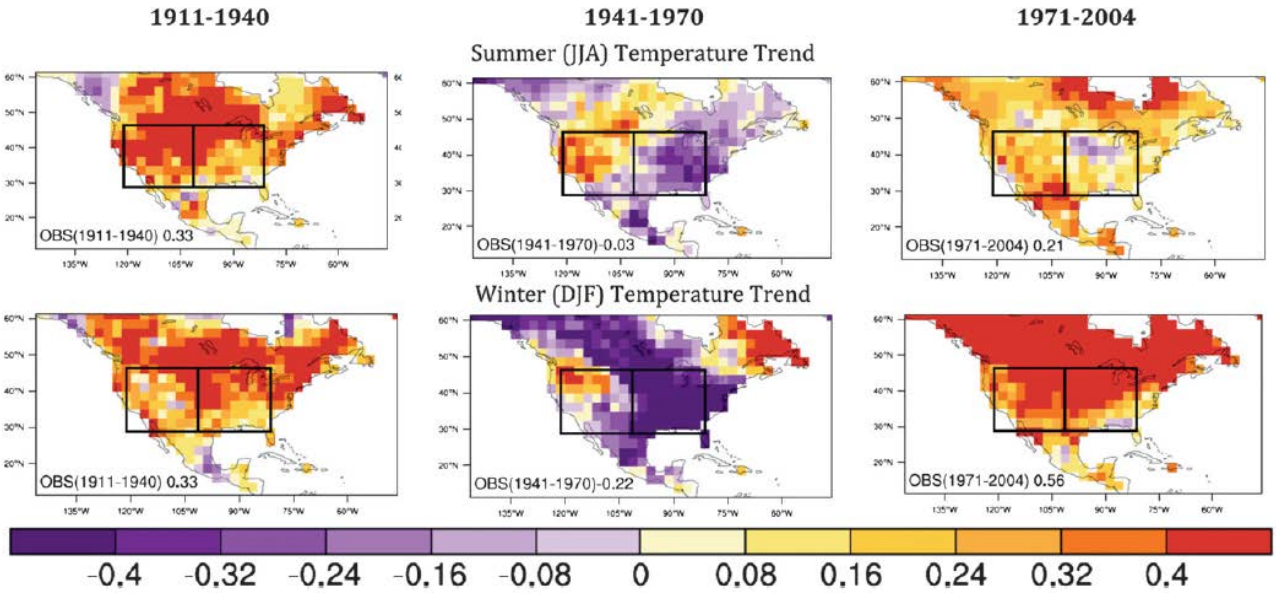

Figure 2.3. Summer (top) and Winter (bottom) Observed Temperature Trends for Three Non-Overlapping 30-Year Periods of (left) 1911–1940, (middle) 1941–1970, and (right) 1971–2004 in °C per Decade. The number in each panel represents the North American land-only temperature trend in the corresponding period and the spatial average for the entire land region shown in the figure. The two boxes in the eastern and western United States are used in subsequent analysis described in the paper by Kumar et al. (2013) from which this figure was derived.

As shown in Figure 2.4, the annual precipitation trends in the eastern United States are correlated with the AMO phase. More specifically, Kumar et al. (2013) found that the summer AMO explains 76 percent of the variance in the annual temperature trend, 70 percent of the variance in the summer temperature trend, and 62 percent of the variance in the winter temperature trend (all statistically significant) in the eastern United States, but the winter AMO is not significantly correlated with eastern United States temperature trends. Generally GCMs in CMIP5 have limited capability in simulating aspects of the warming hole in North America, but Kumar et al. (2013) found that climate models that better captured the AMO are also more likely to reproduce the observed warming hole.

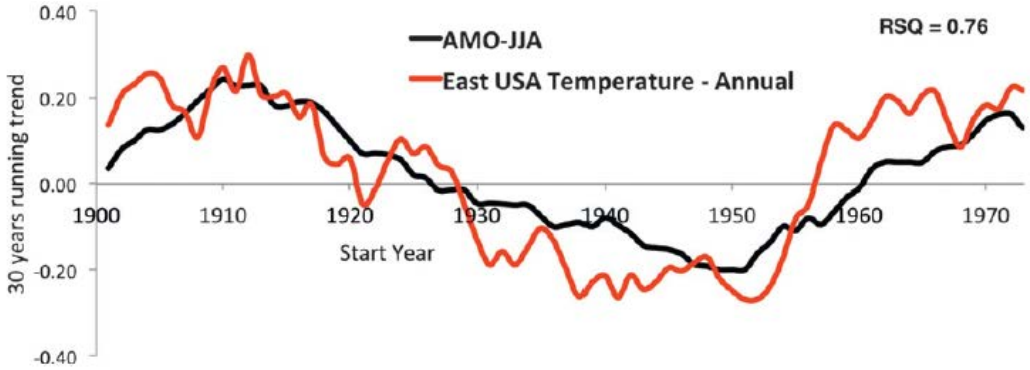

Figure 2.4. Multidecadal Variability in Summer AMO and Temperature Trend (°C per decade) in the Eastern United States. AMO is an index of North Atlantic Ocean sea surface temperature anomalies. (Source: Kumar et al. 2013)

The Southeast Region occasionally experiences hot days (daily maximum temperature ≥95°F or daily minimum temperature ≥75°F) during summer and cold days (daily minimum temperature ≤32°F) during winter (Ingram et al. 2013). Elevated heat in the interior of the region is influenced by an upper-level ridge of high pressure that forms over the Mississippi River drainage area, which when combined with high humidity, can adversely affect human health, agriculture, water supply, and energy production. Local variations in elevated heat events are moderated by elevation effects and sea breezes.

Record high temperatures in the Southeast Region can range from 75°F in January to 115°F in August (NCEI 2016a). Across the Southeast Region, maximum daily average temperatures can exceed 90°F from 2 to 26 days in July and August (NCEI 2016a). Record low temperatures in the Southeast Region can range from 70°F in August to -24°F in January (NCEI 2016a). Across the Southeast Region, minimum daily average temperatures do not fall below freezing from June through August but can fall below freezing up to 24 days in January (NCEI 2016a).

Consistent with the lack of long-term warming trends (i.e., the warming hole), most stations in the Southeast Region have experienced little change in the number of days featuring maximum (minimum) temperatures >95°F (75°F) in the last century. Similarly, most stations have experienced little change in the number of days with minimum temperature <32°F. Further, no observable overall trends are apparent in the number of elevated hot and cold events (Kunkel et al. 2013a).

2.2 Projected Temperature Changes

- No warming hole is projected for the temperature changes in the United States.
- Milder warming is projected along the coast relative to inland areas and the higher latitudes; warming trends are larger in higher emission scenarios.
- The annual maximum number of consecutive days with daily maximum temperature >95°F is projected to increase by 4 to 20 day/year comparing 2041–2070 with 1980–2000.

Consistent with the projections of global surface warming, temperatures in the Southeast Region are projected to increase in the future with greater warming in the A2 compared to the B1 scenarios. For 2035, the annual mean warming in the region is projected to be between 1.5 and 3.5°F, with small differences between the two scenarios. After the mid-century, differences between the two emissions scenarios increase over time; thus, in 2085, warming in the A2 scenario is between 4.5 to 8.5°F compared to between 2.5 and 5.5°F for the B1 scenario. In general, the spatial variations of the warming signals are small, except for larger warming increases from the southeast to the northwest. No warming hole is found in the multimodel mean warming, but analyzing the CMIP5 projections from 22 models, Kumar et al. (2013) found a 10–20 percent chance of the warming hole returning in the second half of the 21st century. Figure 2.5 shows the NARCCAP-projected changes in annual number of days with a maximum temperature greater than 95°F; it displays an increase in both the annual number of days and annual maximum number of consecutive days with a maximum temperature greater than 95°F.

Diffenbaugh and Ashfaq (2010) investigated the changes in hot extremes and heat waves using a regional climate model at 25 km grid resolution, which is twice the resolution used in NARCCAP. A single regional model was driven by five ensemble members of a single GCM from CMIP3 for the A1B scenario, which has lower emissions of GHGs compared to the A2 scenario used in NCA3 (Figure 2.5).

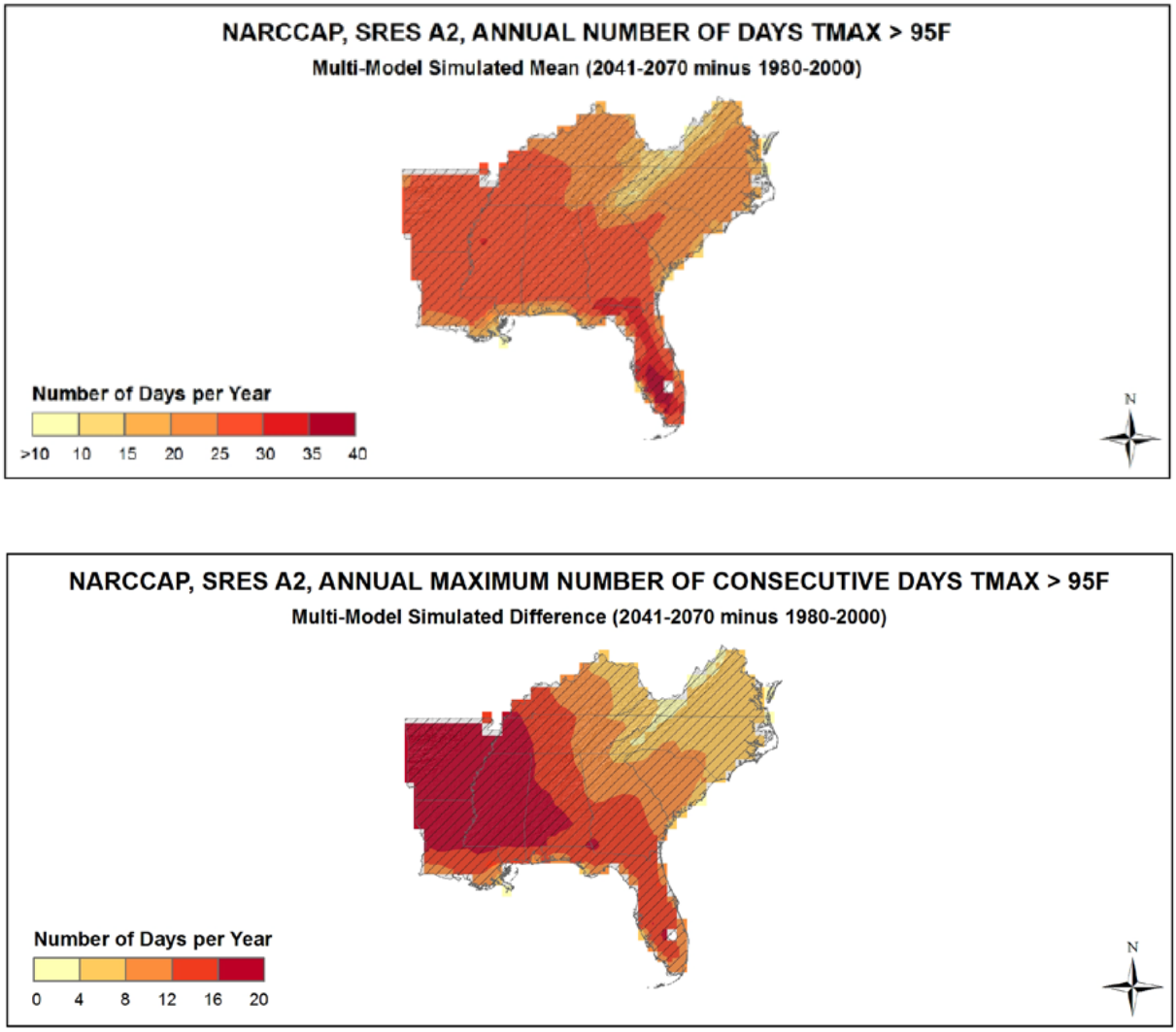

Figure 2.5. (Top) Projected Difference in the Mean Annual Number of Days with Daily Maximum Temperature >95°F for (2041–2070) Relative to (1980–2000) and (bottom) Similar to the Top Panel, but for the Annual Maximum Number of Consecutive Days with Daily Maximum Temperature >95°F. The results are shown for the multimodel differences for both top and bottom. Color with hatching indicates that more than 50 percent of the NARCCAP models show a statistically significant change in the number of days, and more than 67 percent agree on the sign of the change. (Source: Kunkel et al. 2013a)

The study found substantial intensification of hot extremes within the next three decades when global mean warming is below 2°C.

Figure 2.6 shows the changes in heat extremes in the first three decades of the 21st century compared to 1951–1999. By 2030–2039, the 95th percentile daily maximum temperature heat events are projected to increase by 30 to 50 events per year, and the historical longest heat waves are projected to increase by 1 to 5 events per decade in the Southeast Region. Using a regional model at a much higher grid resolution of 4 km for a domain covering the eastern United States, Gao et al. (2012) downscaled climate projections from a CMIP5 GCM for the RCP8.5 scenario. Their results showed an increase in heat wave intensity by 1–3°C and an increase in heat wave frequency by up to seven events per year comparing simulations in a mid-century period (2057–2059) and the present (2001–2004).

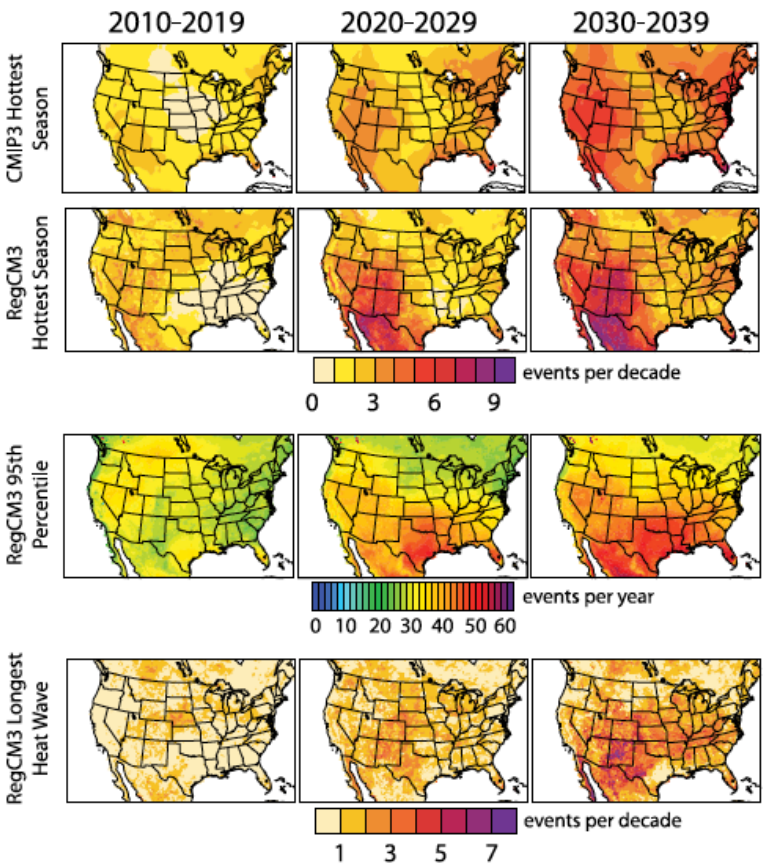

Figure 2.6. Projected Changes in Heat Extremes in the First Three Decades of the 21st Century. The top two rows show the decadal occurrence of the 1951–1999 hottest-season 95th percentile daily maximum temperature threshold (T95), and the third and fourth rows show the decadal occurrence of T95 and the historical hottest-heat-wave threshold in an A1B scenario. As with the historical hottest-season exceedance, the baseline and exceedance values are calculated at each grid point and for each decade of the 2010–2039 period. (Source: Diffenbaugh and Ashfaq 2010)

In Gao et al. (2012), a heat wave is defined as the longest continuous period satisfying three criteria including (1) the maximum daily temperature remains above T1 for at least three continuous days, (2) the mean daily maximum temperature is higher or equal to T1, and (3) in each day, the daily maximum temperature is no lower than T2. T1 and T2 are the 97.5th and 81st percentiles of daily maximum temperature in the present climate (2001–2004). These studies consistently found increases in hot extremes and heat waves as the mean temperature increases in a warmer climate.

Besides heat waves that have large implications for human population and ecosystems, climate change may increase wet bulb temperatures that are directly linked to heat stress. Wet bulb temperature accounts for both heat and humidity and is equivalent to the temperature felt by wet skin exposed to air. Hyperthermia can result from a sustained period when the wet bulb temperature of the environment is close to or higher than the temperature of the human skin (~35°C), because no conductive or evaporative cooling can relieve the metabolic heat generated by the body. Although not relevant to the southeastern United States, Sherwood and Huber (2010) found a strong linear relationship between the wet bulb temperature and the global or tropical mean temperature, plausibly because of the links between air in the tropics and aloft in midlatitudes, which can be used to project regional changes in wet bulb temperature. They found that a global mean warming of roughly 7°C would create small zones where metabolic heat

dissipation would become impossible. This study suggested the need to consider the consequences of very large warmings to rationalize decision-making about climate mitigation. A more recent study using a regional climate model projected that changes in wet bulb temperature in the Persian Gulf could exceed the critical threshold of 35°C in the business-as-usual scenario (Pal and Eltahir 2015).

3.0 Precipitation in the Southeast Region

This chapter summarizes the observed precipitation in the Southeast Region. The data were obtained from the NOAA NCEI, United States Geological Survey (USGS), and from published papers and reports in the broad climate research community. The chapter includes information related to historical trends in observed precipitation and recent record flooding events, and it summarizes the projected precipitation and hydrologic impacts in the Southeast Region from published papers and reports.

3.1 Observed Precipitation

This section reviews observed changes in mean and extreme precipitation over the Southeast Region (Section 3.1.1) and highlights a few recent flood events that exceeded previously recorded historical maximums that result from unusual combinations of hydrometeorological conditions (Section 3.1.2).

3.1.1 Precipitation Changes

- There are no significant changes in annual mean precipitation in the Southeast Region comparing 1986 to 2015 with 1901 to 1960.
- Despite the lack of long-term trends in annual mean precipitation, the 5-year extreme precipitation has increased by 8 percent during the same time period.

The NOAA NCEI summarizes the average precipitation in the form of maps to visualize the information. The NCEI currently uses an averaging period of 1981 to 2010 to create climatology maps (NCEI 2016b). For the Southeast Region, annual average precipitation varies based on influences of location with respect to moisture sources and topographic effects (i.e., orographic lifting and rain shadow; see Figure 3.1). Annual average precipitation at locations along the Gulf and Atlantic Coasts can be 60 to 70 in., whereas interior locations can receive lower amounts. At higher elevations in southwestern North Carolina and in eastern Puerto Rico, annual average precipitation can exceed 100 in. (Ingram et al. 2013). Snowfall is more common in the northern parts of the region, where annual average snowfall ranges from 5 to 25 in. and locally exceeds 100 in. at higher elevations of the Appalachian Mountains (Ingram et al. 2013).

The seasonality of precipitation varies within the Southeast Region (Ingram et al. 2013). Thunderstorms result in summertime maximum precipitation along coasts, the Florida peninsula, and some inland areas. Cool-season extratropical cyclones result in precipitation albeit with much spatial variability in the region. The northern coast of the Gulf of Mexico and interior of the region receive precipitation from mid-latitude cyclones that transport moisture from the Gulf of Mexico in the cool season. The Florida peninsula, located south and east of the cool-season frontal systems, exhibits a winter precipitation minimum.

There have been no statistically significant long-term trends in precipitation across the Southeast Region in the last 100 years, except along the northern coast of the Gulf of Mexico. However, the interannual variability of precipitation has increased in the last few decades. This is partly related to the variability in the strength and location of the Bermuda High, also called the North Atlantic Subtropical High (NASH), which are linked to the sea surface temperatures in the North Pacific (Li et al. 2011) and North Atlantic (Misra et al. 2011) Oceans. Using global reanalysis data for the period of 1948–2007, Li et al. (2012) found that the NASH has become more intense in the last 30 years, a condition attributed to anthropogenic warming. The NASH has also moved westward, with enhanced north-south movement that increased the interannual variability of precipitation in the southeastern United States.

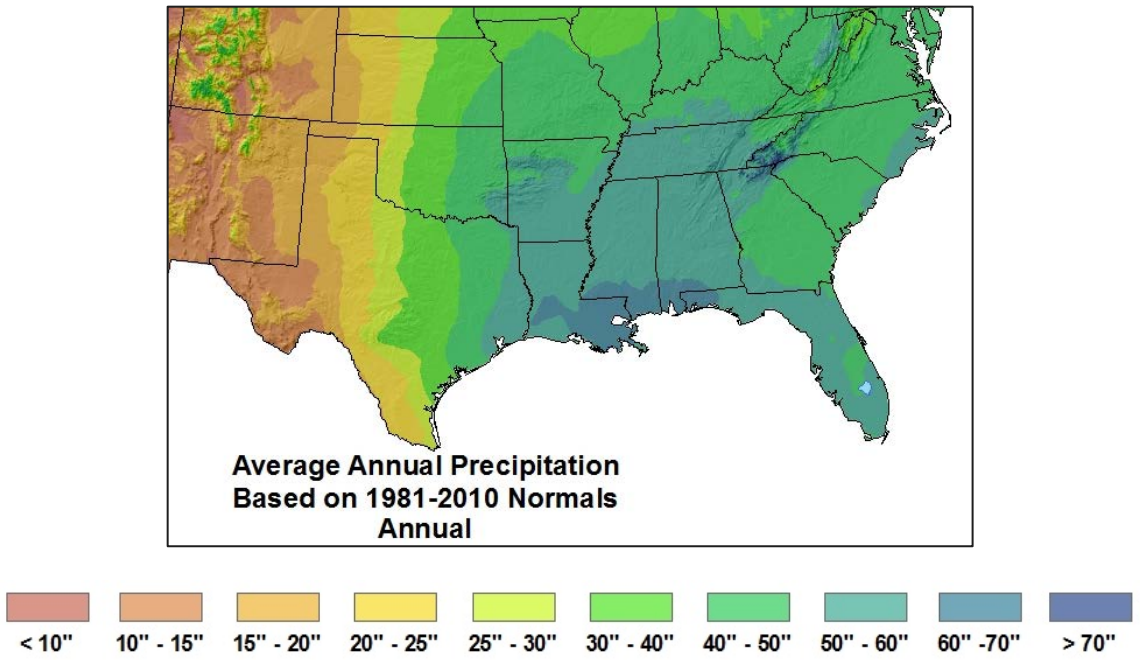

Figure 3.1. Average annual precipitation (1981–2010 normals). (Source: NCEI 2016b)

Although the long-term trends in seasonal mean precipitation are not statistically significant, changes have been observed in different aspects of heavy precipitation. Figure 3.2 shows the observed change in 20-year return period value of daily precipitation by season between 1948 and 2015. In the Southeast, larger changes are observed in fall and winter for increases of 0.41 and 0.15 in., respectively.

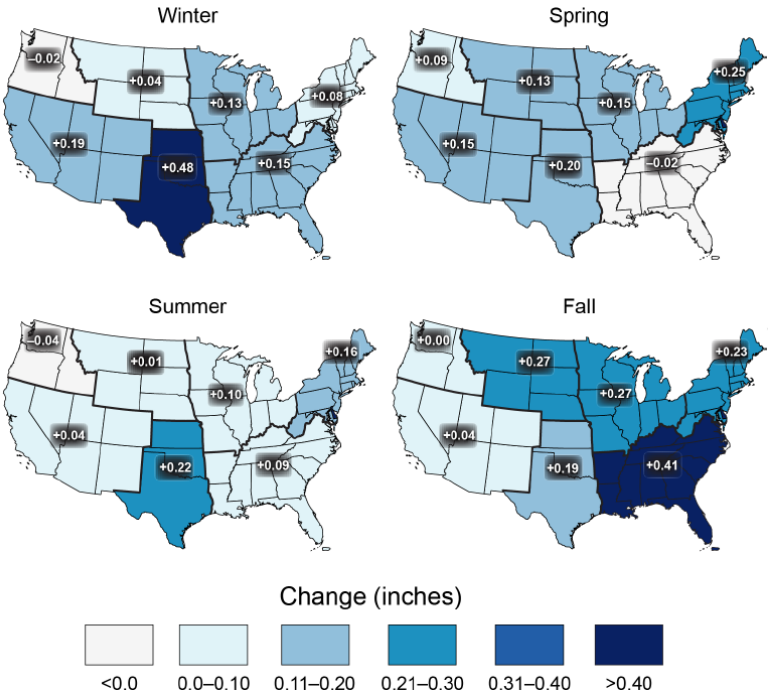

Figure 3.2. Observed changes in the 20-year return period value of the seasonal daily precipitation totals over the period from 1948 to 2015 using data from Global Historical Climatology Network data set. (Source: USGCRP 2017)

Figure 3.3 shows the change in several metrics of extreme precipitation over the entire periods of 1901–2016 or 1958–2016.

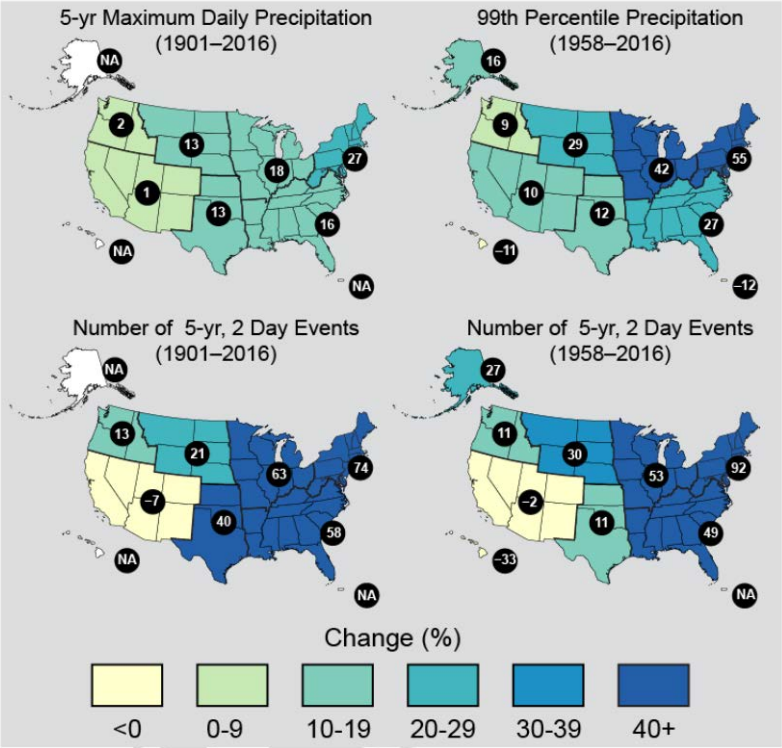

Figure 3.3. The change in several metrics of extreme precipitation by NCA4 region, including (upper left hand panel) the maximum daily precipitation in consecutive 5-year blocks, (upper right hand panel) the amount of precipitation falling in daily events that exceed the 99th percentile of all non-zero precipitation days, (lower left hand panel) the number of 2-day events exceeding the 5-year recurrence interval threshold, calculated over 1901–2016, and (upper right hand panel) the number of 2-day events exceeding the 5-year recurrence interval threshold, calculated over 1958–2016. The numerical value is the percent change over the entire period, either 1901–2016 or 1958–2016. The percentages are first calculated for individual stations, then averaged over 2° latitude by 2° longitude grid boxes, and finally averaged over each NCA4 region. (Source: USGCRP 2017)

The metrics include (1) the maximum daily precipitation in consecutive 5-year blocks from 1901 to 2016 calculated at individual stations, then averaged within each 2° latitude by 2° longitude box, and then aggregated by region to calculate a trend; (2) daily precipitation in the top 1 percent of all days for 1958–2016; and (3) the number of 2-day events exceeding the 5-year recurrence interval threshold for 1958–2016 and 1901–2016. While changes over the Southeast Region are generally small or even negative, the region has seen large increases above 40 percent in the number of 2-day events exceeding the 5-year recurrence interval threshold and an increase of 27 percent in the 99th percentile daily extreme precipitation in 1958–2016. Lastly, Figure 3.4 shows a linear increasing trend in extreme precipitation index for the occurrence of 1-day, 1 in 5-year extreme precipitation events in the southeastern United States. Events are first identified for each individual station by ranking all daily precipitation values and choosing the top N/5 events, where N is the number of years of data for that particular station. Then, event numbers for each year are averaged for all stations in each 1x1° grid box. Finally, a regional average is determined by averaging the values for the individual grid boxes. This regional average is the extreme precipitation index shown in Figure 3.4, with a statistically significant trend depicted.

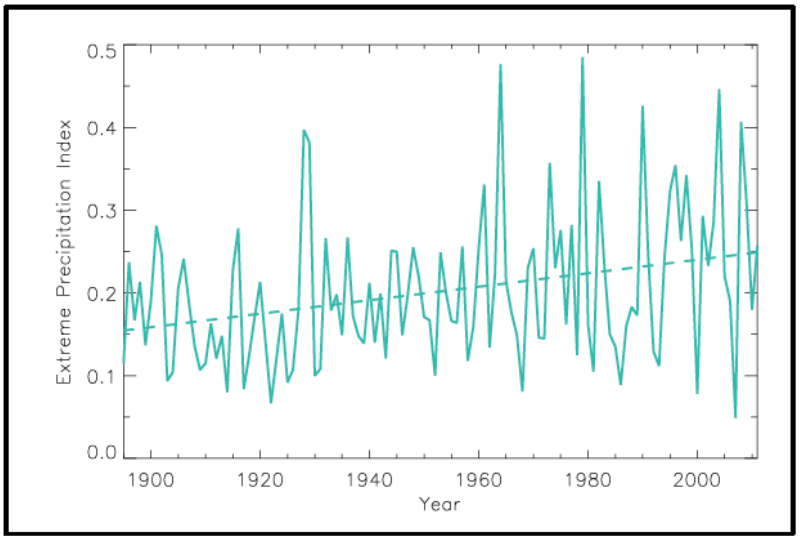

Figure 3.4. Time series of the extreme precipitation index for the Southeast Region for the occurrence of 1-day, 1 in 5-year extreme precipitation events. The dashed line indicates the best linear fit by minimizing the chi-square error statistics. Based on daily Cooperative Observer Network data from long-term stations in the National Climatic Data Center's Global Historical Climate Network data set. (Source: Kunkel et al. 2013a)

Along the Atlantic coast of the Southeast Region, tropical cyclones contribute to 10 to 15 percent of all extreme rainfall events (Figure 3.5) (Knight and Davis 2009). They also contribute significantly to the region's rainfall climatology, with the Appalachian Mountains acting as a barrier to create a spatial gradient of the tropical cyclone rainfall influence (Knight and Davis 2009). More discussions of tropical cyclones and hurricanes are presented in Chapter 4.0.

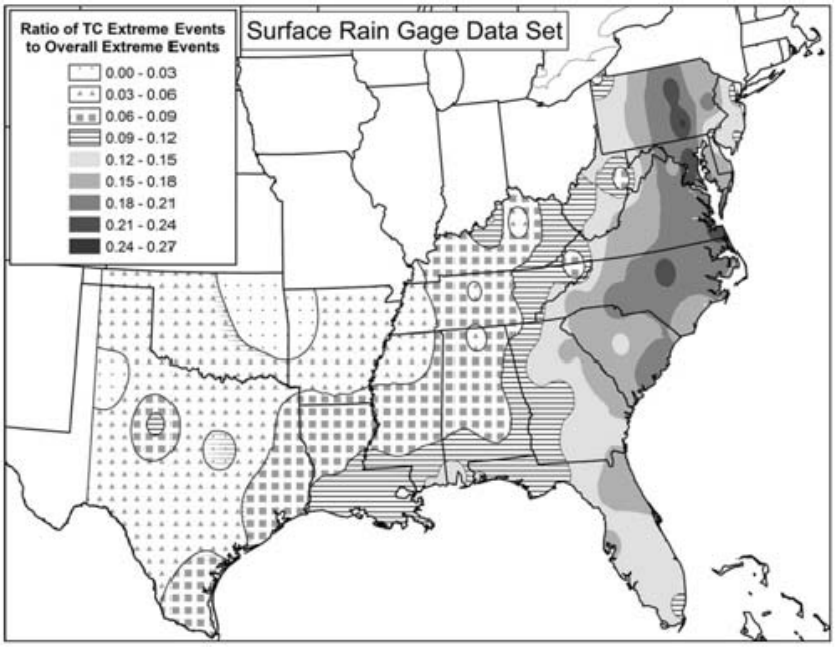

Figure 3.5. Ratio of the number of tropical cyclone extreme rainfall events to overall extreme rainfall events from all weather systems combined; derived from 85 surface weather observation stations in the southeastern United States. (Source: Knight and Davis 2009)

3.2 Future Changes in Precipitation

- Projected changes in annual mean precipitation over the Southeast Region are generally small, with variable spatial distribution.
- The daily, 20-year extreme precipitation is projected to increase by up to 21 percent in the Southeast Region in the higher emission scenario by the late 21st century.
- Convection permitting simulations show a four-fold increase in the probability of exceedance of the present day 99.95 percent hourly precipitation over the Southeast Region in summer comparing 2071–2100 with 1976–2005.

Figure 3.6 shows the projected changes in annual and seasonal mean precipitation from the CMIP3 global models and NARCCAP regional models.

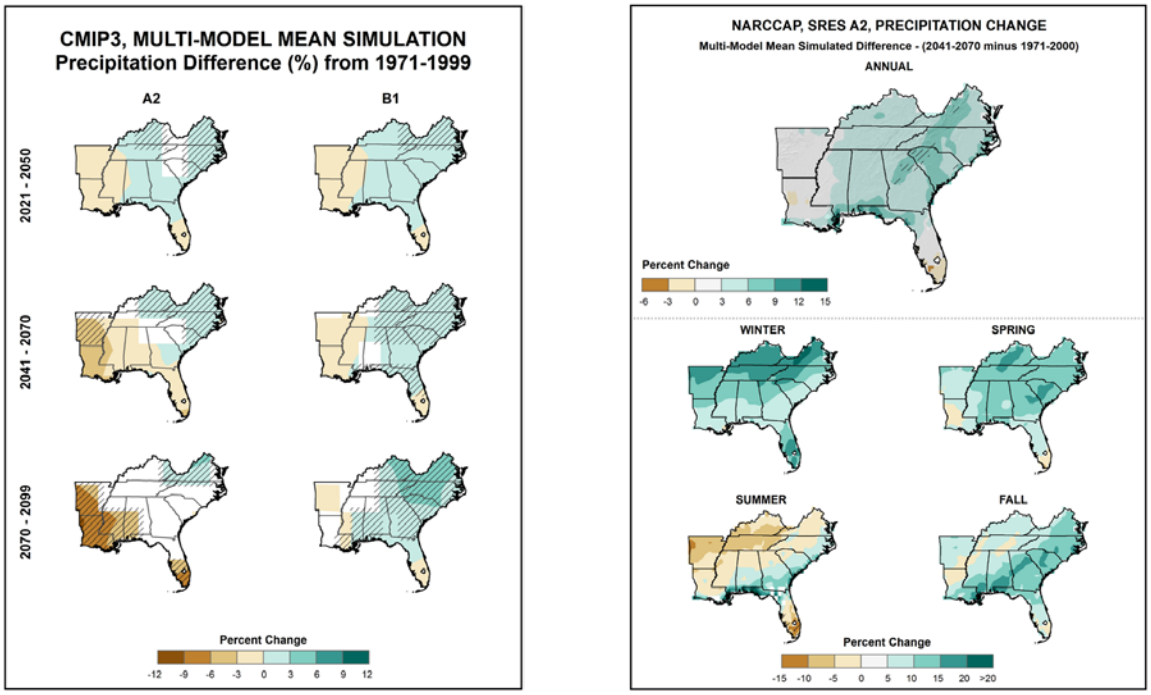

Figure 3.6. (Left) Simulated difference in annual mean precipitation (percent) for the Southeast Region, for (2021–2050, 2041–2070, and 2070–2099) with respect to the reference period of 1971–1999 from the CMIP3 global models for the A2 and B1 emissions scenarios. (Right) Simulated difference in annual and seasonal mean precipitation (percent) for 2041–2070 with respect to the reference period of 1971–2000 from the NARCCAP regional simulations for the A2 emissions scenario. In both panels, color only (Category 1) indicates that less than 50 percent of the models show a statistically significant change in precipitation. Color with hatching (Category 3) indicates that more than 50 percent of the models show a statistically significant change in precipitation, and more than 67 percent agree on the sign of the change. Whited out areas (Category 2) indicate that more than 50 percent of the models show a statistically significant change in precipitation, but less than 67 percent agree on the sign of the change. (Source: Kunkel et al. 2013a)

From the CMIP3 models, annual mean precipitation is projected to generally increase and decrease in the eastern and western part of the Southeast Region, respectively, and the east-west contrast tends to increase over time. The dynamically downscaled changes show a similar east-west contrast, but the drying is reduced in the west and the increase is larger along the Appalachian Mountains. Differences between the CMIP3 and NARCCAP projections could be related to the higher grid resolution, smaller number of global models, and differences in model formulations used in the NARCCAP models. There is a large contrast in winter versus summer precipitation changes projected by NARCCAP. However, NARCCAP-projected changes are mostly not statistically significant, and model agreement is low except for the annual changes along the Appalachian Mountains.

As the atmospheric water-holding capacity increases with warming, extreme precipitation is generally projected to increase even in the absence of changes in atmospheric large-scale circulation. In NCA3, extreme precipitation changes were assessed by comparing the annual number of days with precipitation greater than 1 in. using the NARCCAP regional climate projections. The projected changes for the mid-century show an increase throughout the Southeast Region, with the largest changes again occurring in the Appalachian Mountains (Figure 3.7).

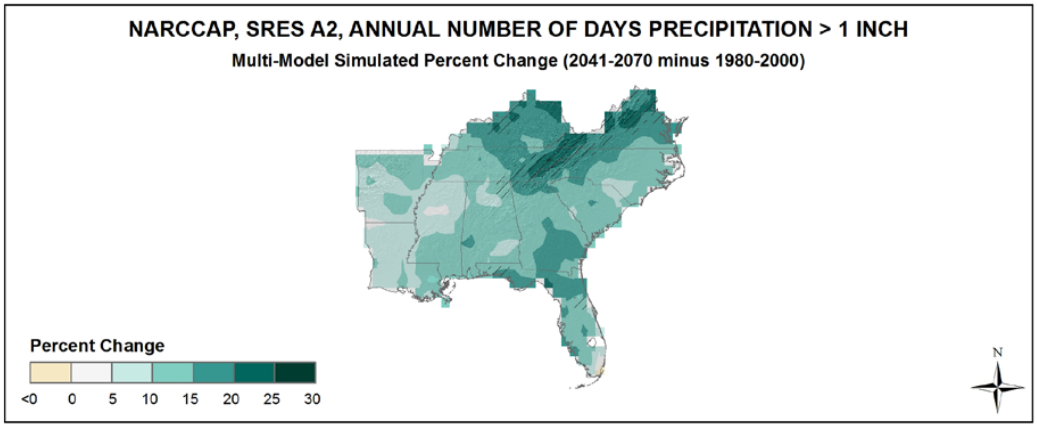

Figure 3.7. Similar to Figure 3.6, but for simulated differences in the annual number of days with precipitation >1 in. from the NARCCAP projections for the mid-century. Color and crosshatching have the same meaning as Figure 3.6. (Source: Kunkel et al. 2013a)

In USGCRP (2017), the changes in extreme precipitation are also summarized by depicting the changes in the 20-year return value of daily precipitation (Figure 3.8). The 20-year return value was calculated based on statistically downscaled data using the Localized Constructed Analogs (LOCA) method (Pierce et al. 2014) applied to CMIP5 GCM outputs. The LOCA method assumes that meteorological processes produce cyclostationary statistical relationships between large-scale and finer-scale values of a climatological field. By finding the day with observed values from a fine-scale gridded observation data, and best matching the GCM simulation in the wider region as well as in the local neighborhood around a model grid point, the GCM value is downscaled to 1/16^{o} using the historical analog, scaled to match the amplitude of the model day being downscaled. The 20-year return values from the LOCA data show increases everywhere in the United State in both the lower (RCP4.5) and higher (RCP8.5) emissions scenarios.

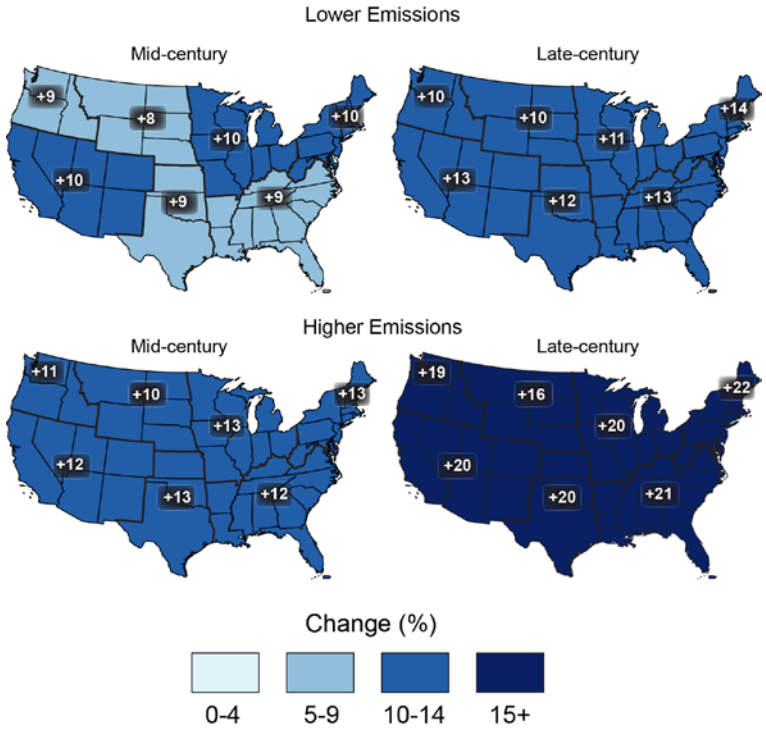

Figure 3.8. Projected change in the 20-year return period amount for daily precipitation for mid- and late-21st century for RCP4.5 and RCP8.5 emissions scenarios using LOCA downscaled data. (Source: USGCRP 2017)

Most of the current state-of-the-art GCMs and regional climate model (RCMs) operate at horizontal grid spacings of approximately 100 km and 10 km, respectively, although climate mitigation and adaptation measures are evaluated and applied at local to regional levels. This scale gap is a fundamental challenge when assessing regional and local climate change impacts, In addition to the mismatch in spatial scales between available models and practitioners' needs, important physical and thermodynamic processes that are not resolved with grid spacings of climate models must be parameterized, which is a major source of model errors and uncertainty in future climate projections. However, with advances in computing resources, it is now more feasible for very high-resolution simulations to be performed using RCMs. At grid resolutions of about 4 km or less, convection can be explicitly resolved rather than parameterized using cumulus schemes. Simulations at convection-permitting resolutions have been shown to be more capable of (or have less biases in) representing precipitation dominated by convection processes, such as mesoscale convective systems, squall lines, and tropical cyclones (Prein et al. 2015).

Recent studies of precipitation response to warming using convection-permitting regional models in Europe found a larger scaling rate of extreme precipitation with temperature compared to mean precipitation (Kendon et al. 2014). Prein et al. (2017) performed a set of convection-permitting simulations over the contiguous United States at 4 km grid resolution. In the control simulation, the regional model was driven by large-scale circulation from a global reanalysis for 2000–2013. Another simulation, called the pseudo global warming (PGW) experiment, was performed for the same period. In the PGW experiment, the model was driven by large-scale circulation that includes monthly mean perturbations corresponding to the ensemble mean climate change signals (i.e., difference between 2071–2100 and 1976–2005) determined from the CMIP5 multimodel ensemble for the RCP8.5 scenario added to the large-scale circulation of the global reanalysis for 2000–2013. Note that the PGW method differs from the more typical method used in NARCCAP and other dynamical downscaling experiments in which the regional model is driven directly by large-scale circulation simulated by the GCMs for the

historical and future periods. An advantage of the PGW method is that biases in the GCMs do not influence the quality of the regional simulations because only the GCM-simulated climate change signals are used. However, the PGW method imposes only the long-term monthly mean climate change signals as perturbations to the global reanalysis boundary conditions, so it ignores potential changes in interannual variability in a warmer climate and it does not address uncertainty using the multimodel ensemble of GCMs. Comparing the PGW and the control simulations showed that extreme (99.95th percentile) hourly precipitation increases almost across the entire domain for both winter and summer (Figure 3.9), while the mean and moderate (97.5 percentile) hourly precipitation exhibits both increases and decreases regionally. Although the 99.95 percentile hourly precipitation is considered rather extreme in the climate modeling community that has been limited by availability of hourly data, it represents the top four largest hourly precipitation events in a year, which is not rare from a hydrologist perspective in the context of extreme precipitation and flood.

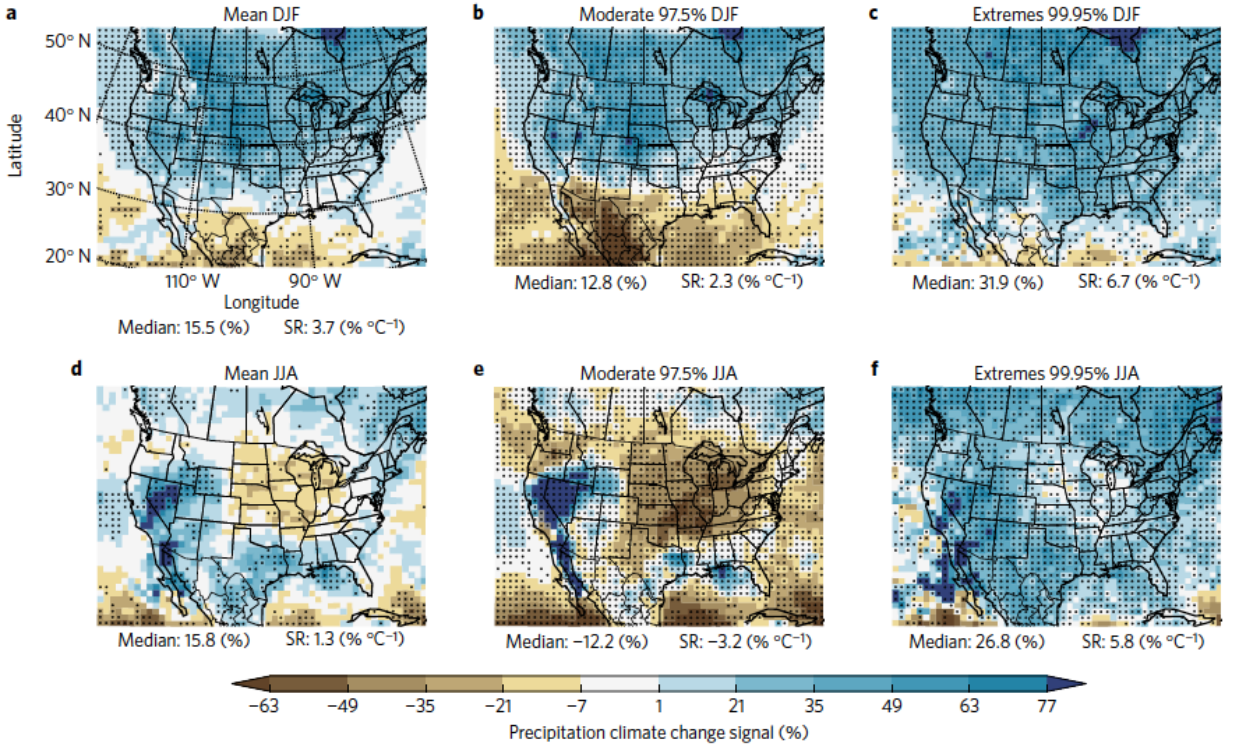

Figure 3.9. Relative changes in mean (a, d), moderate 97.5 percent (b, e), and extreme 99.95 percent (c, f) hourly precipitation for winter (DJF) (upper panels) and summer (JJA) (lower panels) comparing the PGW and control simulations. Dots highlight regions with significant changes. The relative changes correspond to the climate change signals calculated based on the difference between (2071–2100) and (1976–2005) from the multimodel CMIP5 mean for RCP8.5 used in the PGW method. (Source: Prein et al. 2017)

Changes in the probability of exceedance are shown in Figure 3.10 based on the 99.95th percentile hourly precipitation intensity in the control simulation. While the changes are larger in the north during winter, the northern Gulf Coast is projected to experience a fourfold or more increase in the 99.95th percentile hourly precipitation occurring in the future during summer. Large changes are also seen in North and South Carolina in the summer, but the changes are much smaller in the Central and Northern Great Plains and the Midwest.

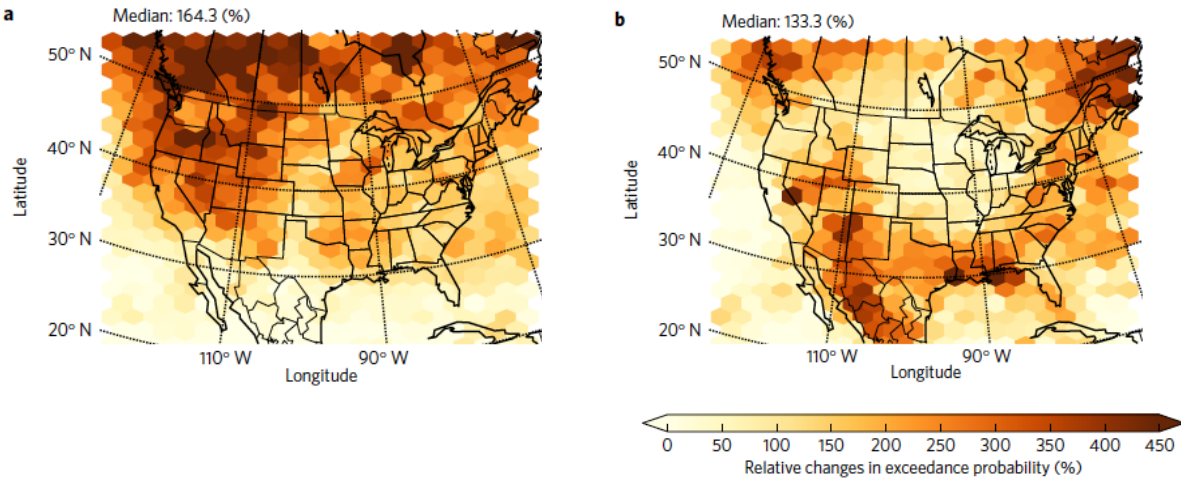

Figure 3.10. Relative changes in probability of exceedance of the control period 99.95th percentile hourly precipitation intensities for winter (DJF) (a) and summer (JJA) (b). A 300 percent relative change in probability of exceedance means a fourfold higher chance of an extreme occurring in the future (2071–2100) compared to the present (1976–2005) under the RCP8.5 scenario. (Source: Prein et al. 2017)

An important factor that contributes to model biases and model sensitivity to resolution is how convection is represented in climate models. Convection has important influences on both weather and climate, not just on the local formation of clouds and precipitation. Through the release of latent heat, convection affects regional and global atmospheric circulation, which plays a key role in the global distribution of precipitation. In recent years, advances in computing have enabled regional models to be applied at sub-kilometer grid spacing over relatively large domain size (e.g., country- or continental-scale). At such resolutions, convection is explicitly resolved rather than parameterized, which results in more realistic simulations of precipitation. Prein et al. (2015) provided a review of convection-permitting regional modeling and highlighted recent efforts demonstrating improvements that can be achieved with this approach. Applying this method to the contiguous United States, Prein et al. (2017) provided important insights into changes in hourly extreme precipitation. However, it should be noted that the study used a perturbation method in which climate change scenarios are generated by adding perturbations to the observed large-scale boundary conditions to the regional model based on the mean changes derived from the CMIP5 multimodel ensemble. While this method has the benefit of reducing computational cost, because only one set of simulations is needed to capture the response to the mean climate change signal from the multimodel ensemble, it does not provide information about the uncertainty associated with individual models of CMIP5. The latter requires a larger number of simulations, which is computationally expensive for the large U.S. domain at 4 km grid spacing. Climate models being used in CMIP6 are not expected to have significantly higher spatial resolution, but in one component of CMIP6 called HighResMIP (Haarsma et al. 2016), about 20 modeling groups will be participating in a coordinated set of experiments at roughly 1° and 0.25° resolution to systematically investigate the impacts of horizontal resolution. Although these simulations still rely on convective parameterizations, they will advance understanding of model behaviors and uncertainty that result from resolution sensitivity.

4.0 Hurricane, Sea-Level Rise, and Storm Surge in the Southeast Region

This chapter summarizes the observed and projected changes in tropical cyclones and hurricanes, sea-level rise, and storm surge in the southeaat region. Major sources of information include the NCA3 regional report for the Southeast, the NCA4 reports, and peer-reviewed literature.

4.1 Observed and Projected Changes in Hurricanes

4.1.1 Observed Changes

- The frequency of landfalling hurricanes and major hurricanes exhibits large interdecadal variability associated with the Atlantic multidecadal oscillation.
- There has been a robust increase in Atlantic tropical cyclone activity since the 1970s and a slight decline in landfalling hurricane in the last century.

Hurricanes have caused major economic losses due to the strong winds, inland flooding, tornadoes, and storm surge they produce in the Southeast Region. The return period for hurricane (>64 knot sustained wind speeds) along the coastline of the region is between 5 to 16 years, with isolated areas near the Mississippi delta, the southern tip of Florida, and the coastline of North Carolina featuring the shortest return period of 5 years. This means on average, 20 Category 3 or greater hurricanes passed within 58 mi of those areas in the last 100 years (Figure 4.1). For major hurricanes (>96 knot sustained wind speed; hurricanes of Saffir-Simpson Category 3 or above), the return period along the southeastern Atlantic coastline varies between 14 and 290 years, with the shortest return periods being related to North and South Carolina, Louisiana, Alabama, and the Florida tip.

Detecting long-term changes in tropical cyclone (TC) activity is difficult because of issues with the historical records related to changing technology and methodology (Landsea et al. 2004). Despite the data issues, an increasing trend in Atlantic TC frequency is robustly observed from around 1970 since the availability of satellite data (Figure 4.2), but the period is too short to make inferences about longer-term trends (Kunkel et al. 2013b). Assessing the longer-term trend is particularly challenging because TC activity exhibits strong multidecadal variability and responds to both natural factors (e.g., meridional overturning circulation, volcanic eruptions, and Saharan dust outbreaks) and external forcings (e.g., GHGs and anthropogenic aerosols). While substantial efforts have been devoted to understanding how TC frequency and intensity respond to internal and external influences, Kossin et al. (2014) found some evidences of poleward migrations of the locations where TCs reach their peak intensity in both northern and southern hemispheres during the past 30 years. The changes are consistent with the expansion of the tropics, and have the potential to substantially change patterns of TC hazard, exposure, and mortality risk (USGCRP 2017).

For landfalling hurricanes and major hurricanes, their frequencies exhibit large interdecadal variability associated with the AMO and other factors, but they showed a slight decline in the last century (Kunkel et al. 2013a). Trends and variability in U.S. landfalling hurricanes are not simply related to the trends and variability in Atlantic hurricanes. While the latter are strongly influenced by sea surface temperatures in the North Atlantic, the fraction of Atlantic hurricanes making landfall in the United States depends on steering winds, wind shear, and other factors.

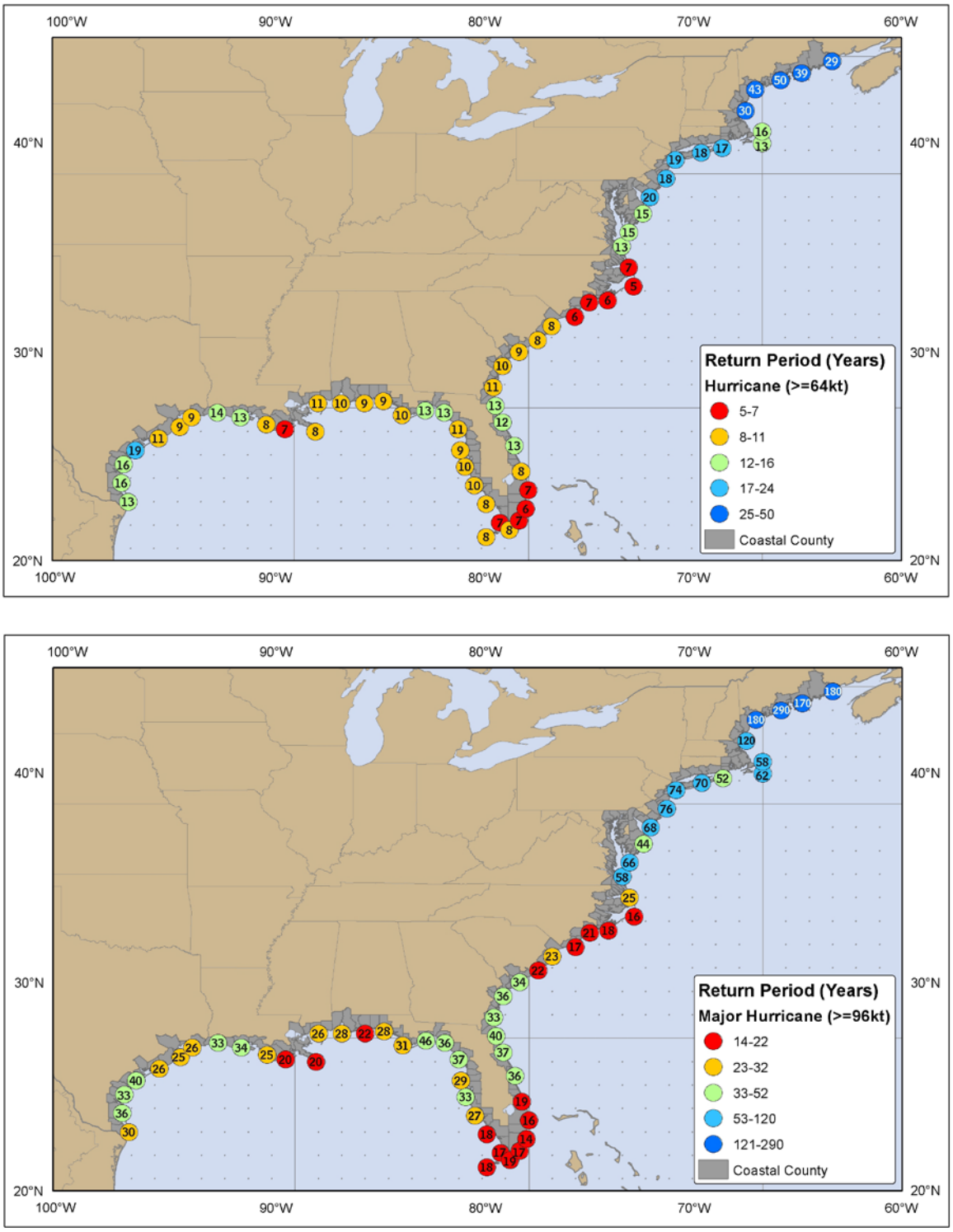

Figure 4.1. Estimated return period in years for hurricanes (top) and major hurricanes (bottom) passing within 50 nautical miles of various locations on the U.S. Coast. (Source: NOAA http://www.nhc.noaa.gov/climo/)

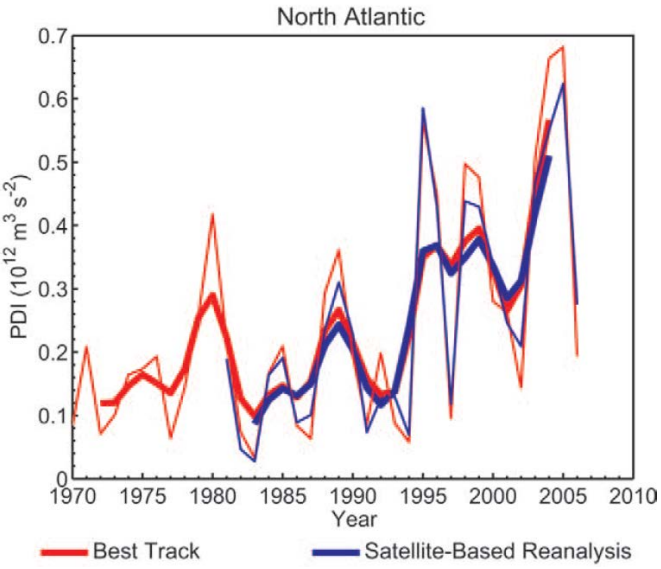

Figure 4.2. Comparisons of TC Power Dissipation Index (PDI; defined by Emanuel [2005]) in the North Atlantic. Red curves show the annual values derived from the best-track data; blue curves show annual values derived from the more homogeneous satellite-based intensity reconstructions. Thin lines show the raw values, thick lines show the smoothed time series, and least squares linear trend lines calculated from the raw series are shown. (Source: Kunkel et al. 2013b)

4.1.2 Projected Changes

- Projections of the tropical cyclone (TC) counts in the North Atlantic are uncertain; CMIP5 models show both increases and decreases in the future.
- Analysis of the Power Dissipation Index (PDI) in CMIP5 shows an increase in TC intensity in the North Atlantic in all scenarios, and the PDI increases significantly more in RCP8.5 compared to RCP2.6 and RCP4.5 toward the end of the 21st century.
- High-resolution simulations show increasing frequency of Category 4 and 5 TCs by about 0 to 3 storms per decade in the Gulf of Mexico and North Atlantic comparing the late-21st century with the present day.

As discussed in Section 1.1, GCMs do not have sufficient grid resolution to resolve TCs so they tend to produce weaker storms that rarely reach Category 4 and 5 hurricanes. Hence, Kunkel et al. (2013a) did not report on model projections of hurricanes, because the statistical downscaled data used in NCA3 only include information about temperature and precipitation over the conterminous United States, and the NARCCAP RCM domain does not cover the whole Gulf of Mexico and Atlantic Ocean for downscaling of TCs from the global models. However, key findings related to future changes in TCs and hurricanes relevant to the Southeast Region can be summarized from peer-reviewed literature. As discussed by Emanuel (2013), three approaches have been used to project TC changes in the future climate. In GCM studies, TC statistics can be analyzed by tracking the simulated TCs despite the general limitations in simulating hurricanes and the lack of a universally agreed on TC tracking algorithm appropriate for climate models with inherent biases. However, analysis can also be performed using indices (e.g., Genesis Index) defined by the TC large-scale thermodynamical environment simulated by the models that are

proxies for the genesis locations and frequency. Dynamical downscaling has been used to better resolve TCs, but the results can be influenced by the inherent limitations of regional models related to the imposed boundary conditions. Studies using each of the three approaches are discussed to highlight their findings and consistency and/or differences.

Camargo (2013) applied the Camargo and Zebiak (2002) TC tracking algorithm to the global climate simulations from CMIP5 to investigate the projected changes in TCs globally and in the North Atlantic and North Pacific. The tracking algorithm used model- and basin-dependent thresholds of vorticity, wind speed, and vertically integrated local virtual temperature anomaly to account for differences in model resolution. Many models have too few or no TCs in the North Atlantic (Figure 4.3, top), and they tend to produce too few TCs during the active season but too many TCs during the inactive season (Figure 4.3, bottom). Therefore, only 5 out of 14 CMIP5 models with 6-hourly data available for TC detection and tracking were used in their analysis of North Atlantic TC changes. Figure 4.4 shows the number of TCs (NTC) in the North Atlantic simulated for the historical (1951–2000) and future (2051–2100) periods for the RCP4.5 and RCP8.5 emissions scenarios. As discussed earlier, the RCP4.5 and RCP8.5 emissions scenarios are comparable to the B1 and A2 SRES scenarios, respectively (Figure 1.5). NTC varies significantly among the five models, and there is no robust signal of TC changes across the models. The latter is consistent with the results of Villarini and Vecchi (2012), who analyzed statistically downscaled TC changes; however, dynamical downscaling of CMIP3 and CMIP5 models suggested a decrease in NTC in the Atlantic (Knutson et al. 2013).

Villarini and Vecchi (2013) analyzed PDI (Emanuel 2005; 2007), which is a metric that integrates storm duration, frequency, and intensity. Using a statistical model of PDI (Villarini and Vecchi 2012) that relates the location parameter of the gamma distribution to sea surface temperatures in the Atlantic and the tropics simulated by CMIP5 models, PDI values derived from GCM-simulated sea surface temperatures in the North Atlantic were analyzed for the 1986–2005 reference period and future periods as PDI anomalies. Figure 4.5 shows an increase in PDI in North Atlantic in all scenarios, with the PDI increasing significantly more in RCP8.5 compared to RCP2.6 and RCP4.5 toward the end of the 21st century. Because the NTC is not projected to change (Villarini and Vecchi 2012), the increase in PDI suggests an increase in intensity, duration, or a combination thereof for TCs in the North Atlantic in response to greenhouse warming. Changes in storm tracks may have important implications for U.S. landfall. Camargo (2013) found a westward expansion of the subtropical high in the CMIP5 models, which may increase the likelihood of more landfalls in the Southeast Region due to the impacts of the subtropical high on the steering winds.

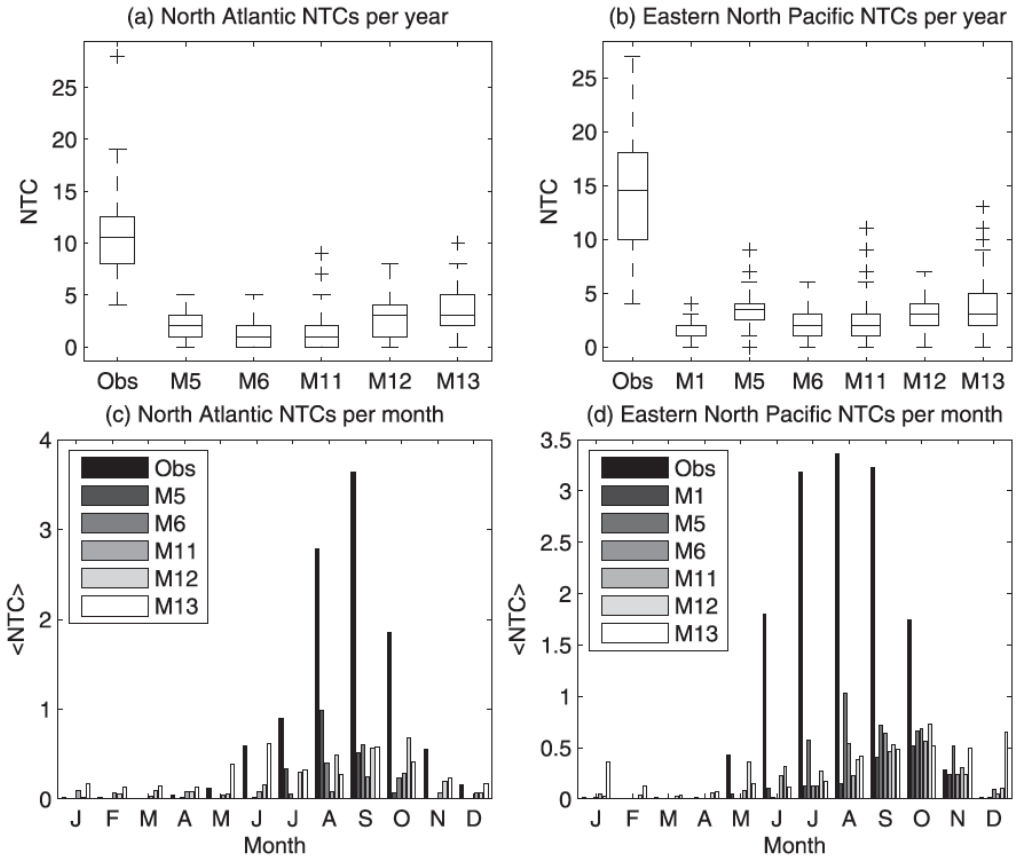

Figure 4.3. (Top) Distribution of the number of tropical cyclones (NTC) in North Atlantic and eastern North Pacific in the period 1950–2005 for five CMIP5 models (M5: Geophysical Fluid Dynamics Laboratory [GFDL] CM3; M6: GFDL-ESM2M; M11: MIROC5, M12: MPI-ESM-LR, M13: MRI-CGCM3) and observations per year. (Bottom) Mean NTC per month in the North Atlantic and Eastern North Pacific from observations (black) and five models (shaded). (Source: Camargo et al. 2013)

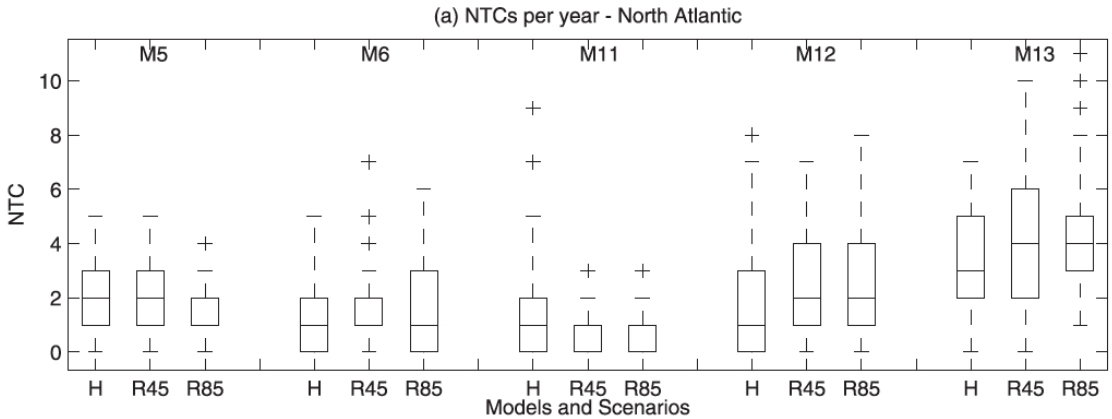

Figure 4.4. NTC per year simulated by five CMIP5 models (see caption of Figure 4.2 for details) in the North Atlantic for the historical period (H; 1951–2000) and future (RCP4.5 and RCP8.5) scenarios (2051–2100). (Source: Camargo 2013)

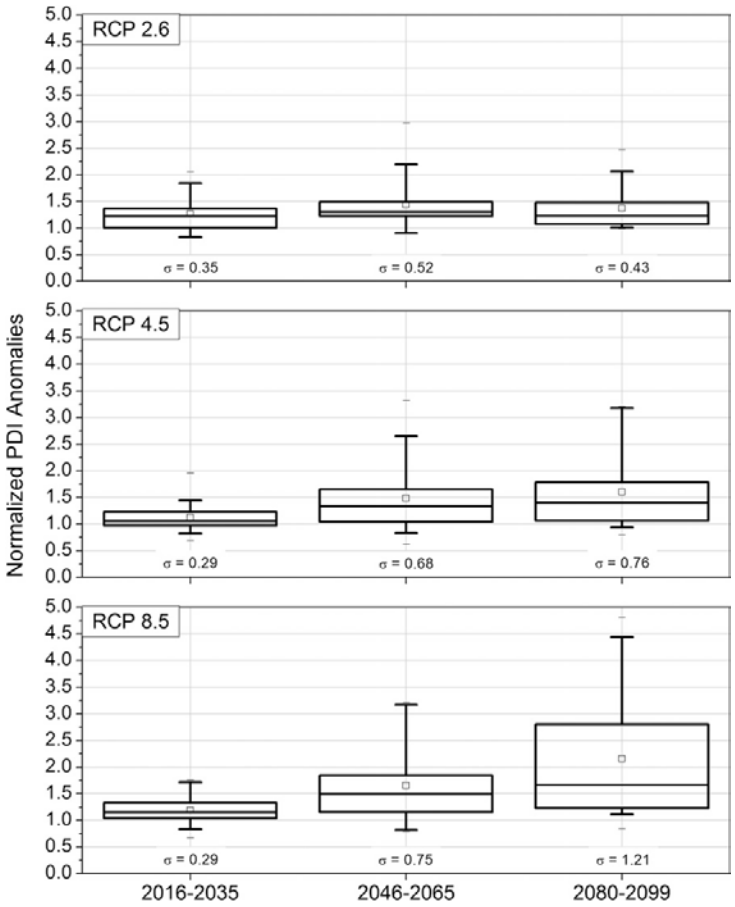

Figure 4.5. Box plots of the averaged projected PDI for three periods normalized by their values over 1986–2005. The projections are based on 17 CMIP5 global climate models. Results are shown for three emissions scenarios: RCP2.6 (top), RCP4.5 (middle), and RCP8.5 (bottom). The whiskers represent the 10th and 90th percentiles, the limits of the boxes correspond to the 25th and 75th percentiles, and the horizontal line and square are the median and mean values, respectively. The horizontal dashes represent the minimum and maximum values. (Source: Villarini and Vecchi 2013)

Knutson et al. (2015) projected changes in intense TC activity in a warmer climate using a two-step downscaling procedure including the use of a global high-resolution model (GFDL) at 50 km grid resolution to simulate TC genesis, followed by the use of a very-high-resolution hurricane model (GFDN) with a grid spacing of about 6 km in a regional domain centered at the genesis locations. Figure 4.6 and Figure 4.7 shows the simulated tracks and occurrence of Category 4 and 5 hurricanes in the present day and the late 21st century under the RCP4.5 scenario. From Figure 4.6, there is more of a tendency for the Category 4 and 5 hurricanes to be shifted toward the Gulf of Mexico and Florida in the future from downscaling of the CMIP5 than the CMIP3 runs. However, the authors cautioned that the hurricane model was run for a maximum of 5 days so the experiments have limited utility for examining U.S. landfalling storm behavior. The hurricane model projected an increase in Category 4 and 5 hurricanes by 0 to 3 storms per decade in the Gulf of Mexico and western Atlantic that has implications for hurricane activity in the Southeast Region (Figure 4.7).

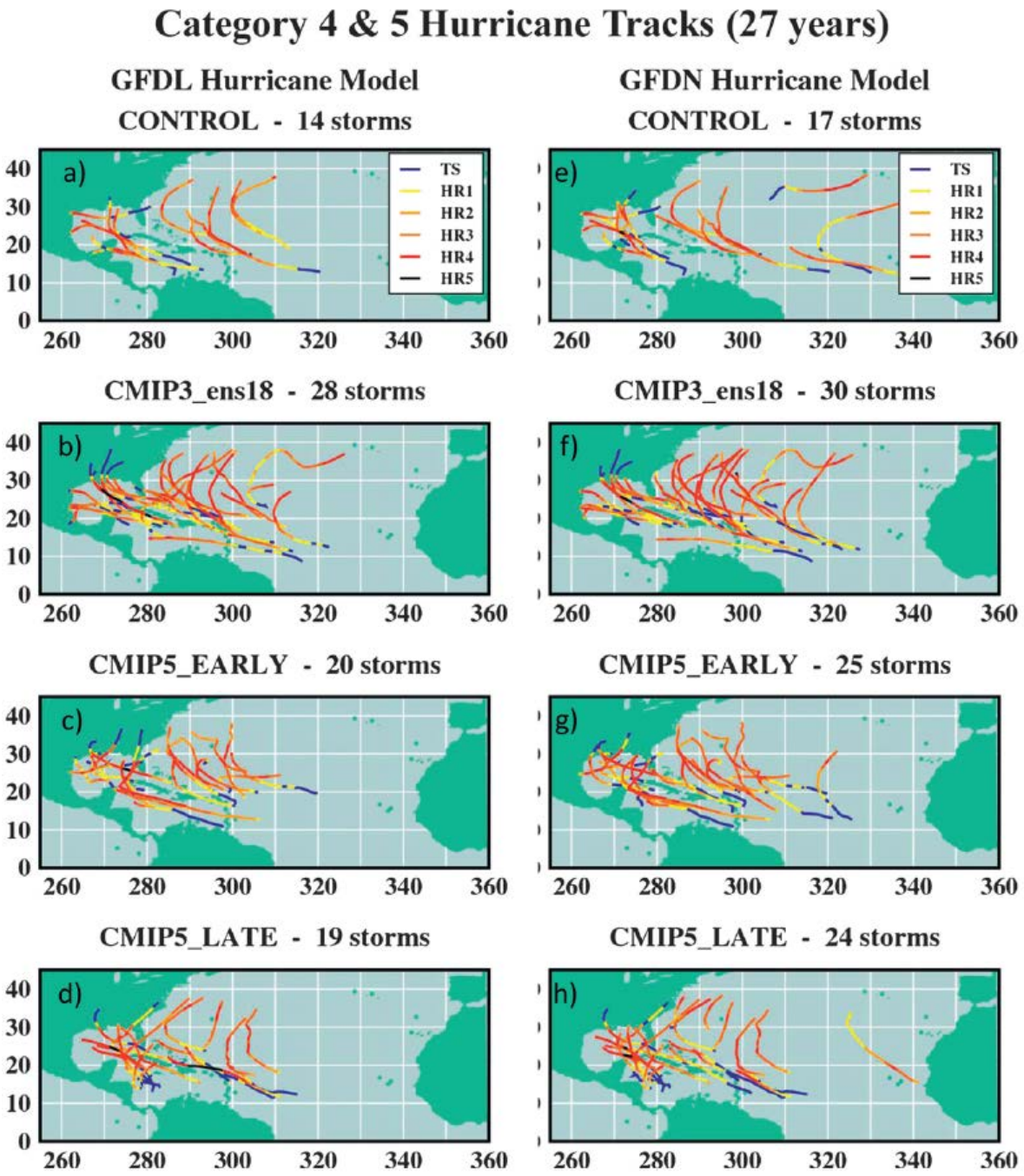

Figure 4.6. Tracks and intensities of all storms reaching Category 4 or 5 intensity ($\geq$ 59 ms^{-1}) in the GFDL hurricane model downscaling experiments (27 seasons), using model versions (left) GFDL or (right) GFDN for the nested model. Results shown for the (a),(e) control climate; (b),(f) CMIP3–A1B 18-model late-21st-century ensemble climate change; (c),(g) CMIP5–RCP4.5 early-21st-century ensemble; and (d),(h) CMIP5–RCP4.5 late-21st-century ensemble. (Source: Knutson et al. 2013)

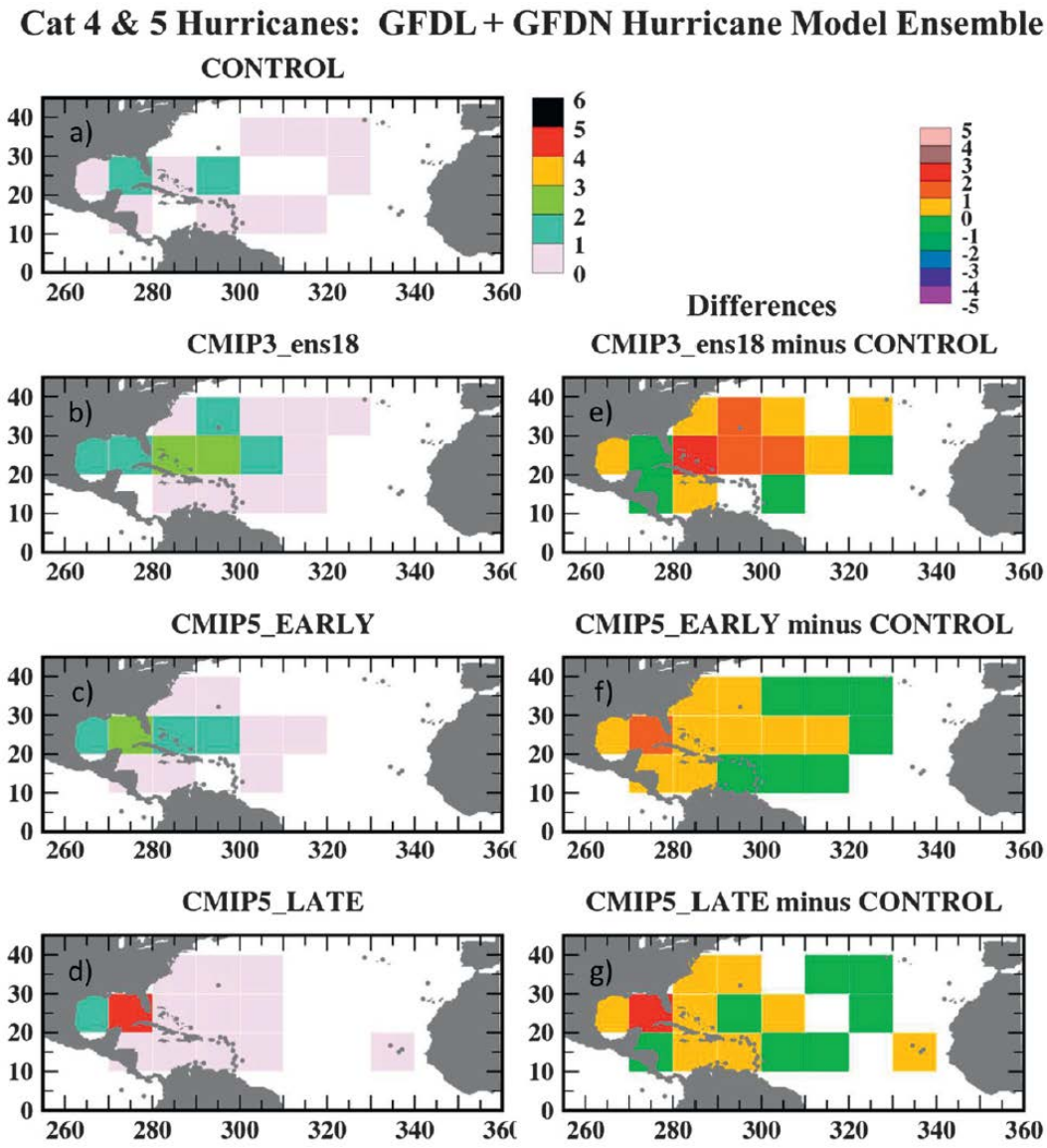

Figure 4.7. Geographical distribution of the (left) projected rate of occurrence or (right) change in rate of occurrence of Category 4 and 5 storms (surface winds of at least 59 m/s or 130 mph) for (a) control; (b),(e) CMIP3–A1B late-21st-century ensemble; (c),(f) CMIP5–RCP4.5 early-21st-century ensemble; and (d),(g) CMIP5–RCP4.5 late-21st-century ensemble. The combined results obtained using the GFDL and GFDN versions of the GFDL hurricane model (scaled as storm occurrences per decade in 10^{o}x10^{o} grid boxes) are shown. (Source: Knutson et al. 2013)

Besides the dynamical downscaling method discussed above, Emanuel (2013) pioneered a new downscaling approach that combines a stochastic model that seeds TCs randomly in space and time with a beta-and-advection model that simulates TC tracks, as driven by GCM-simulated winds, and a coupled atmosphere-ocean model that simulates TC intensity. Using this method, Emanuel (2013) downscaled TCs simulated by 6 CMIP5 models in the RCP8.5 scenario. An increase in both TC frequency (Figure 4.8, top) and intensity was found in most regions during the 21st century. The increase in TC frequency contrasts with previous studies using CMIP3 models that showed a small decrease in TC frequency and previous studies using CMIP5 models that showed no consistent changes.

However, the increase in TC frequency is consistent with increases in Genesis Potential Intensity that was developed independently, based on observed seasonal, spatial, and climate variability of tropical cyclones. Furthermore, the increase in TC intensity is consistent with changes derived from PDI calculated directly from the GCMs (Figure 4.8, bottom). Because the results are based on only 6 GCMs that include all the data needed to apply the downscaling method, the projections reported in the study remain uncertain, although the method produced good predictions of spatial, seasonal, and short-term climate variability of TCs over the past few decades.

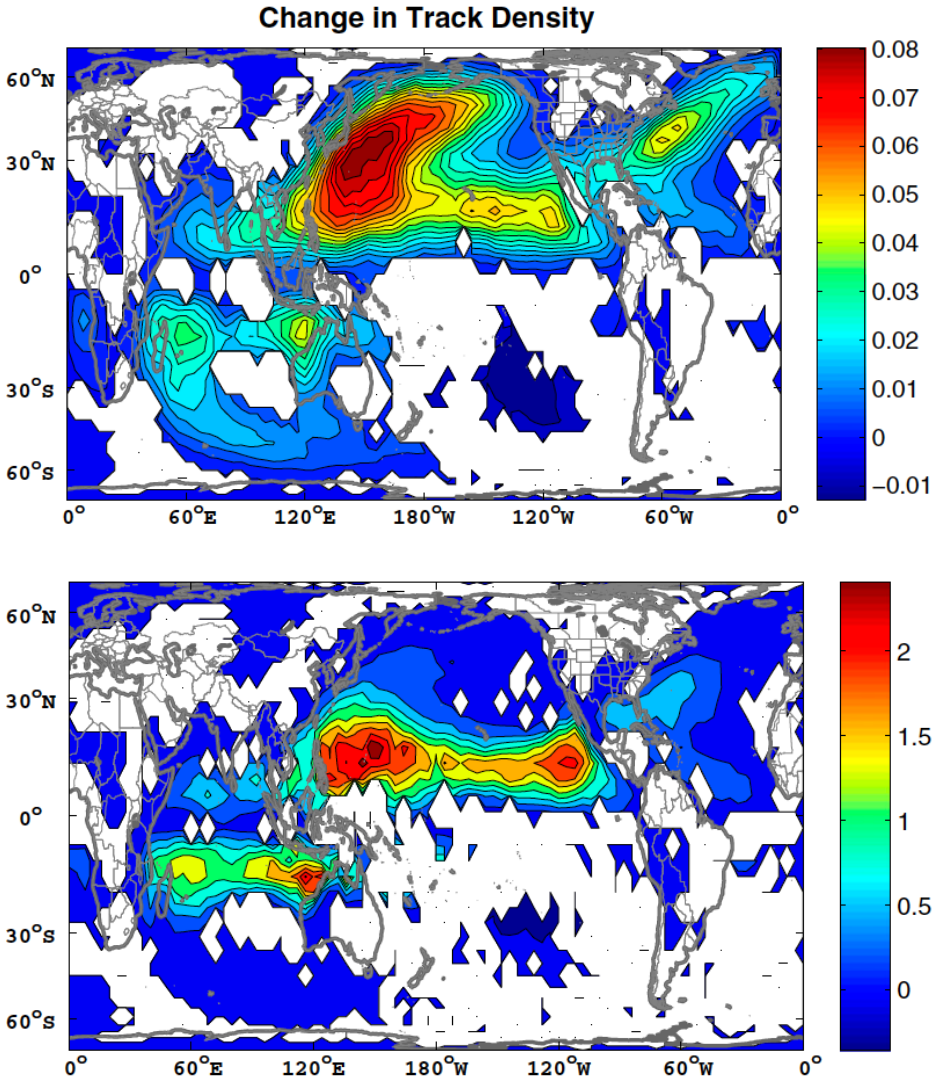

Figure 4.8. (Top) Change in track density, measured in number of events per 4° x 4° grid box per year, averaged over six CMIP5 models used in the study. The change is the average over the period 2006–2100 minus the average over 1950–2005. The white regions are where fewer than five of the six models agree on the sign of the change. (Bottom) Change in PDI averaged over the six models, per 4° latitude grid box. This is defined as the difference between power dissipation averaged over the period 2006–2100 and that averaged over 1950–2005. Units are 10^8 m^3s^{-2} per 4° x 4° square, and white areas show regions in which fewer than five of the six models agree on the sign of the change. (Source: Emanuel 2013)

With the active Atlantic hurricane season of 2017, several studies investigated the role of climate change in hurricanes that made landfall in the United States that year. Hurricane Harvey was a particularly notable hurricane because of the extreme precipitation it produced when it made landfall on the coast of Texas on August 26, 2017, causing significant damages with the unprecedented amount of rain that fell on the greater Houston area (Figure 4.9). Applying covariate-based extreme value statistical analysis to historical data, Risser and Wehner (2017) found that human-induced climate change likely increased the chances of the observed precipitation accumulations during Hurricane Harvey by a factor of at least 3.5 in the most affected areas of Houston. They further noted that the increase in precipitation accumulations is larger than what would be expected from the Clausius-Clapeyron scaling of 6–7 percent for each degree of warming.

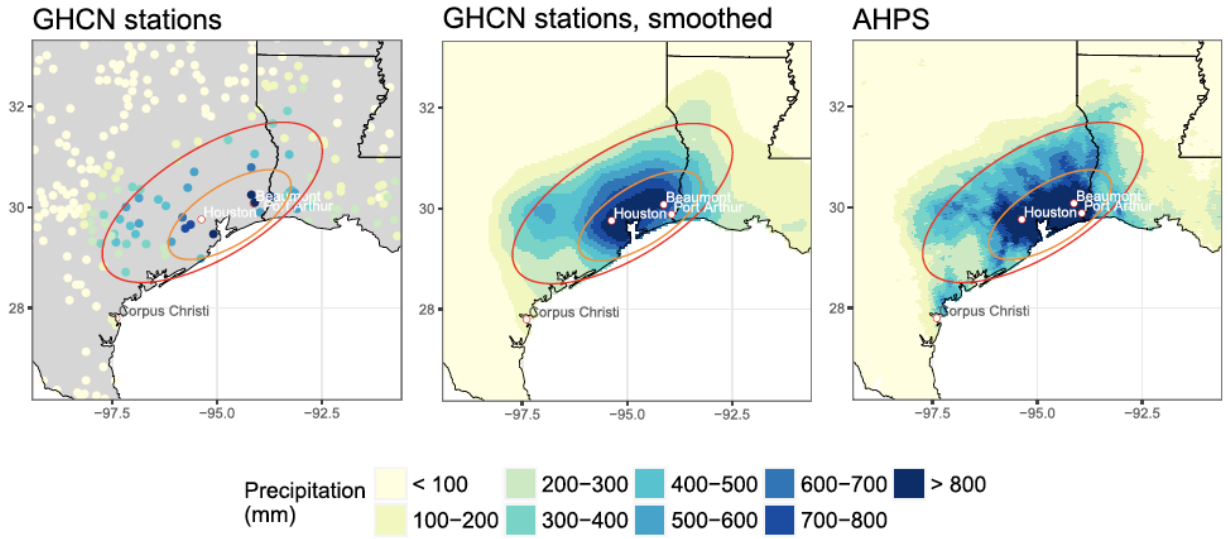

Figure 4.9. Precipitation totals (mm) for the Houston, Texas, region from August 25–31, 2017, from (left) Global Historical Climatology Network stations with at least five non-missing daily measurements during the time window; (middle) smoothed estimates; (right) NOAA's Advanced Hydrologic Prediction Service estimates, based on radar and rain gauge data. The orange and red ellipses correspond to the small and large regions, respectively. (Source: Risser and Wehner 2017)

Focusing also on extreme rainfall from Hurricane Harvey, van Oldenborgh et al. (2017) analyzed observations as well as an ensemble of three global and regional high-resolution simulations at 25 km resolution. They found that since 1880, the intensity of extreme precipitation in Houston and the surrounding area has increased between 12 and 22 percent, roughly two times the increase in atmospheric moisture holding capacity expected for a 1°C warming (the Clausius-Clapeyron scaling). Among the three climate simulations comparing pre-industrial to present day, one shows that extreme rainfall in the region has increased following 2x the Clausius-Clapeyron scaling and another shows a 1× the Clausius-Clapeyron scaling, with the third member not realistically simulating extreme rainfall in the Gulf Coast. Taken together, this study concluded that global warming made the precipitation of Hurricane Harvey about 15 percent more intense, or made that event three times more likely.

Using a regional model that realistically simulates Hurricane Harvey, Wang et al. (2018) performed another study to attribute Harvey's extreme rainfall to climate effects. With a 60-member ensemble simulations of Hurricane Harvey, they suggested that post-1980 climate warming could have contributed to the extreme precipitation of the event.

Lastly, the present and future probability of Hurricane Harvey's rainfall was assessed by Emanuel (2017) using a large NTC (3700) over the period 1980–2016 generated from three climate reanalyses and six climate models using statistical models of cyclone tracks and precipitation. The TCs were selected from a larger set on the basis that they pass within 300 km of Houston, Texas, with peak wind speeds of at least 40 knots (22 m/s) while within 300 km of Houston. The study estimated that the probability of Houston rainfall larger than 500 mm is about once in 2000 years in the period 1981–2000, and it will increase to once in about 100 years over the period 2081–2100 under the RCP8.5 scenario (Figure 4.10).

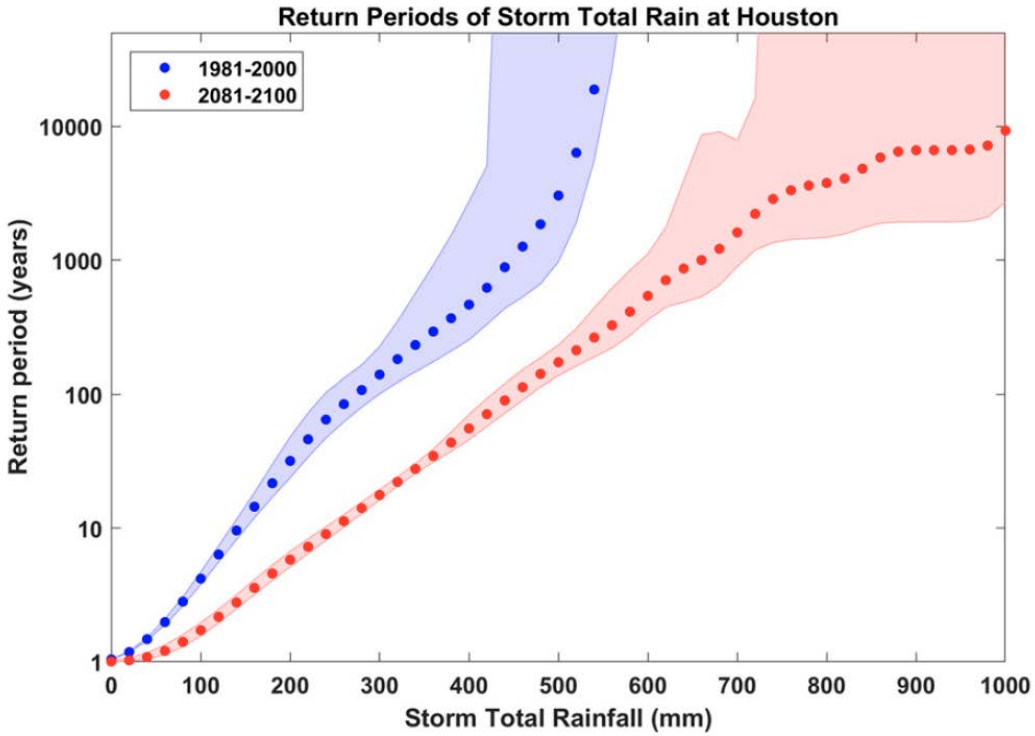

Figure 4.10. Return periods of hurricane total rainfall (mm) at the single point of Houston, Texas, based on 3700 simulated events each from six global climate models over the period 1981–2000 from historical simulations (blue), and 2081–2100 from RCP 8.5 simulations (red). The dots show the mean of the six climate simulations and the shading shows one standard deviation in storm frequency, remapped into return periods. (Source: Emanuel 2017)

Besides Hurricane Harvey that produced unprecedented rainfall after making landfall, the 2017 Atlantic hurricane season also was unusual in that out of 17 named tropical storms that formed in the Atlantic, 10 developed into hurricanes and 6 achieved major hurricane status. Four hurricanes—Harvey, Irma, Jose, and Maria—reached Category 4 or 5 strengths, and all underwent rapid intensification (RI) during their lifecycle. RI is defined for hurricane increases in intensity by 25 knots or higher in 24 hours. Balaguru et al. (2018) explored changes in RI magnitude over the 30-year satellite period of 1986-2015. They found that in the central and eastern tropical Atlantic (CETA)that includes the main development region, the 95th percentile of 25-hr intensity changes increased at 3.8 knots per decade, but the trend in the western tropical Atlantic is insignificant (Figure 4.11). They identified that warming of the upper ocean coinciding with the positive phase of theAMO, and associated changes in the large-scale environment, favored RI magnitude increases in the CETA. Although the increase in RI has been attributed mainly to the environmental changes induced by the AMO phase, this study did not rule out the role of anthropogenic climate change.

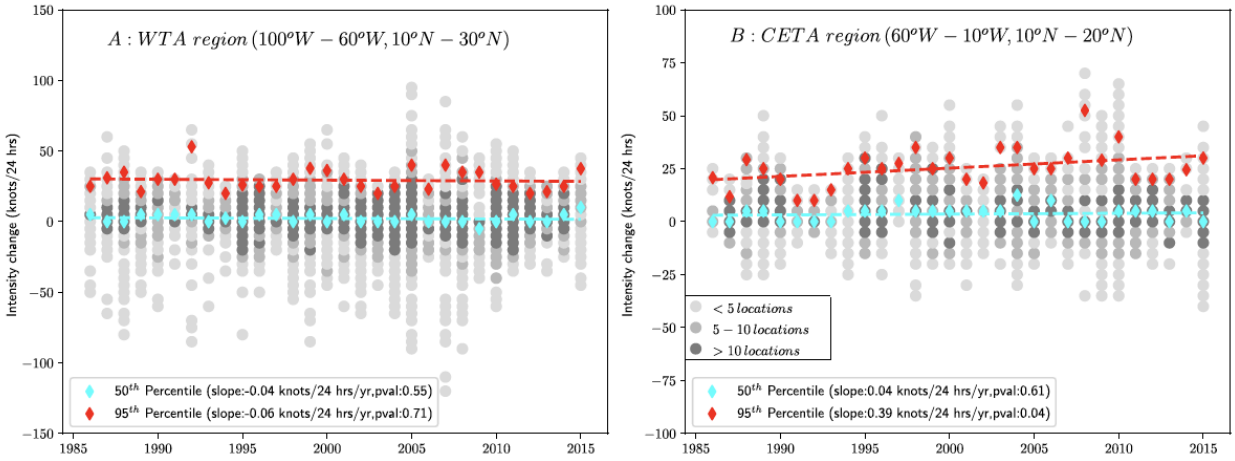

Figure 4.11. Observed trends in quantiles of 24-hr intensity change over the 30-year period 1986–2015 for (a) western tropical Atlantic and (b) central and eastern tropical Atlantic (CETA). Gray circles denote the 24-hr intensity change values at 6-hourly hurricane track locations for each season, with darker shades of gray indicating more locations with that intensity change value. The medium quantile value and the value of the 95th percentile for each season are denoted by cyan and red diamonds, respectively. Trends in time series of medium quantile and the 95th percentile of 24-hr intensity changes are also shown. The slopes of the trend lines and the p-values for statistical significance of those trend lines are provided. (Source: Balaguru et al. 2018)

4.2 Observed and Projected Sea-Level Rise, Tidal Flood, and Storm Surge

4.2.1 Observed Changes

- The rate of global sea-level rise has increased from 1.7 ± 0.3 mm/yr averaged over the 20th century to about 3.2 ± 0.4 mm/yr between 1993 and 2007.
- The Southeast Region's coast has experienced increases in sea surface height between 0 and 1.5 in./decade between 1993 and 2014.
- Associated with the sea-level rise is an increase in the frequency of nuisance tidal flooding along the southern United States coast.

The global mean sea level (GMSL) is the area-weighted mean of the global sea surface height (SSH) anomalies, which can be measured by satellite altimetry. The GMSL is also called the eustatic sea level. SSH also is called geocentric sea level and is defined with respect to a reference ellipsoid. Relative sea level (RSL) is the difference in elevation between SSH and the height of the solid-Earth surface. RSL can be measured by tide gauges. Although the difference between the GMSL and global mean RSL is small, the local difference between RSL and SSH can be quite significant (Kopp et al. 2014).

The GMSL has increased gradually in the last century, driven mainly by (1) thermal expansion of the ocean as it warms, and (2) mass addition from melting of glaciers and the Greenland and Antarctic ice sheets. Satellite and in situ measurements show that about one-third of the GMSL rise since 2004 has been associated with thermal expansion, and about two-thirds has been primarily from the melting of land-based ice (USGCRP 2017) (Figure 4.12). The rate of GMSL rise has increased from 1.7 ± 0.3 mm/yr averaged over the 20th century to about 3.2 ± 0.4 mm/yr between 1993 and 2007 (Merrifield et al. 2009).

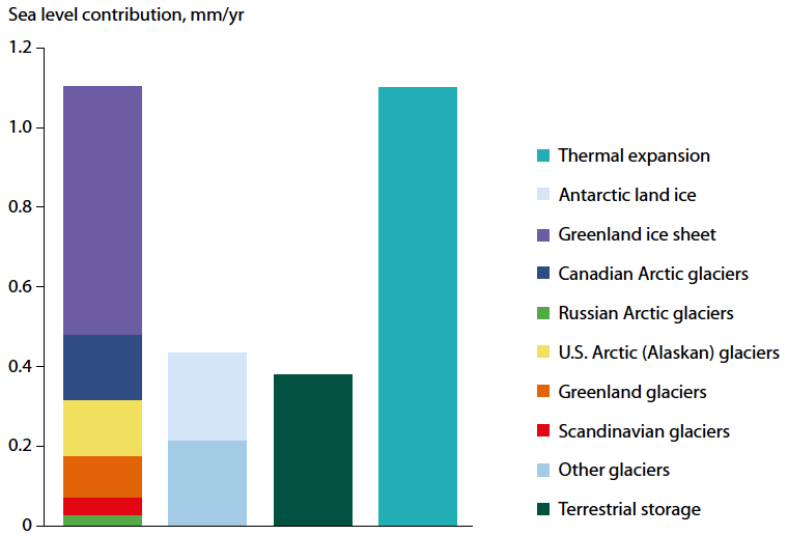

Figure 4.12. During the period 2004–2010, melting Arctic land ice accounted for more than one-third of global sea-level rise, while thermal expansion caused by warming water contributed another one-third, and contributions from Antarctica, other glaciers, and changes in terrestrial storage contributed less than one-third. (Source: AMAP 2017)

Sea-level changes are not uniform globally; their variations are driven by several climatic and non-climatic factors including:

- Regional differences in atmosphere-ocean dynamics that influence the SSH through wind driven circulation and distribution of ocean heat and salinity
- Regional fingerprints of land ice melting
- Land response to ice sheet loss during the Last Glacial Maximum
- Other factors such as vertical land movement and compaction due to sediment and groundwater extraction.

Consistent with the GMSL increase, the sea level across the coastline of the Southeast Region has risen slowly during the last century. After accounting for background rates due to long-term factors such as glacial isostatic adjustment (i.e., land movement due to ice-age glaciers), the spatial pattern of SSH changes between 1993 and 2014 shows a slower-than-global increase in the U.S. Southeast since the 1970s (Figure 4.13). The slowdown along the Southeast Region's coast has been attributed to land subsidence induced by glacial isostatic adjustment (GIA) and weakening of the Gulf Stream that may be related to the weakening of the Atlantic meridional overturning circulation (AMOC) (Yin and Goddard 2013; Rahmstorf et al. 2015).

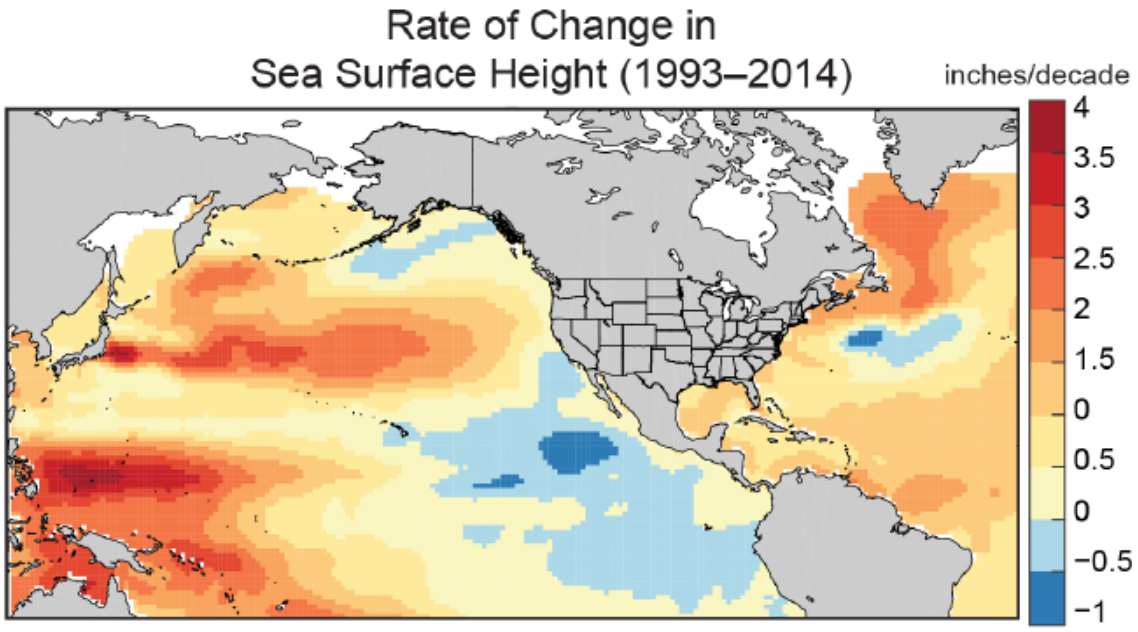

Figure 4.13. Rates of change from 1993 to 2014 in SSH from satellite altimetry data (from Kopp et al. [2015] using data updated from Church and White [2011]). (Source: USGCRP 2017, adapted from Kopp et al. 2015])

A nuisance flood occurs when the water level is above the local NOAA National Weather Service (NWS) threshold for minor impacts that trigger coastal flood advisories. A rise in the RSL can increase "nuisance flooding" or "sunny-day flooding" but the impacts could also be due to changes in the built environment, leading to changes in the threshold for nuisance flooding even if the RSL has been stable. Along the Southeast Region's coast, the nuisance flooding elevation thresholds relative to the mean higher high water are between 15 and 90 cm, depending on the locations. Figure 4.14 shows that nuisance tidal floods occurred more than 30 days/year in some locations in South Carolina and Florida, and nuisance tidal floods have been on an increasing trend since 1960.

Besides tidal floods, the Southeast Region also experiences storm surge from strong winds induced by hurricanes. Storm-surge activity is archived in SURGEDAT, the world's storm-surge information center database. The data identify the magnitude and location of peak storm surge from more than 550 TC-generated surge events around the world since 1880. Figure 4.15 depicts the 195 peak storm-surge events along the U.S. Gulf Coast since 1880. In general, surge magnitude and frequency are larger on the northern and western coast and in the Florida Keys.

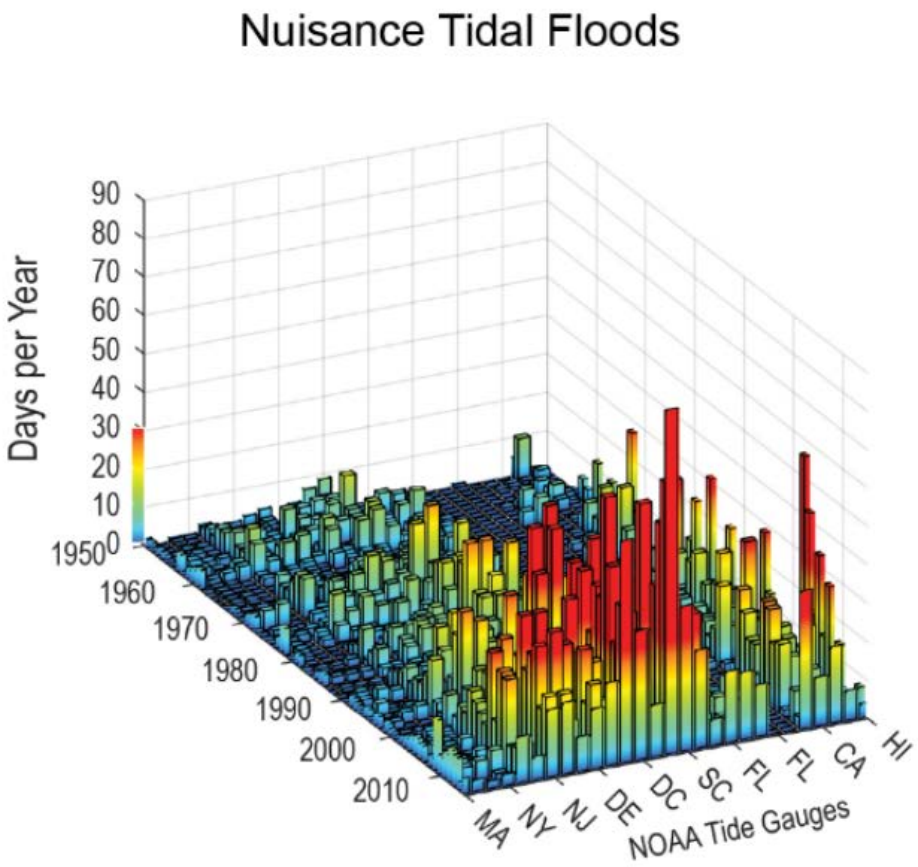

Figure 4.14. Tidal floods (days per year) exceeding NOAA thresholds for minor impacts at NOAA tide gauges through 2015. Three tide gauges in South Carolina and four tide gauges in Florida are included in the analysis. (Source: USGCRP 2017)

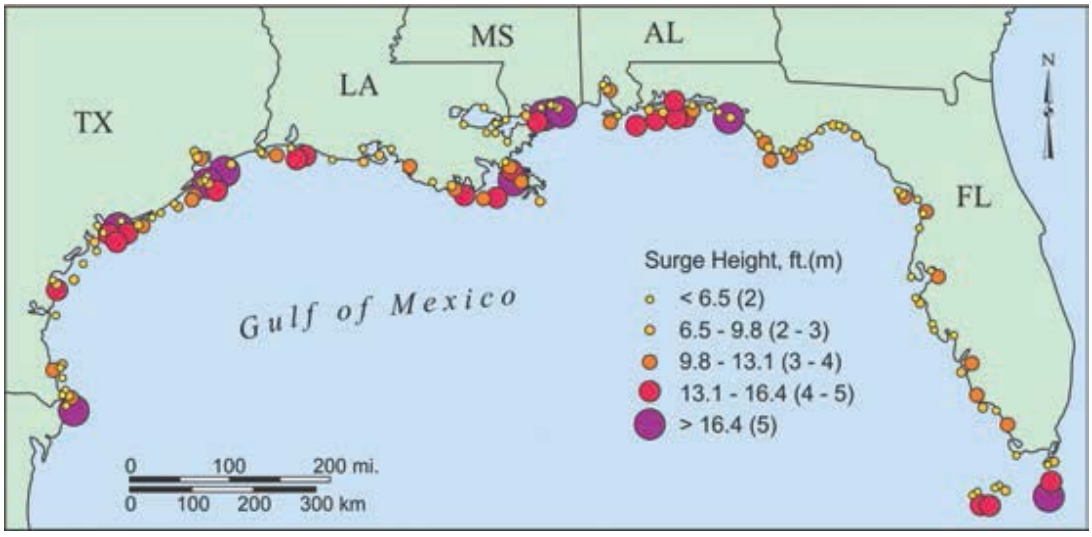

Figure 4.15. A map of the 195 peak storm surges along the U.S. Gulf Coast since 1880. Each circle represents a unique storm-surge event; the darker circles depict higher magnitude storm-surge levels. (Source: Kunkel et al. 2013a)

4.2.2 Projected Changes

- Relative sea level along the Southeast coast is projected to rise by 3–6 feet for 2100 under the intermediate 1 m global sea level rise scenario.
- By 2100, the rise in water level height with a 5-year recurrence interval is between 2 and 3.5 feet along the Southeast coast.
- Nuisance tidal flood in Charleston, South Carolina, is projected to increase from less than 50 days/year at the present to about 350 days/year by 2100.
- Storm surge is projected to increase in the future, with sea-level rise playing a key role while increase in TC intensity contributes 10–15 percent to the storm surge increase.

The Sea-Level Rise and Coastal Flood Hazard Scenarios and Tools Interagency Task Force has revised the GMSL rise scenarios for the United States. The six scenarios provided by the task force are summarized by USGCRP (2017). The interagency approach is similar to the regional sea-level rise scenarios described by Hall et al. (2016) for all coastal U.S. Department of Defense installations worldwide. The scenarios combine probabilistic estimates of contributions to GMSL and RSL rise pooled from Kopp et al. (2014), in which probability distributions of sea-level rise are informed by a combination of expert community assessment, expert elicitation, and process modeling. The latter includes (1) the use of CMIP5 projections of global sea level due to ocean thermal expansion and local sea level due to regional steric and dynamic effects (e.g., wind driven circulation); (2) Antarctic and Greenland ice sheet mass balance changes driven by surface mass balance and ice sheet dynamics; (3) sea-level fingerprints of static-equilibrium sea-level rise; (4) ice mass change estimated from process model of glaciers and ice caps; (5) GMSL change due to changes in water storage on land as variations related to population, reservoir storage, and groundwater depletion; and (6) glacial isostatic adjustment, tectonics, and other non-climatic local effects approximated as linear trends based on the changes in the 20th century. The low scenario of 30 cm (1 ft) GMSL rise by 2100 is consistent with a continuation of the recent, approximately 13 mm/year (1.2 in./decade) rate of rise through 2100, while the five other scenarios span a range of GMSL rise between 50 and 250 cm (1.6 and 8.2 ft) in 2100. The highest scenario of 250 cm (8.2 ft) is consistent with several literature estimates of the maximum physically plausible level of 21st century sea-level rise. Emerging science regarding ice sheet stability suggests that, for high emissions, a GMSL rise exceeding 240 cm (8 ft) by 2100 cannot be ruled out. Table 4.1 summarizes the Interagency GMSL rise scenarios relative to 2000, and the explanations of the scenarios are listed in Table 4.2. Table 4.3 provides the probability of exceeding the Interagency GMSL scenario in 2100 in three RCP scenarios.

Table 4.1. The Interagency GMSL rise scenarios in meters (feet) relative to 2000. All values are 19-year averages of GMSL centered at the identified year. To convert from a 1991–2009 tidal datum to the 1983–2001 tidal datum, add 2.4 cm (0.9 in.) (USGCRP 2017).

Scenario	**2020**	**2030**	**2050**	**2100**
Low	0.06 (0.2)	0.09 (0.3)	0.16 (0.5)	0.30 (1.0)
Intermediate-Low	0.08 (0.3)	0.13 (0.4)	0.24 (0.8)	0.50 (1.6)
Intermediate	0.10 (0.3)	0.16 (0.5)	0.34 (1.1)	1.0 (3.3)
Intermediate-High	0.10 (0.3)	0.19 (0.6)	0.44 (1.4)	1.5 (4.9)
High	0.11 (0.4)	0.21 (0.7)	0.54 (1.8)	2.0 (6.6)
Extreme	0.11 (0.4)	0.24 (0.8)	0.63 (2.1)	2.5 (8.2)

Table 4.2. Interpretations of the interagency GMSL rise scenarios (USGCRP 2017)

Scenario	**Interpretation**
Low	Continuing current rate of GMSL rise, as calculated since 1993 Low end of *very likely* range under RCP2.6
Intermediate-Low	Modest increase in rate Middle of *likely* range under RCP2.6 Low end of *likely* range under RCP4.5 Low end of *very likely* range under RCP8.5
Intermediate	High end of *very likely* range under RCP4.5 High end of *likely* range under RCP8.5 Middle of *likely* range under RCP4.5 when accounting for possible ice cliff instabilities
Intermediate-High	Slightly above high end of *very likely* range under RCP8.5 Middle of *likely* range under RCP8.5 when accounting for possible ice cliff instabilities
High	High end of *very likely* range under RCP8.5 when accounting for possible ice cliff instabilities
Extreme	Consistent with estimates of physically possible "worst case"

Table 4.3. Probability of exceeding the Interagency GMSL scenarios in 2100 per Kopp et al. (2014). New evidence regarding the Antarctic ice sheet, if sustained, may significantly increase the probability of the intermediate-high, high, and extreme scenarios, particularly for RCP8.5, but these results have not yet been incorporated into a probabilistic analysis (USGCRP 2017).

Scenario	RCP2.6	RCP4.5	RCP8.5
Low	94%	98%	100%
Intermediate-Low	49%	73%	96%
Intermediate	2%	3%	17%
Intermediate-High	0.4%	0.5%	1.3%
High	0.1%	0.1%	0.3%
Extreme	0.05%	0.05%	0.1%

Figure 4.16 shows the RSL projected for 2100 under the intermediate 1 m scenario developed by the U.S. Interagency Sea-Level Rise Task Force. Variations along the U.S. coastlines are due to changes in Earth's gravitational field and rotation from melting of land ice, changes in ocean circulation, and vertical land motion (very high confidence). The smaller RSL rise in the southeast coast relative to the northeast coast is a continuation of the observed changes attributable to the weakening of the AMOC circulation (Yin and Goddard 2013). In parts of the southeastern U.S. coast, RSL may increase by more than 180 cm (6 ft) and the water height with a 5-year recurrence may be up to 90 cm (3 ft) by 2100. Increases in RSL may increase daily tidal flooding, also called sunny-day or nuisance flooding, for coastal cities. An example for Charleston, South Carolina, in the Southeast Region (Figure 4.17), shows increases in tidal floods in the recent decades and significant increases projected for the future.

With sea-level rise (SLR) and TC intensity both projected to increase, storm surge could increase along the southeastern U.S. coast. Balaguru et al. (2016) found a statistically significant correlation between the observed potential intensity (PI), which is a measure of the air-sea thermodynamic environment's conduciveness for TC development and the TC lifetime maximum and mean intensity, characterized by the maximum wind speed of the hurricane, in the North Atlantic. Using this correlation and the CMIP5 model-projected changes in PI, Balaguru et al. (2016) showed that the mean intensities of Atlantic hurricanes may increase by 1.8 to 4.2 percent and their lifetime maximum intensities may increase by 2.7 to 5.3 percent when comparing the last two decades of the 20th and 21st centuries. Combining the estimates of hurricane intensity changes with projections of SLR, the Sea, Lake, and Overland Surges from Hurricanes model was used to project changes in storm surge for five historical hurricanes that made landfall in the Gulf of Mexico and Florida. Figure 4.18 shows the tracks of the five historical hurricanes and the percent change in peak surge for a range of SLR and hurricane intensity changes. The results indicate a median increase in storm surge ranging between 25 and 47 percent, and the changes in hurricane intensity contribute to a 10 percent increase relative to the increase caused by SLR alone.

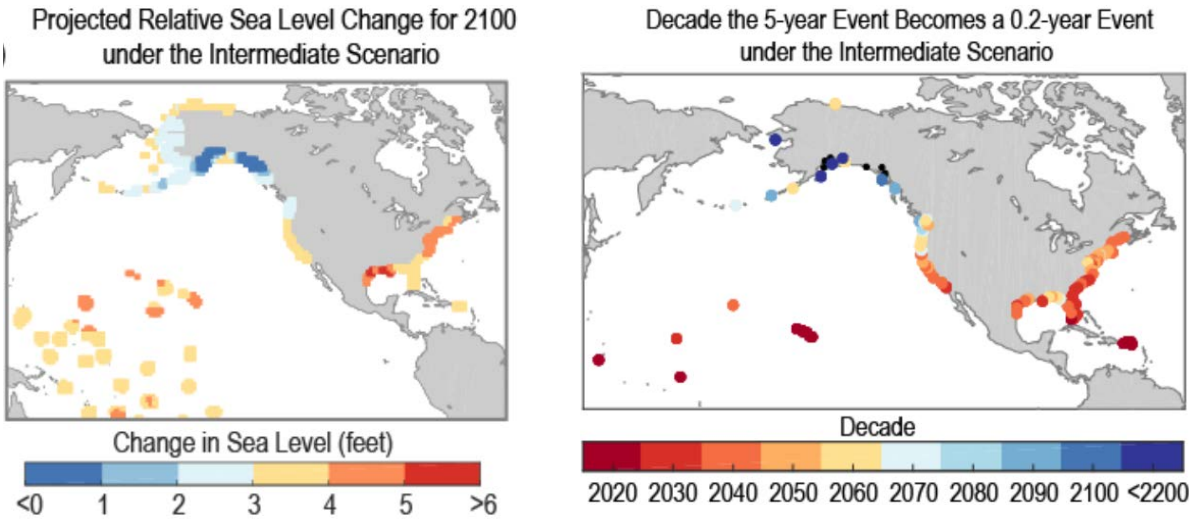

Figure 4.16. (Left) RSL change (ft) in 2100 projected for the interagency intermediate scenario (1-meter GMSL rise by 2100), and (right) the future decade when the 5-year event becomes a 0.2-year (5 or more times a year) event under the interagency intermediate scenario. The black dots on the right side figure imply that a 5-year to 0.2-year frequency change does not unfold by 2200 under the intermediate scenario, after Sweet et al. 2014. (Source: USGCRP 2017)

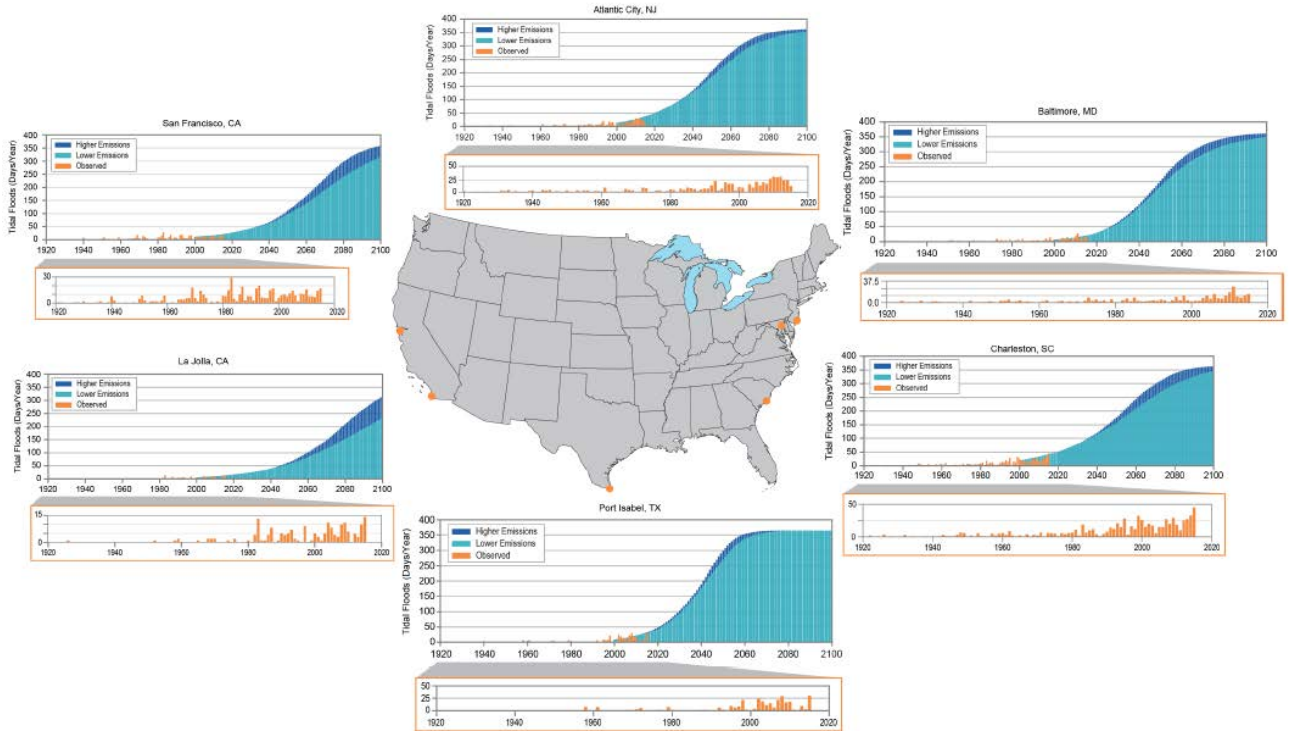

Figure 4.17. Annual occurrences of daily tidal flooding, also called sunny-day or nuisance flooding, for some U.S. coastal cities including Charleston, South Carolina, in the Southeast Region. (Source: USGCRP 2017)

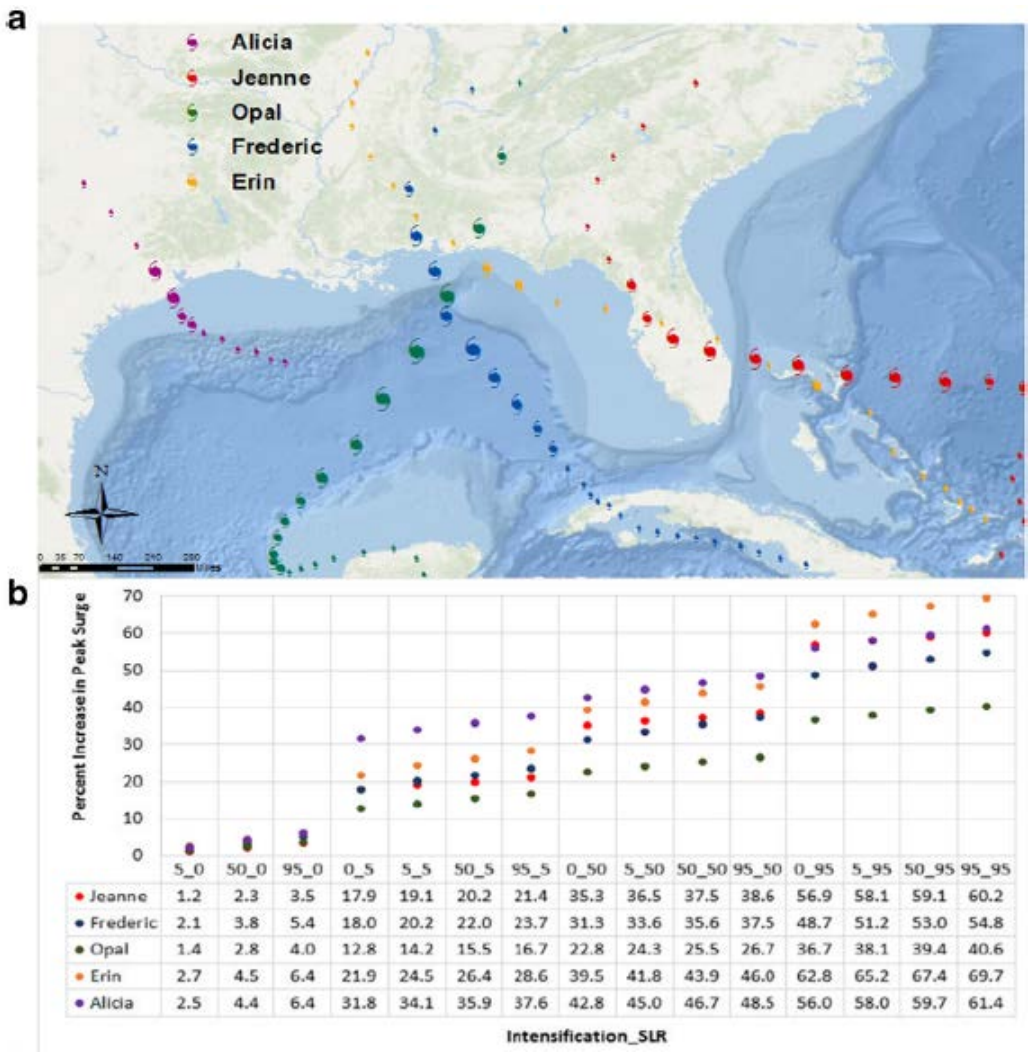

	5_0	50_0	95_0	0_5	5_5	50_5	95_5	0_50	5_50	50_50	95_50	0_95	5_95	50_95	95_95
Jeanne	1.2	2.3	3.5	17.9	19.1	20.2	21.4	35.3	36.5	37.5	38.6	56.9	58.1	59.1	60.2
Frederic	2.1	3.8	5.4	18.0	20.2	22.0	23.7	31.3	33.6	35.6	37.5	48.7	51.2	53.0	54.8
Opal	1.4	2.8	4.0	12.8	14.2	15.5	16.7	22.8	24.3	25.5	26.7	36.7	38.1	39.4	40.6
Erin	2.7	4.5	6.4	21.9	24.5	26.4	28.6	39.5	41.8	43.9	46.0	62.8	65.2	67.4	69.7
Alicia	2.5	4.4	6.4	31.8	34.1	35.9	37.6	42.8	45.0	46.7	48.5	56.0	58.0	59.7	61.4

Figure 4.18. Percentage change in peak surge in storm-surge simulations of five historical hurricanes comparing a base case with no change in hurricane intensity or sea level with scenarios marked as P_Q, representing a Pth percentile increase in hurricane intensification and Qth percentile increase in sea level. (Source: Balaguru et al. 2016)

Little et al. (2015) also considered the joint impacts of SLR and TC changes when assessing future coastal flood risk. While Balaguru et al. (2016) used the PI, which reflects only TC intensity, Little et al. (2015) used the PDI, which is an integrated measure of TC intensity, frequency, and duration. They also developed a flood index (FI) based on the joint probability distribution of SLR and PDI anomaly projected by CMIP5 models (left panel of Figure 4.19). The FI is an aggregate measure of the duration and exceedance of high water during the TC season, normalized so that each site contributes equally. An FI value of 100 implies that the annually integrated flood height over a threshold is 100 times greater compared to the 1986–2005 annual mean. The median 2080–2099 FI value is approximately 16 for RCP2.6 and 100 for RCP8.5, suggesting significantly increased flood height projected in the future. Comparison of the dashed, thin solid, and thick solid lines in the right panel of Figure 4.19 shows that most of the FI changes are driven by SLR. However, the PDI-induced changes in FI are fractionally larger in RCP8.5 than in RCP2.6, and increase into the upper tail. Models that project the largest increase in SLR, PDI, and upper ocean temperatures are responsible for the high-end FI projections.

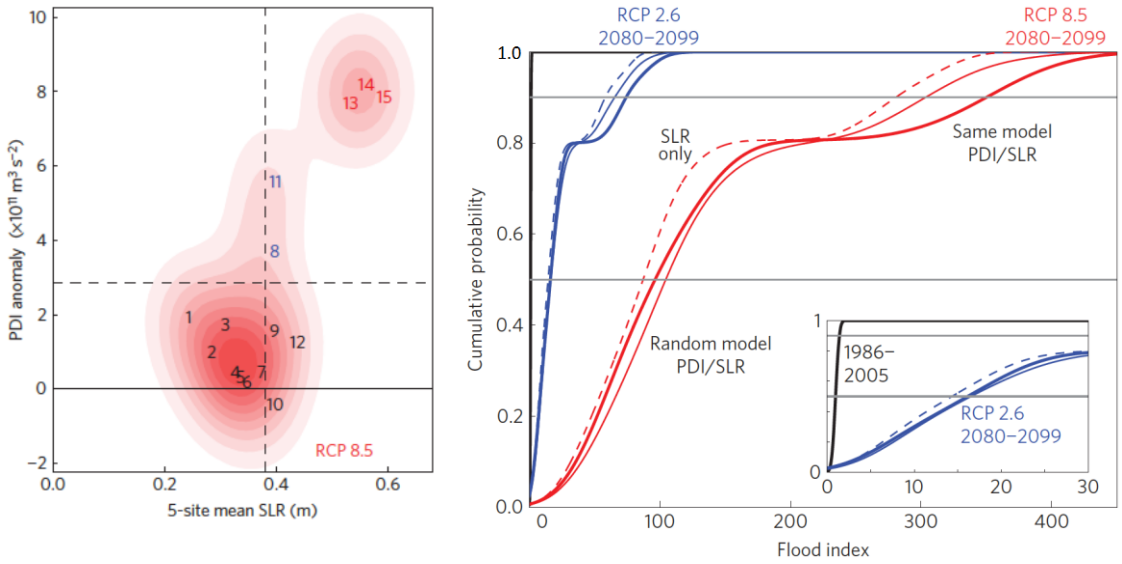

Figure 4.19. (Left) The region, along with the location of the sites, used to develop the FI in the analysis (right) cumulative distribution functions for the 1986–2005 (black) and 2080–2099 FI subject to RCP 2.6 (blue) and RCP 8.5 (red). For the 2080–2099 period, dotted lines show the FI if PDI is unchanged; thin solid lines show the FI distribution if PDI and SLR are drawn randomly from one of the 15 models; thick solid lines show the distribution if PDI and SLR are selected from the same model. The insets expand the x-axis in the range 0 < FI < 30. Gray lines in b indicate the median and 90th percentile of the cumulative probability distribution. (Source: Little et al. 2015)

4.2.2.1 Uncertainty in Projecting Sea-Level Rise

An important source of uncertainty in model projections of SLR arises from limited understanding and model representation of uncertain processes. For example, Oppenheimer and Alley (2016) discussed the issues behind the fall and rise of projected SLR (Figure 4.20) since the IPCC First Assessment Report (AR1).

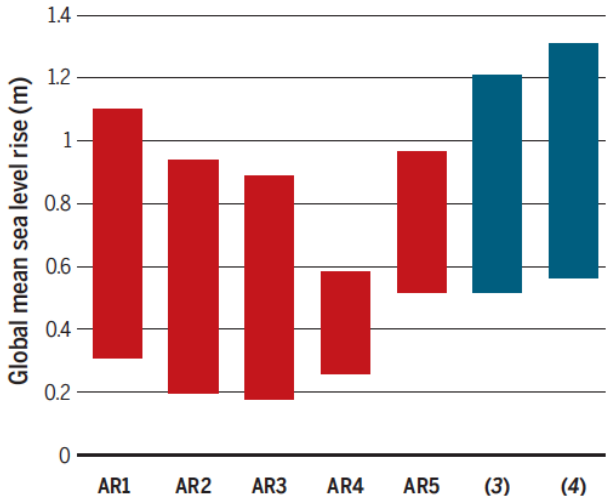

Figure 4.20. Sea-level projections for year 2100 from models used in previous IPCC assessment reports and recent projections from Kopp et al. (2014) and Mengel et al. (2016). (Source: Oppenheimer and Alley 2016)

They noted that the development of ice sheet models from the late 1980s to the late 1990s undercut the notion that ice sheet instability would cause rapid ice loss and SLR. Hence, the projections of were adjusted downward from AR1 to AR4, because thermal expansion and mountain glacier retreat dominated the projections from AR2 to AR4. Improved monitoring in the 2000s captured the spectacular collapse of most of the Antarctic Peninsula's floating Larsen B Ice Shelf and resulting acceleration of its tributary glaciers. This and other findings guided improvements in ice sheet modeling, which also benefited from the use of paleoclimate analogs. In a recent study that makes use of an advanced ice sheet model, which includes the marine ice sheet instability and marine ice cliff instability mechanisms and is calibrated against Pliocene and Last Interglacial sea-level estimates, DeConto and Pollard (2016) estimated that Antarctica has the potential to contribute more than a meter of SLR by 2100. Another uncertain factor in projecting SLR is the strength of the AMOC. As discussed in Chapter 3.0, a weakening of AMOC would accelerate SLR in the northeastern United States relative to the southeastern United States and modulate the RSL rise along the U.S. Atlantic coast. The AMOC is projected to decline in the future (Yang et al. 2016). A full collapse of the AMOC could result in as much as 0.5 m of RSL rise (Gregory and Lowe 2000; Levermann et al. 2013). While the AMOC may weaken with increased freshwater flux from the melting of sea ice, the slowdown of the AMOC may be counteracted by the warming of the deep ocean that tends to strengthen the AMOC. Hence, projecting global and regional SLR remains a significant challenge that requires further advances in understanding and observations to constrain models used in future projections. A slowdown of the AMOC would also lead to cooling over the United States (Jackson et al. 2015), which reduces ocean carbon dioxide uptake. The resulting increase in atmospheric carbon dioxide can accelerate warming. Compounding extreme events (e.g., heat and wildfires) may amplify the climate extremes; thus, assessments of regional climate change should recognize potential unforeseen events that are not currently well modeled or understood.

5.0 Tornadoes and Severe Storms in the Southeast United States

This chapter summarizes the observed and projected changes in tornadoes and severe storms in the Southeast Region. Assessment of these changes is challenging because of three major sources of uncertainties. First, there is no reliable, long-term record of severe thunderstorms and tornadoes to systematically analyze variability and trends and attribute them to internal and external influences. For example, there are well known biases in the U.S. database of tornado reports, although quantification of tornado activity in terms of tornado days instead of raw numbers of tornado reports may reduce some biases (USGCRP 2017). Second, climate models do not have sufficient resolution and process fidelity to simulate individual storms and their interactions with the large-scale environments. These limit the usefulness of climate models in understanding and projecting changes in severe thunderstorms. Third, although environmental proxies can be used to analyze historical trends and project future changes, warming can influence the environmental proxies in competing ways, making robust quantification and attribution more difficult. Furthermore, the environmental proxies are related to both thermodynamical and dynamical processes. While the thermodynamical response to climate change may be more robustly simulated by climate models, large uncertainty in projecting the dynamical or circulation response to warming may limit even the use of environmental proxies in projecting future changes in severe thunderstorms. This chapter summarizes information synthesized by Kunkel et al. (2013a) and USGCRP (2017) and peer-reviewed literature.

5.1 Observed Changes in Tornadoes and Severe Storms

- Since the 1970s, the United States has experienced a decrease in the number of days tornadoes have occurred.
- However, the frequency of tornado outbreaks in the United States has increased since 1960, and the rate of increase is higher for more extreme outbreaks (outbreaks with more than 12 tornadoes of F1 and greater magnitiude on the Fujita scale).
- Comparing tornado counts between two 25-year periods since the 1950s shows a spatial redistribution of tornado activity with the maximum tornado count shifting from Oklahoma to Tennessee.
- There is moderate evidence of increasing extratropical storm activity around the U.S. coastlines including the Gulf coast during the cold season since 1950.

Severe thunderstorms occur in the Southeast Region most frequently in late winter and spring. Damaging winds and large hail have the highest frequency of occurrence in Alabama, Mississippi, Arkansas, western Tennessee, and northern Louisiana (Ingram et al. 2013). The southeast experiences the highest number of strong tornadoes (F2 and greater) and more killer tornadoes than the notorious “Tornado Alley” of the Great Plains (Ashley 2007). Figure 5.1 displays the spatial distribution of the number of tornadoes of F2 intensity and greater in the Southeast, showing larger numbers in Arkansas, Alabama, and central Florida.

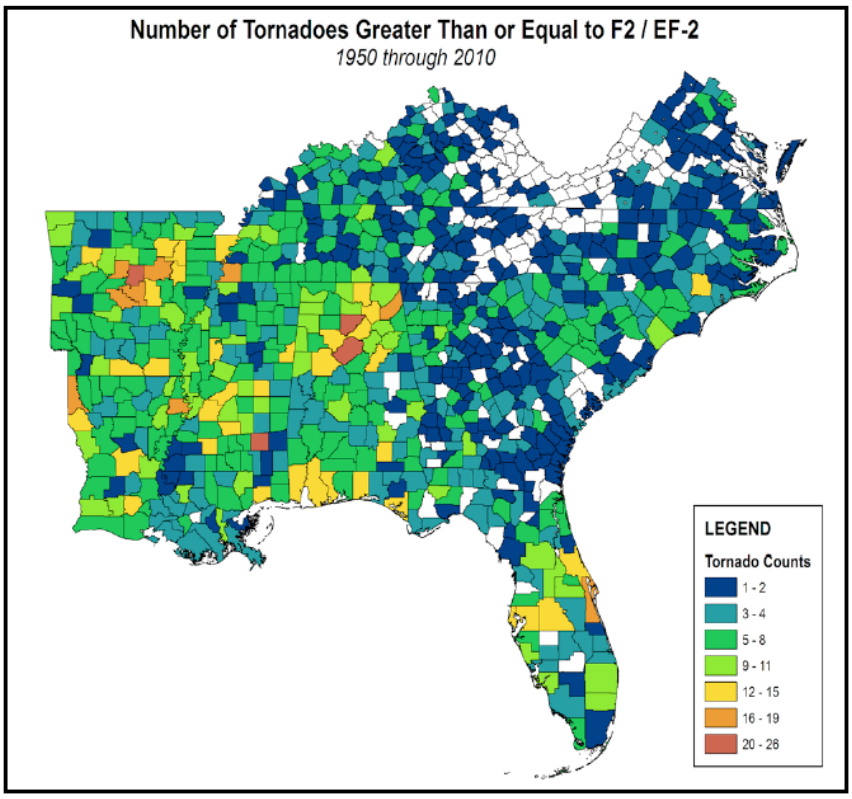

Figure 5.1. Number of tornadoes of F2/EF-2 intensity and greater by county from 1950 to 2010 for the Southeast Region. (Source: Kunkel et al. 2013a)

Analysis of the tornado report database shows that the United States has experienced a decrease in the number of days per year on which tornadoes occur since the 1970s. However, there is an increase in the number of tornadoes that form on those days (Brooks et al. 2014). Using extreme value analysis, Tippett et al. (2016) found an increasing frequency of U.S. tornado outbreaks, defined as sequences of six or more tornadoes rated F1 and greater on the Fujita scale or rated EF1 and greater on the Enhanced Fujita scale. Using the Generalized Pareto approach to model the extreme outbreaks (i.e., outbreaks with 12 or more tornadoes that are rated F1 and greater), they found a higher increasing rate for outbreaks that are more extreme (Figure 5.2). To determine what environmental factors contribute to the tornado outbreak trend, they analyzed two environmental proxies for tornadoes: convective available potential energy (CAPE) and storm relative helicity, which is a measure of vertical wind shear (Brooks et al. 2003). The increase in CAPE in a warmer climate has been associated with increasing frequency of severe storms projected by climate models for the future (Diffenbaugh et al. 2013). However, conditioning the outbreaks on CAPE did not reproduce the observed trend. Instead, Tippett et al. (2016) found that conditioning the outbreaks on storm relative helicity reproduced the observed increasing trend in extreme tornado outbreaks. Their results suggested that the observed increased frequency of tornado outbreaks could be part of the multidecadal variability associated with the AMO that influences vertical wind shear, rather than as a consequence of warming that increases CAPE. In addition to the increasing number of tornadoes per outbreak, another study by Tippett (2012) identified an increasing extent of the season for tornado activity, with an earlier calendar day start of the season of high activity.

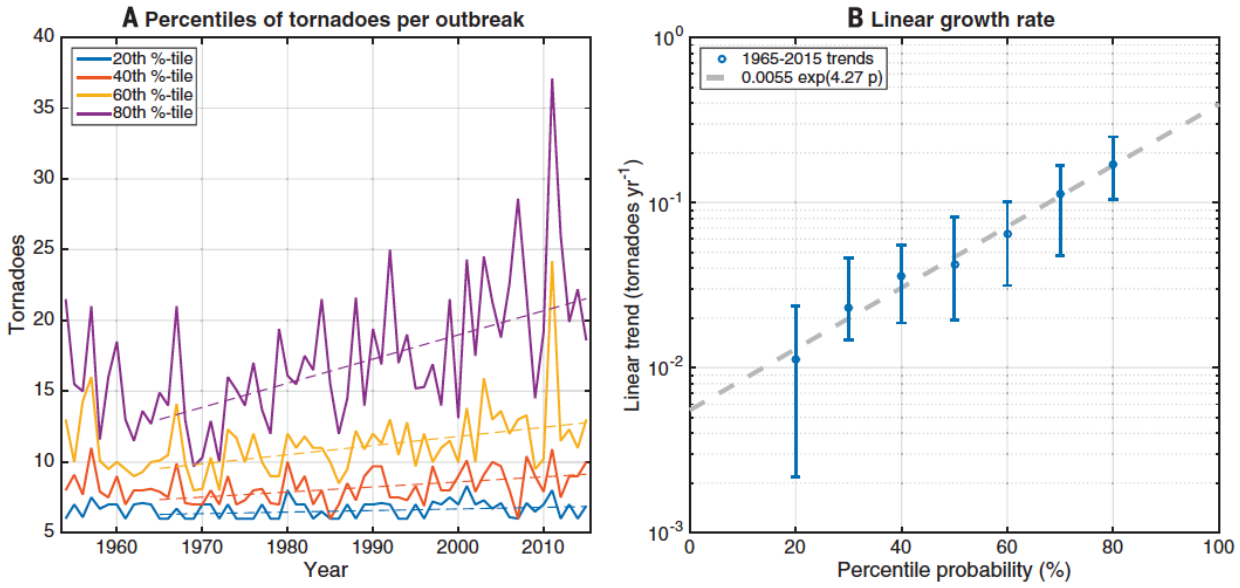

Figure 5.2. (A) Annual 20th, 40th, 60th, and 80th percentiles of the number of tornadoes that are F2 or greater per outbreak between 1954 and 2015 and the quantile regression fits from 1965 to 2015 assuming linear growth in time (dashed lines). (B) Linear growth rates as a function of the percentile probability. (Source: Tippet et al. 2016)

A recent study analyzed tornado counts and days in the United States during the past 50 years. Comparing two 25-year periods featuring regional cooling and warming trends between 1954 and 2013, Agee et al. (2016) noted a spatial redistribution of the tornado counts and days for the (E)F1–(E)F5 tornado events (Figure 5.3). Statistical analysis showed significant decreases in annual tornado activity in the traditional "Tornado Alley," which centers over Oklahoma, and the emergence of a new maximum center of tornado activity over Tennessee or the "Dixie Alley." These results suggest that this may be due to possible warming effects during the second 25-year period and the impact on tornado activity. However, this study did not analyze the large-scale environment in the two 25-year periods, so it is not clear what environmental factors other than the warming and cooling may have contributed to the spatial shift in tornado activity. More research is needed to establish the mechanisms responsible for the spatial redistribution of tornadoes.

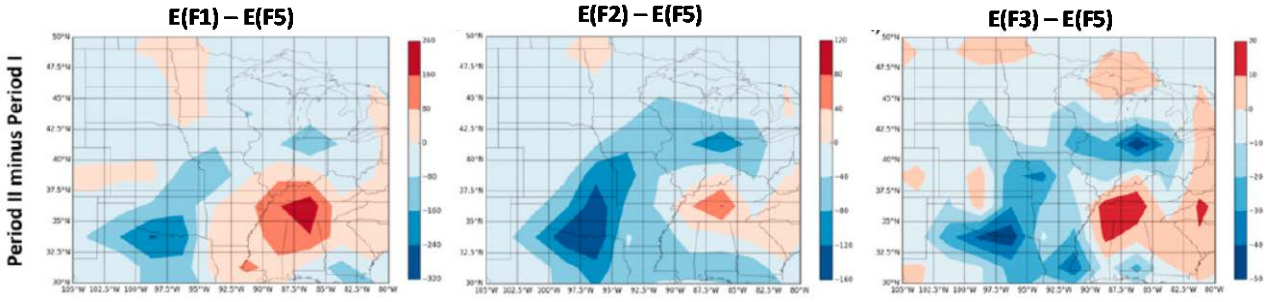

Figure 5.3. Tornado counts (left) (E)F1-(E)F5, (center) (E)F2-(E)F5, and (right) (E)F3-(E)F5 for the difference between Period II (1984–2013) and Period I (1954–1983). (Source: Agee et al. 2016)

The southeastern United States is influenced not only by severe convective storms. Extratropical storms account for the majority of extreme winds during the cold season, and extreme waves are largely driven by extreme winds. Extratropical storms are synoptic-scale low-pressure systems generally formed in the zones of marked temperature contrasts (Vose et al. 2014). Based on global reanalysis data, there is moderate evidence that both storm frequency and intensity during the cold season have increased since 1950 in both mid- and high-latitude zones, corresponding to a poleward shift of storm track (Wang et al. 2013). Increases are also seen around the U.S. coastlines, but in the Southeast Region, there is a reduction in extratropical cyclone activity, although the change is not statistically significant (Figure 5.4).

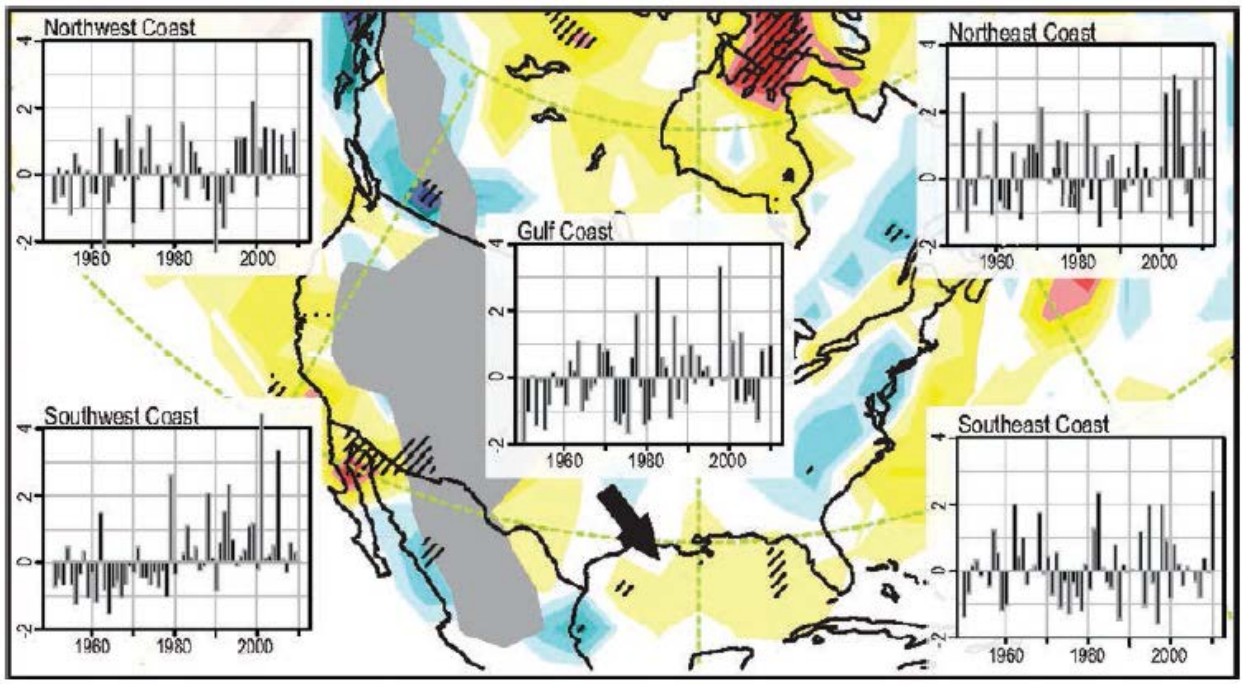

Figure 5.4. Difference in extratropical storm activity between 1979–2010 and 1948–1978 during the cold season. Activity is defined using a standardized index that represents the seasonal total of cyclones in a given area, multiplied by their mean intensity (Wang et al. 2013). Extratropical storms were derived using the NCEP–NCAR reanalysis (Kalnay et al. 1996) as input, and the term "standardized" implies deviations from the long-term average that has been divided by the spread in the data. Yellows and reds indicate a higher level of activity in the more recent period, blues indicate a lower level of activity, gray indicates high-elevation areas for which no cyclones are defined, and hashed lines indicate statistically significant differences. Inset boxes depict time series of standardized anomalies of the cyclone activity index for specific coastal regions, each consisting of all reanalysis grid points within approximately 500 km of the coast. The Northwest region includes coastal British Columbia, and the Northeast coast includes the maritime provinces of Canada. The increasing trends along the Southeast and Gulf Coasts are statistically significant for the 1948–2010 period. (Source: Vose et al. 2014)

Arctic sea-ice loss has been argued to promote extreme weather events in the midlatitudes through circulation changes such as enhanced block patterns and jet stream speed. Evidence for changes in atmospheric circulation associated with Arctic sea ice is particularly compelling for the boreal summer. Modulation of anticyclonic circulation by low Arctic sea-ice extent may modulate synoptic-scale forcing and atmospheric temperature, humidity, and winds to favor intense-thunderstorm formation. Trapp and Hoogewind (2018) explored the connections between Arctic sea ice and U.S. tornadoes using observation

data. They found robust statistical correlations between tornado activity and sea-ice extent during boreal summer, specially in July. In particular, the daily mean (F/EF1+) July probability of 0.45 over 1990–1999 has decreased to 0.33 over 2006–2015, a period of particularly rapid declines in sea-ice extent (Figure 5.5). There is evidence for the statistical relationship that low (high) Arctic sea-ice extent provides unfavorable (favorable) conditions for tornado-bearing thunderstorm formation through anomalous regional circulation and storm track.

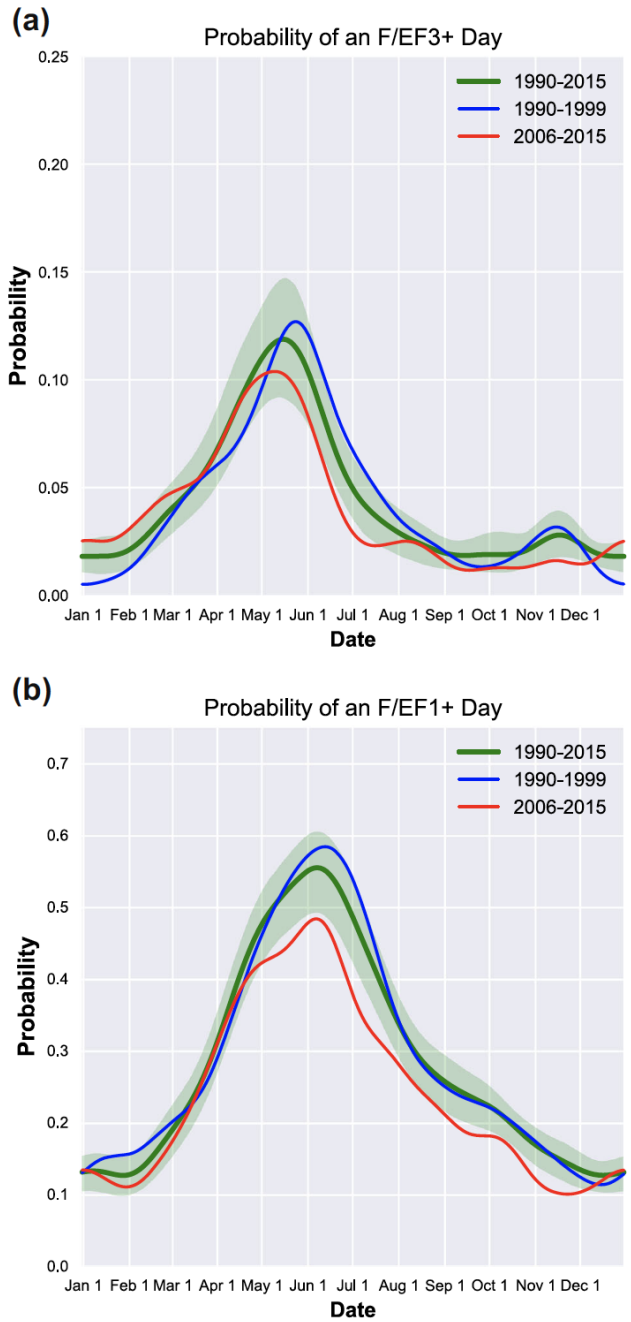

Figure 5.5. Probability of a tornado day within the United States as a function of calendar day for tornadoes rated (a) F/EF3 and greater, and (b) F/EF1 and greater for 1990–2015 (green line for the 26-year mean and lighter green shading for the 95th confidence intervals) and the 10-year mean of 1990–1999 (blue) and 2006–2015 (red). (Source: Trapp and Hoogewind 2018)

5.2 Future Changes in Tornadoes and Severe Storms

- Severe convective thunderstorm environment is projected to increase in the Southeast Region during spring; projected changes are inconsistent among models for summer.
- Some studies have shown a reduction in extratropical cyclone activity, particularly the intense storms, in the eastern United States in the future.

Currently, neither global models nor RCMs have sufficient spatial resolution to simulate tornadoes, which involve very fine-scale dynamical and cloud processes. Hence, projections of tornado changes have been evaluated based on changes in the large-scale atmospheric environment for hazardous convective weather, including primarily vertical wind shear and CAPE (Brooks et al. 2007; Brooks 2013; Tippett et al. 2012). Analyzing the severe thunderstorm environment simulated by CMIP5 models in the RCP8.5 scenario, Diffenbaugh et al. (2013) found that the changes are largest during spring, with an increase of 2 days per model grid point by the end of the 21st century (Figure 5.6). The changes are due to increase in CAPE, but weaker reduction in wind shear compared to other seasons is responsible for the larger increase in severe storm environment during spring.

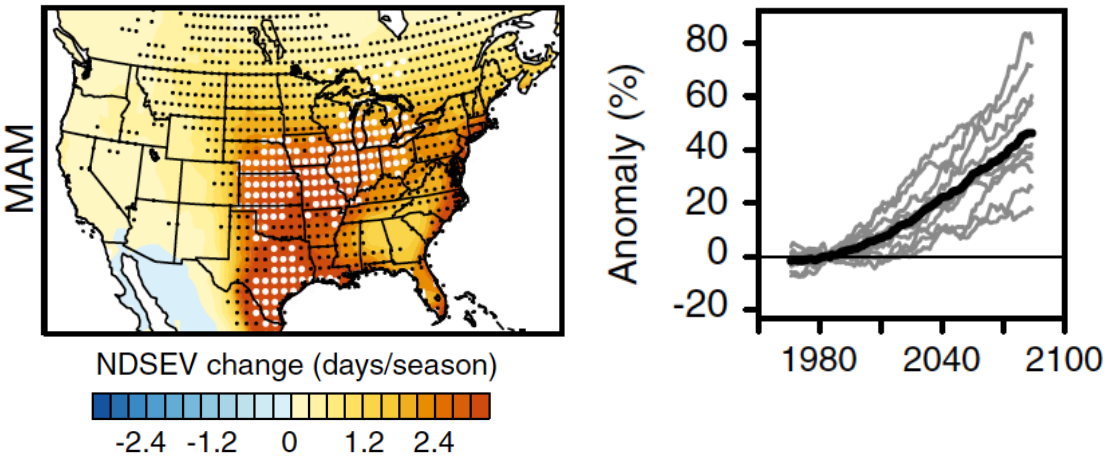

Figure 5.6. (Left) Changes in number of days with spring (March-April-May) severe thunderstorm environment (NDSEV) comparing 2070 to 2099 with 1970 to 1999 from CMIP5 models in the RCP8.5 scenario. Black (gray) dots identify areas where the ensemble signal exceeds one (two) standard deviations of the ensemble noise. (Right) Anomaly in the regional average NDSEV value over the eastern United States (105-67.5^{o}W, 25-50^{o}N and land points only), calculated for each year in the 21st century, with the anomaly expressed as a percentage of the 1970–1999 baseline mean value. A 31 yr running mean is applied to each time series. Each gray line shows an individual model realization. (Source: Diffenbaugh et al. 2013)

Seeley and Romps (2015) analyzed changes in severe-thunderstorm-favorable environments (STEnvs, defined as grid cells where the product of CAPE and vertical shear exceed a 3 percent exceedance threshold) simulated by the CMIP5 models. Based on their skill in reproducing STEnvs constructed from observations (Stratosphere-troposphere Processes And their Role in Climate radiosonde data for CONUS), they down-selected four models (GFDL CM3, GFDL-ESM2M, MRI-CGCM3, and NorESM1-M) from 11 CMIP5 models. These four GCMs were then used to explore the changes in the severe storm environment by comparing the future (2079–2088) with the present (1996–2005) for both RCP4.5 and

RCP8.5 scenarios. Figure 5.7 shows the changes in STEnv projected by the four models for spring (MAM) and summer (JJA). For spring, the models projected larger increases in STEnv in the central United States, but the Southeast Region may also experience increases in STEnv, although model differences are notable. In summer, uncertainty in projecting changes in STEnv increases, and models project both increases and decreases in STEnv. The model-divergent response in summer is related to uncertainty in projecting the changes in boundary layer humidity, which affects projections of CAPE.

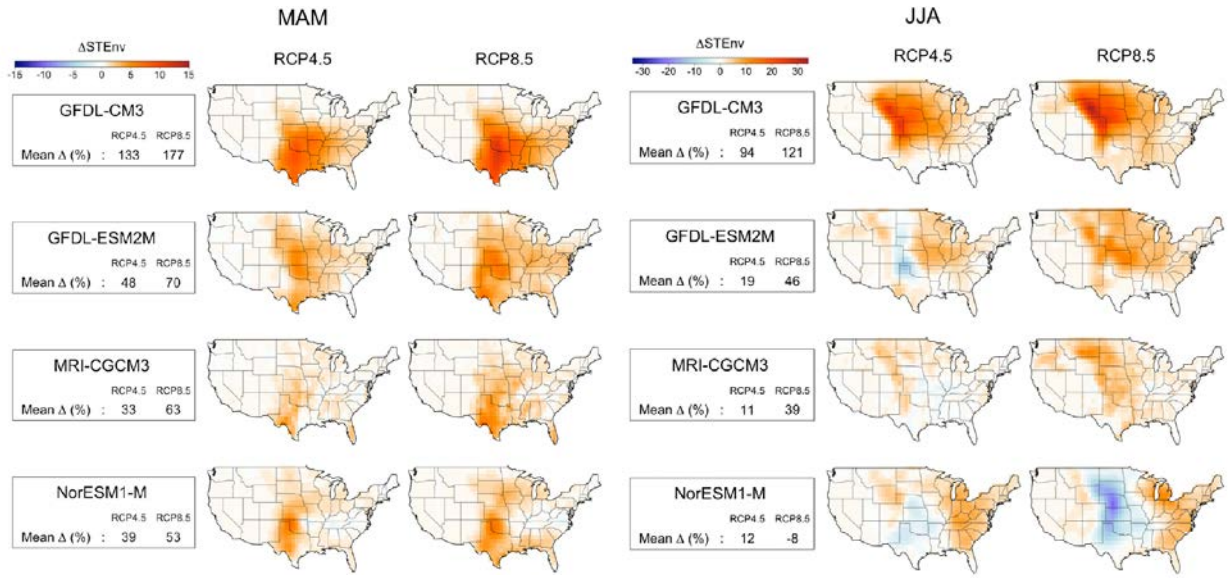

Figure 5.7. Changes in mean STEnv in spring (MAM; left) and summer (JJA; right) projected by four global models for the RCP4.5 and RCP8.5 scenarios. Changes are calculated as the difference in means for 1996–2005 and 2079–2088. A summary of the fractional continental United States mean changes is given for each model in the boxes at left. (Source: Seeley and Romps 2015)

Besides Diffenbaugh et al. (2013) and Seeley and Romps (2015), several studies also consistently found an increase in the spring severe storm environment projected by GCMs in a warmer climate. To address the limitations of the environmental proxy approach, very high-resolution simulations have been performed in a few studies to explicitly simulate severe storms. Trapp and Hoogewind (2016) selected three high-end supercellular tornado events that occurred in Oklahoma in May of 2007, 2010, and 2013 for their experiments. Ensemble simulations were performed using a regional model with a larger domain at 3 km grid resolution to characterize the large-scale environment and a smaller domain at 1 km grid resolution to simulate storm-scale processes. The PGW approach was used to simulate potential changes in the tornado events under perturbations of the large-scale boundary conditions corresponding to the difference between May 2090–2099 and May 1990-2099, as simulated by three GCMs in CMIP5 under the RCP8.5 scenario. Consistent with parcel theory that an increase in CAPE in a warmer climate leads to stronger updraft, the simulations showed a 15 percent increase in updraft in the perturbed simulations relative to the control. However, the increase in updraft is much smaller than that which can be supported by the increase in CAPE, partly due to precipitation loading that reduces the updraft. Changes in vorticity due to changes in vertical wind shear are also small, due to the dependence of the vorticity on both updraft (which increases) and wind shear (which generally decreases). The results do not support a change in convective morphology of the supercellular tornadic events in the PGW experiments. A more recent study using dynamical downscaling for climate simulations shows increases in both the frequency and intensity of severe convective storms in the future (Hoogewind et al. 2017). However, the study also found that the environment-event frequency relationship can be altered in the future climate such that the

increase in storm frequency is not as high as would be expected from the increase in favorable environment. These studies highlight the need to use very high-resolution modeling to further distangle the influence of CAPE and wind shear on tornado activity and their often competing impacts in a warmer climate.

Several mechanisms have been explored to understand and project changes in winter storms. First, polar amplification (i.e., larger warming in the polar regions relative to the rest of the world) has been postulated to reduce the meridional temperature gradient and weaken the strength of the jet streams. The latter has been hypothesized to stall the movement of the jet streams, leading to more blocking and cold air outbreaks (Francis and Vavrus 2012), though more recent studies did not find supporting evidence for this hypothesis (Barnes and Polvani 2015). Second, weaker meridional temperature at the surface due to polar amplification reduces the available potential energy for extratropical storms (Bengsston et al. 2009). Third, expansion of the Hadley circulation may shift the storm tracks poleward, leading to dipole changes in winter storm activity in the high- and mid-latitude zones (Lu et al. 2007; Chang et al. 2015).

Consistent with the weaker meridional temperature gradient from polar amplifications, GCMs projected reductions in the extratropical cyclone frequency globally and in the northern hemisphere, but projection of changes in storm intensity is more uncertain (Colle et al. 2015). Many studies have also shown a decrease in the number of mid-latitude cyclones in North America. Colle et al. (2013) found a 10–40 percent increase in more intense (<980 hPa) cyclones and 20–40 percent more rapid deepening rates just inland of the U.S. East Coast (Figure 5.8). They attributed the increase in cyclone intensity to the increase in latent heat release due to increased water vapor in a warmer climate that intensifies the storms.

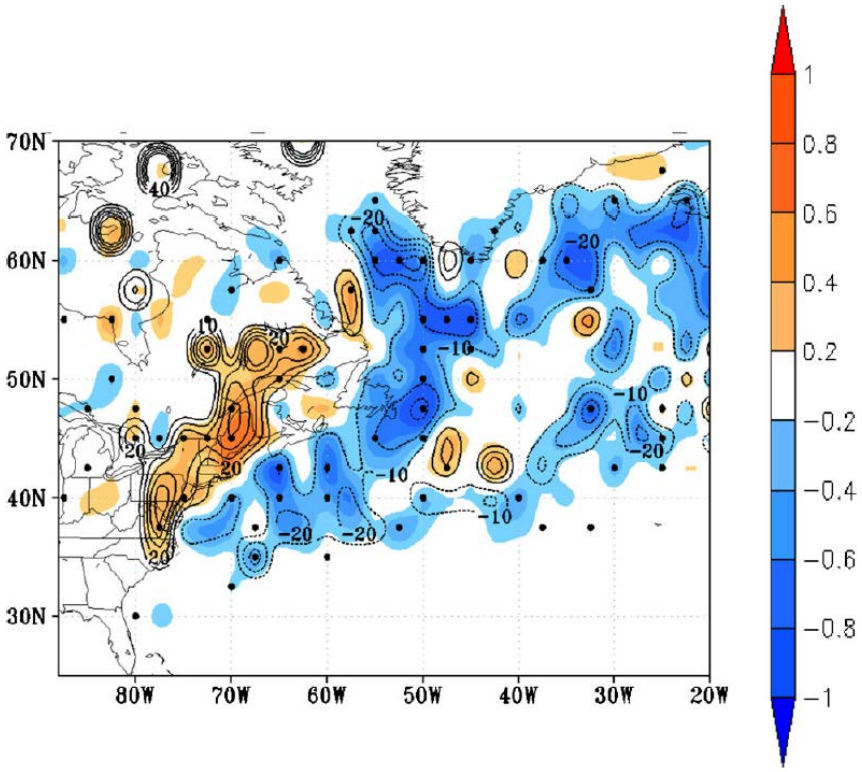

Figure 5.8. Change in the number of 6 h cyclone deepening rates >5 hPa (shaded as the number of cyclone tracks per five cool seasons) per 50,000 km^2 and the percentage change (contour every 10 percentwith negative dashed) between the 2039–2068 future period minus the 1979–2004 historical period. The dots are locations in which six of the seven best models agree with the sign of the change. (Source: Colle et al. 2013)

6.0 Hydrologic Impacts of Climate Change in Southeastern United States

This chapter describes the hydrological impacts of climate change in the Southeast Region. The focus is on two metrics—floods and low flows, resulting from precipitation and/or snowmelt events under climate change scenarios. Because both of these metrics are manifestations of runoff from precipitation and/or snowmelt, conditions other than just precipitation and snowmelt are also important to consider. For example, precipitation or snowmelt events that are similar in magnitude can differ in the amount of runoff from the drainage area because of differences in antecedent soil-moisture conditions or differences in the degree of imperviousness. The duration of the precipitation event is also important (e.g., a stalled storm system producing a low-intensity but longer-duration precipitation event can result in significantly greater flood magnitude compared to a higher-intensity shorter-duration storm for the same antecedent and physiographic conditions). Other factors that affect runoff include land use and cover, water-supply management, and urbanization. Some of these hydrometeorologic parameters are not directly addressed in the NCAs.

6.1 Historical Flood Events

Floods in the Southeast Region can be produced by several mechanisms including (1) locally heavy precipitation (e.g., thunderstorms and mesoscale convective complexes), (2) slow-moving extratropical cyclones during the cool season, (3) TCs during summer and fall, (4) late spring rainfall on snowpack, (5) storm surge near coastal areas from hurricanes, and (6) occasional large releases from upstream dams. Some recent floods are briefly described in this section. The reason these recent flood events are highlighted is that they resulted from unusual combinations of hydrometeorological conditions and exceeded previously recorded historical maximums. In general, the climate research community has not focused on evaluating trends and impacts on low annual exceedance probability (AEP) meteorological (and by extension, flood) events that are of interest to the NRC in a PFHA for permitting and licensing. Current climate models have significantly increased uncertainties for low-AEP events approaching those of interest to the NRC. The events described below highlight unusual combinations of hydrometeorological conditions that open a potential avenue to identifying similarly unusual combinations in climate simulations and how their frequencies are affected under various climate scenarios. This information could inform the NRC of combinations of hydrometeorological conditions relevant to PFHA.

6.1.1 August 2016 Louisiana Floods

The National Hurricane Center stated that a storm system that developed near Florida and Alabama on August 5, 2016, might transform into a tropical depression after moving into the Gulf of Mexico (Schleifstein 2016). However, the system moved over land slowly to the west and, on August 12, 2016, became nearly stationary over southern Louisiana (van der Wiel et al. 2016). Watson et al. (2017) described the system as a slow-moving sheared inland tropical depression that gained energy and moisture as it moved from the southeast across the Gulf Coast into Louisiana and southwestern Mississippi. Over the next 3 days, multiple thunderstorms produced heavy precipitation; a Livingston, Louisiana, rain gauge recorded 25.5 in. of rain during this period (Figure 6.1).

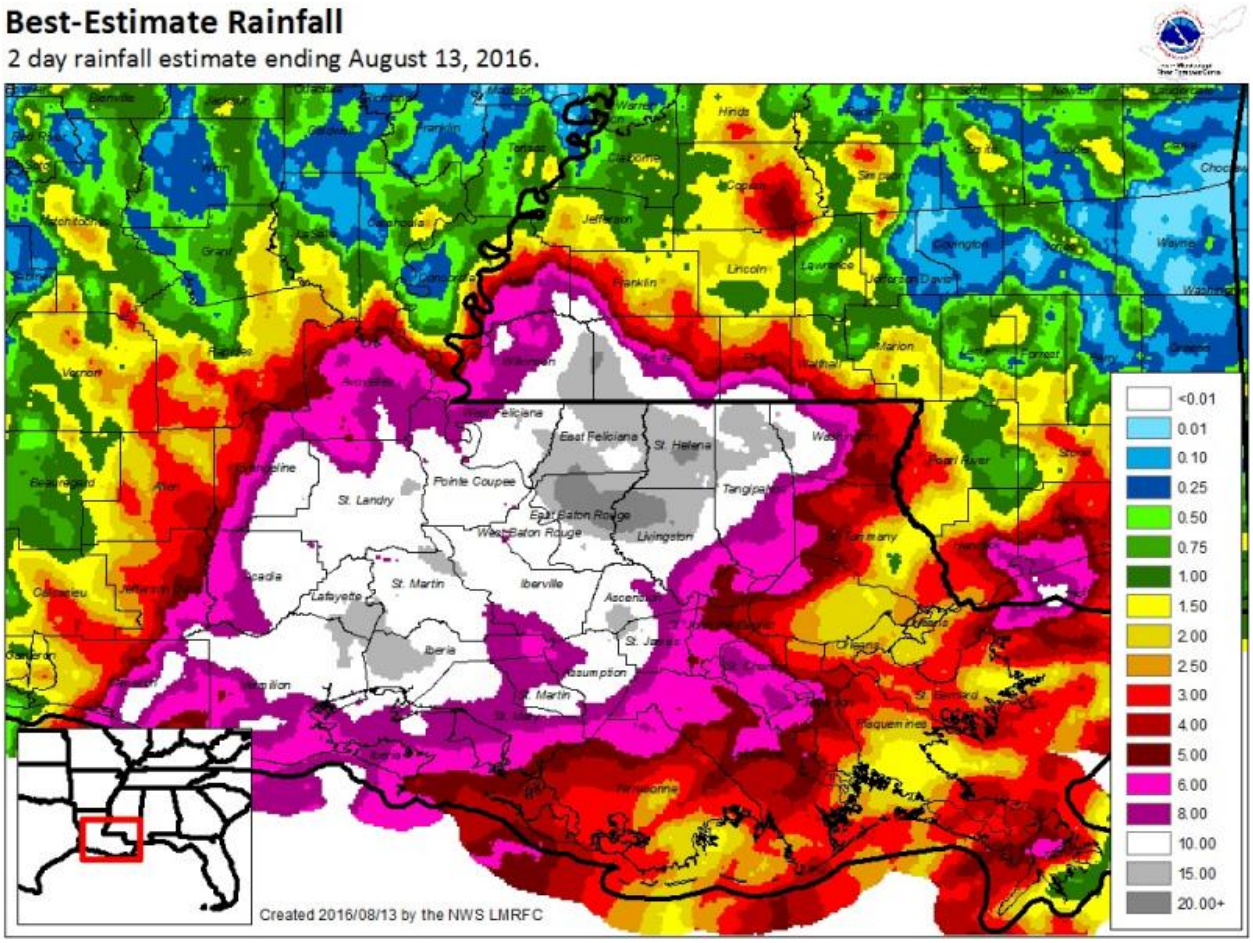

Figure 6.1. Cumulative 2-day rainfall estimates for the August 2016 event. (Source: NOAA 2016d)

Rainfall rates exceeded 3 in./hr in places. The 3-day total precipitation exceeded three times the climatological August total and three times the annual maximum 3-day precipitation (van der Wiel et al. 2016). The city of Watson, Louisiana, about 20 mi northeast of Baton Rouge, received 31.4 in. of rainfall over the duration of this event (Figure 6.2). In response to the intense precipitation, local drainages and rivers that ultimately drain to Lakes Pontchartrain and Maurepas flooded. The Comite River near Comite exceeded the NWS flood stage on August 12, and the Amite River near French Settlement exceeded the NWS flood stage on August 14, 2016. At both locations, the maximum stages exceeded the corresponding historical records (Figure 6.3).

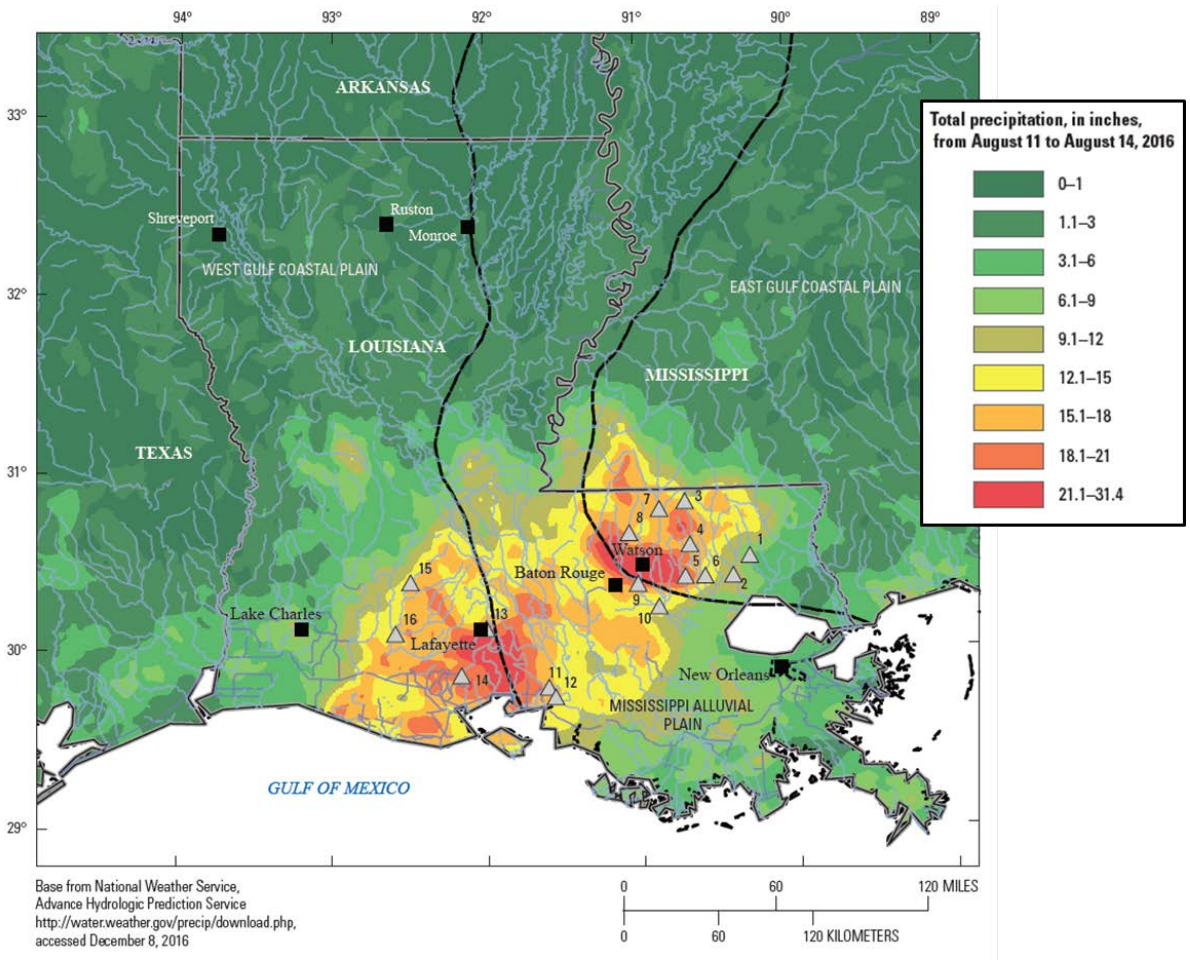

Figure 6.2. Total precipitation depths during August 11-14, 2016 during the August 2016 event. (Source: Watson et al. 2017)

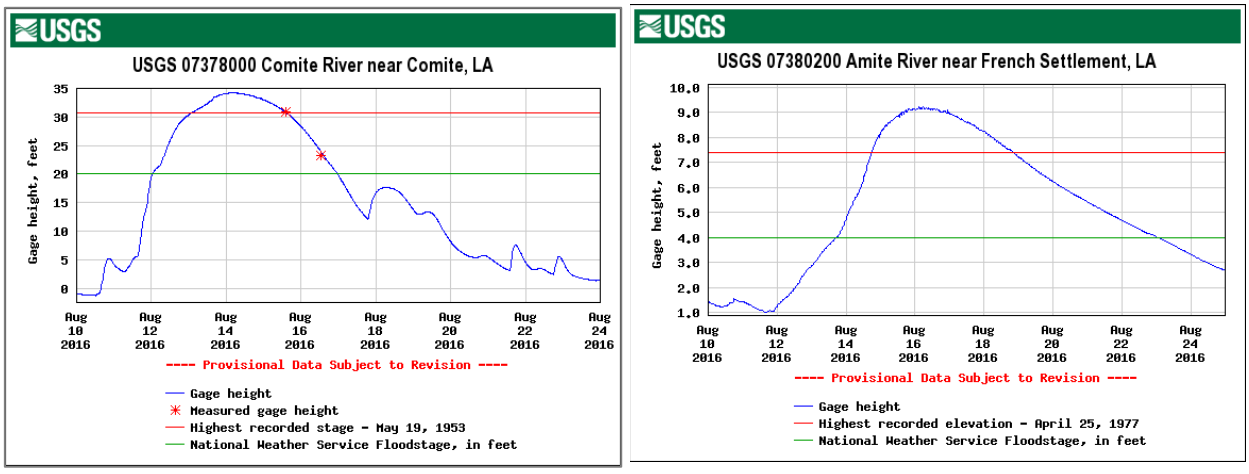

Figure 6.3. Flooding in the Comite River (left) and Amite River (right) during the August 2016 Louisiana storm. (Source: USGS National Water Information System 2016a)

Van der Wiel et al. (2016) performed a rapid attribution of this Louisiana flood to climate change. Observational data indicate that the local return period of the August 12–14 precipitation event is about 550 years, and that since 1900, the probability and intensity of extreme precipitation of this return period have increased. In addition, high-resolution GCMs also suggest that the regional probability of 3-day extreme precipitation is increasing by more than a factor of 1.4 due to anthropogenic climate change. Wang et al. (2016) performed another attribution study of the Louisiana flood, focusing on the historical and projected changes in the synoptic conditions that contributed to the extreme event. They emphasized two synoptic ingredients: (1) the eastward moving upper-level trough and (2) a slow-moving tropical low-pressure system. Their coincidental occurrence enhanced the moisture transport from the Gulf of Mexico that fueled the storm. Observations in the past three decades show a likelihood for more and stronger upper-level troughs propagating out of the western United States, increasing the likelihood of such extreme events. Analysis of a large ensemble of global climate simulations and regional modeling experiments by Wang et al. (2016) suggests that the warming trend that increases atmospheric moisture could have increased event precipitation by 20 percent. Watson et al. (2017) mention that the 2-day total precipitation in East Baton Rouge, Livingston, and St. Helena Parishes exceeded that of AEP 0.002.

Watson et al. (2017) also described estimation of the AEPs for the peak streamflow that occurred during the August 2016 floods at nine streamflow gauges. They used the USGS PeakFQ software to estimate discharges corresponding to 15 specific AEPs ranging from 0.995 to 0.002. To estimate AEPs for the peak streamflow discharges during the August 2016 flood, Watson et al. (2017) created generalized additive models (GAM) with integrated smoothness estimation. The GAMs were used to estimate the AEPs for the peak streamflow discharges at the nine gauges during the August 2016 event (Table 6.1). Of the nine streamflow gauges listed in Table 6.1, the August 2016 peak discharges at eight gauges exceeded the previous historical maximum.

There has been a remarkable interest in activity in extreme event detection and attribution in the past decade. A report published by National Academy of Sciences, Engineering, and Medicine (2016) examines the science of attribution of specific extreme weather events to human-caused climate change and natural variability. The report reviewed current understanding and capabilities, assessed the robustness of the methods for different classes of events and attribution approaches, and provided guidance for interpreting analyses and identified priority research needs. The report noted that "… unambiguous interpretation of an event attribution study is possible only when the assumptions and choices that were made in conducting the study are clearly stated and uncertainties are carefully estimated." Moving forward, there is a need to improve extreme event attribution capabilities, including models such as those used in the studies discussed above, and focused effort to improve understanding of specific aspects of weather and climate extremes could improve the ability to perform extreme event attribution.

Table 6.1. Estimated annual exceedance probabilities for the observed peak streamflow discharges at nine gauges for the August 2016 flood event (top panel). The bottom panel shows the peak streamflow discharges corresponding to AEPs 0.01, 0.005, and 0.002 along with the corresponding 95-percent confidence intervals. (Source: Watson et al. 2017)

Site identification number (fig. 1)	Station number	Flood data			AEP for observed August 2016 flood			
						66.7 percent confidence interval		
		Peak streamflow (ft^3/s)	Rank/number of annual peak streamflows in record	Number of years in annual peak analysis	Estimate (percent)	Lower (percent)	Upper (percent)	Upper
1	07375000	32,700	2/73	73	1.0	0.8	4.4	139,000
2	07375500	120,000	1/78	78	<0.2	<0.2	2.3	204,000
3	07375800	43,000	1/60	60	0.8	0.2	3.0	200,000
4	07375960	120,000	1/44	44	<0.2	<0.2	4.1	272,000
5	07376000	35,800	1/76	76	<0.2	<0.2	2.4	57,900
6	07376500	22,100	1/73	73	<0.2	<0.2	2.5	33,800
7	07377000	116,000	1/68	68	1.0	0.2	2.6	341,000
8	07377500	78,000	1/74	74	<0.2	<0.2	2.4	153,000
9	07378500	205,000	1/78	78	<0.2	<0.2	2.3	307,000

Site identification number (fig. 1)	Station number	Expected peak streamflows for selected AEP with 95 percent confidence intervals								
		1 percent AEP (100-year recurrence)			0.5 percent AEP (200-year recurrence)			0.2 percent AEP (500-year recurrence)		
		Estimate (ft^3/s)	95 percent confidence interval		Estimate (ft^3/s)	95 percent confidence interval		Estimate (ft^3/s)	95 percent confidence interval	
			Lower	Upper		Lower	Upper		Lower	Upper
1	07375000	34,400	23,200	66,100	43,000	27,500	92,000	56,400	33,500	139,000
2	07375500	76,200	56,200	121,000	89,500	63,400	153,000	108,000	72,400	204,000
3	07375800	41,100	25,900	88,900	52,200	31,000	128,000	69,400	38,000	200,000
4	07375960	52,800	33,500	122,000	65,800	39,600	174,000	86,000	47,900	272,000
5	07376000	25,200	19,300	37,500	28,600	21,300	45,500	33,300	23,500	57,900
6	07376500	12,500	9,600	19,800	14,700	10,800	25,100	17,800	12,500	33,800
7	07377000	118,000	84,600	199,000	139,000	95,100	253,000	169,000	108,000	341,000
8	07377500	47,600	34,100	82,100	57,400	39,300	108,000	71,900	46,300	153,000
9	07378500	136,000	104,000	200,000	154,000	114,000	243,000	180,000	126,000	307,000

6.1.2 March 2016 Southern Floods

In mid-March 2016, an unusual combination of a low-pressure system to the southwest of the Southeast Region, a high-pressure system to the east of the region, and the jetstream over Mexico (much farther south than normal), caused large amounts of moisture from tropical Gulf of Mexico to be transported to the southeastern United States (Figure 6.4) (Di Liberto 2016). Breaker et al. (2016) stated that the system resulted from a slow-moving southward dip in the jetstream shifted eastward across Mexico, funneling tropical moisture into parts of U.S. Gulf Coast states and the Mississippi River valley. During the period from March 8–13, 2016, northern Louisiana, southeast Arkansas, and southwest Mississippi received rainfall totals ranging from 1 to 2 ft (Figure 6.5).

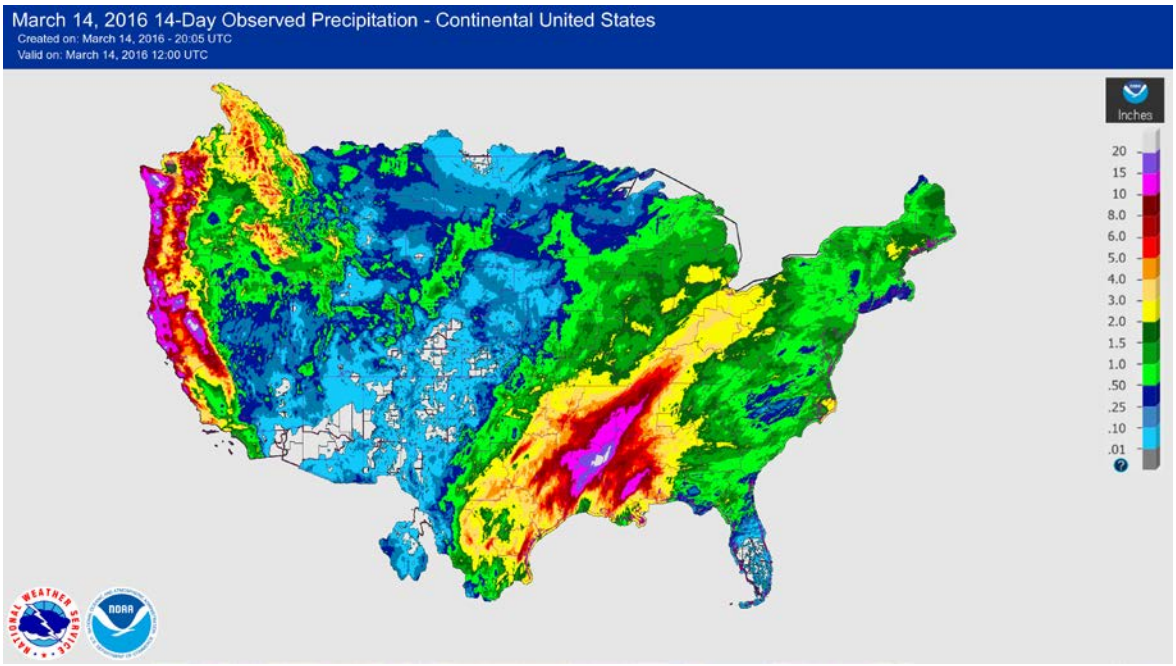

Figure 6.4. Cumulative 14-day precipitation for the continental United States. (Source: NOAA 2016c)

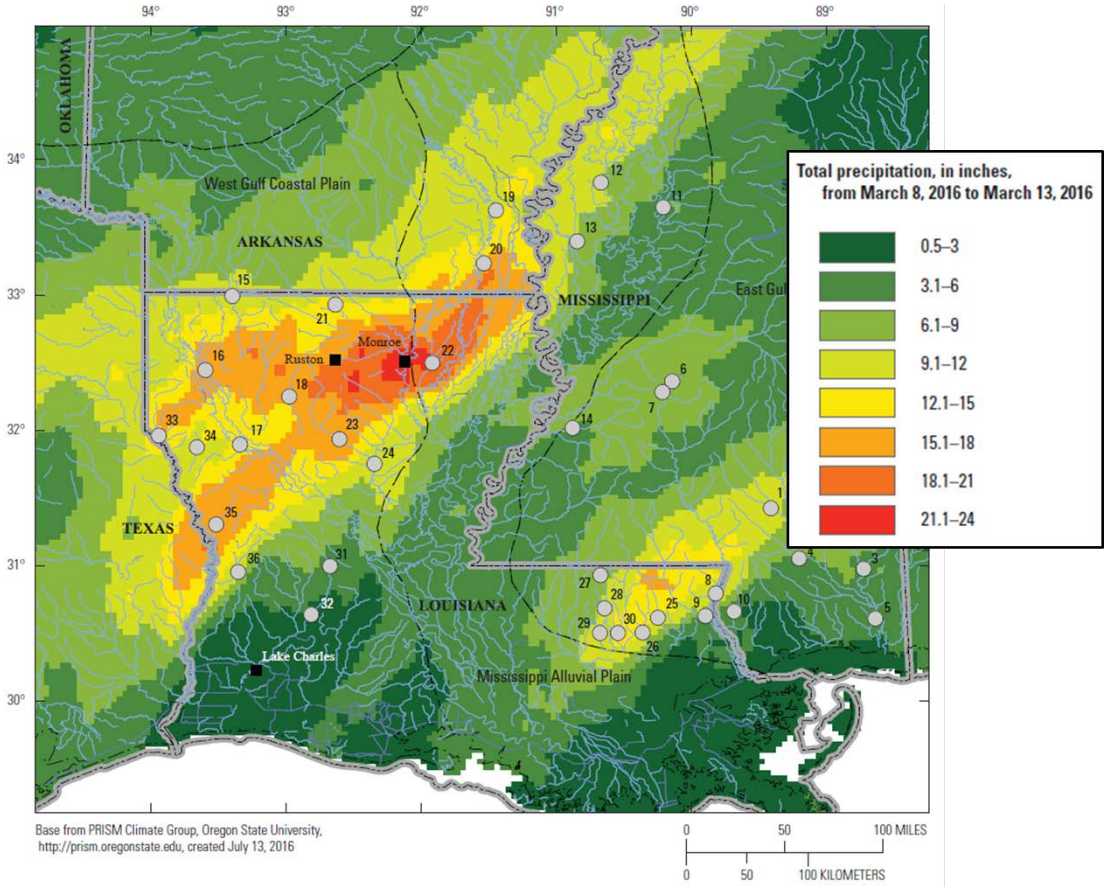

Figure 6.5. Total precipitation depths during March 8–13, 2016 during the March 2016 event. (Source: Breaker et al. 2017)

Widespread flooding in the region occurred as a result of this event. Bayou Dorcheat at Lake Bistineau exceeded its historical peak stage of 147.8 ft recorded on April 18, 1991, by 2.4 ft to crest at 150.2 ft (left panel of Figure 6.6). The stage did not fall below flood level until March 26, 2016. Bouge Chitto River near Bush, Louisiana, exceeded its previous historic gauge height of 21.2 ft recorded on April 8, 1983, to peak at 21.4 ft (right panel of Figure 6.6). The stage would fall below flood stage on March 18, 2016.

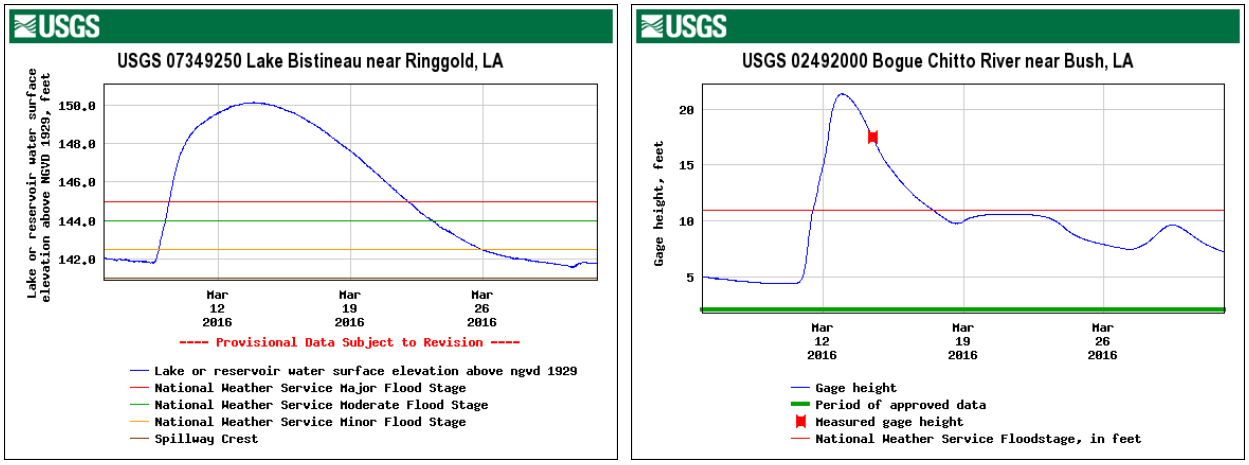

Figure 6.6. Flooding in Bayou Dorcheat (left) and Bogue Chitto River (right) during the March 2016 storm. (Source: USGS National Water Information System 2016b)

Breaker et al. (2016) analyzed 36 streamflow gauges in the region. At 14 of these gauges, the previously recorded historical maximum peak discharge was exceeded during the March 2016 floods. At 29 of the 36 gauges, peak streamflow discharge was among the five greatest recorded discharges. Using the same approach as that of Watson et al. (2017), Breaker et al. (2016) estimated that the AEPs corresponding to the peak discharges during the March 2016 floods were ≤0.002 at 3 gauges and between 0.002 and 0.01 at 13 gauges.

6.1.3 October 2016 Hurricane Matthew Floods

Hurricane Matthew became the first tropical system since Hurricane Felix in 2007 to become a Saffir-Simpson Category 5 hurricane in the Atlantic Basin (NWS 2017). It passed the eastern seaboard from October 7–9, 2016 (Figure 6.7) (NWS 2016). Hurricane Matthew made landfall on October 8, 2016, near McClellanville, South Carolina, as a Category 1 storm and resulted in rainfall depths of 10–20 in. in the eastern Carolinas (Figure 6.8) with hourly estimates of up to 7 in./h (NWS 2017). AEPs of 24-hr rainfall were 0.002 or less in many areas of the coastal plains in North and South Carolina (Figure 6.9). Precipitation from the hurricane caused rivers to flood (Figure 6.10) and coastal areas were affected by storm surge (Figure 6.11).

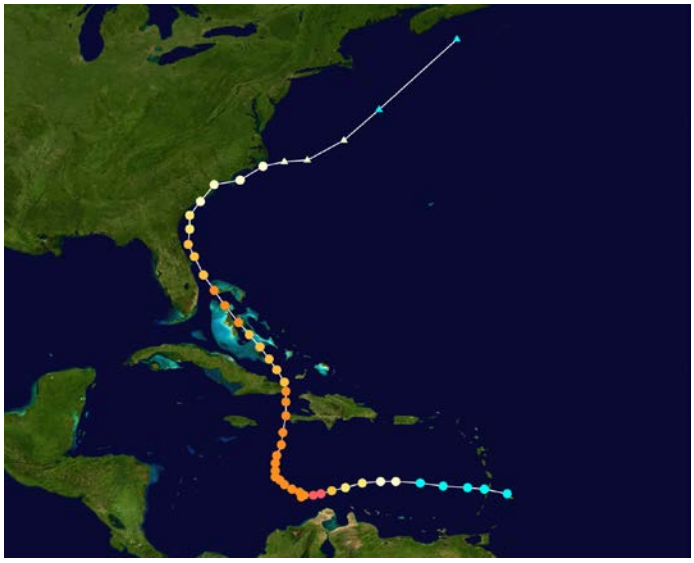

Figure 6.7. Track of Hurricane Matthew from September 28 through October 10, 2016. (Source: NOAA 2016b)

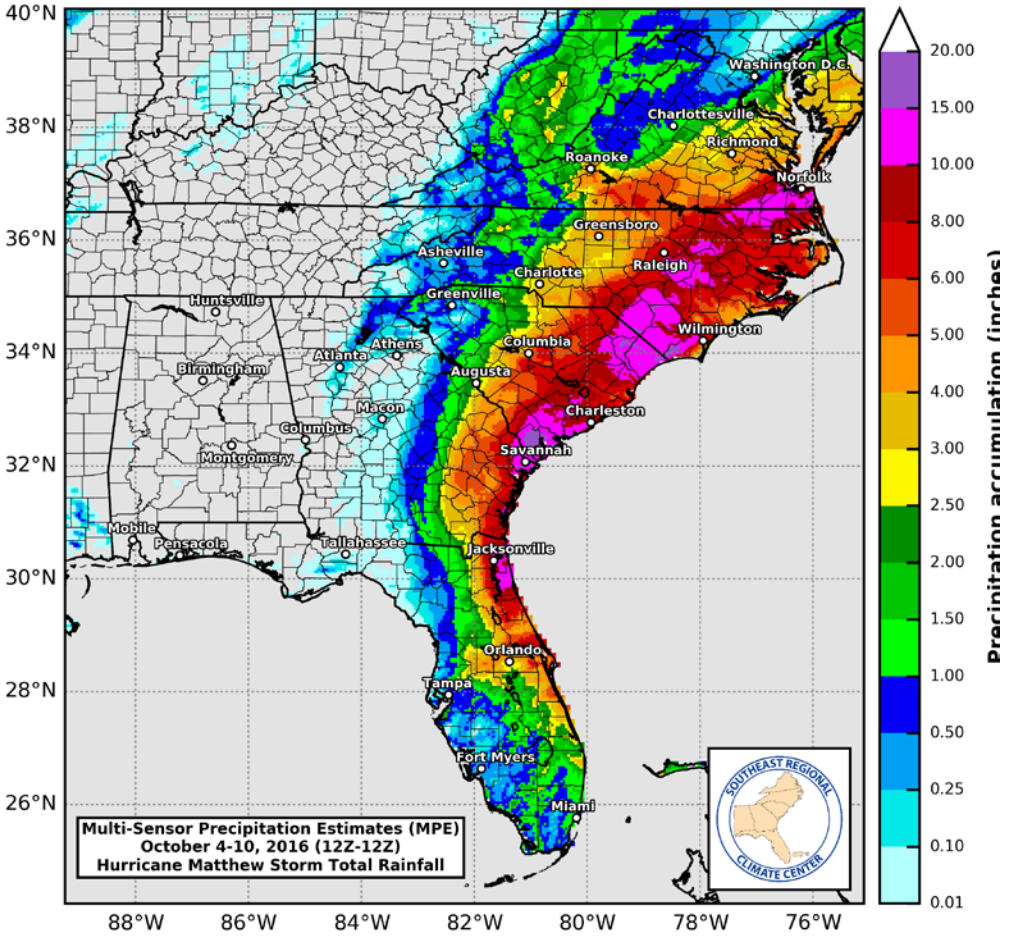

Figure 6.8. Total rainfall from Hurricane Matthew during October 4–10, 2016. The map shows multi-sensor precipitation estimates. (Source: Southeast Regional Climate Center 2016)

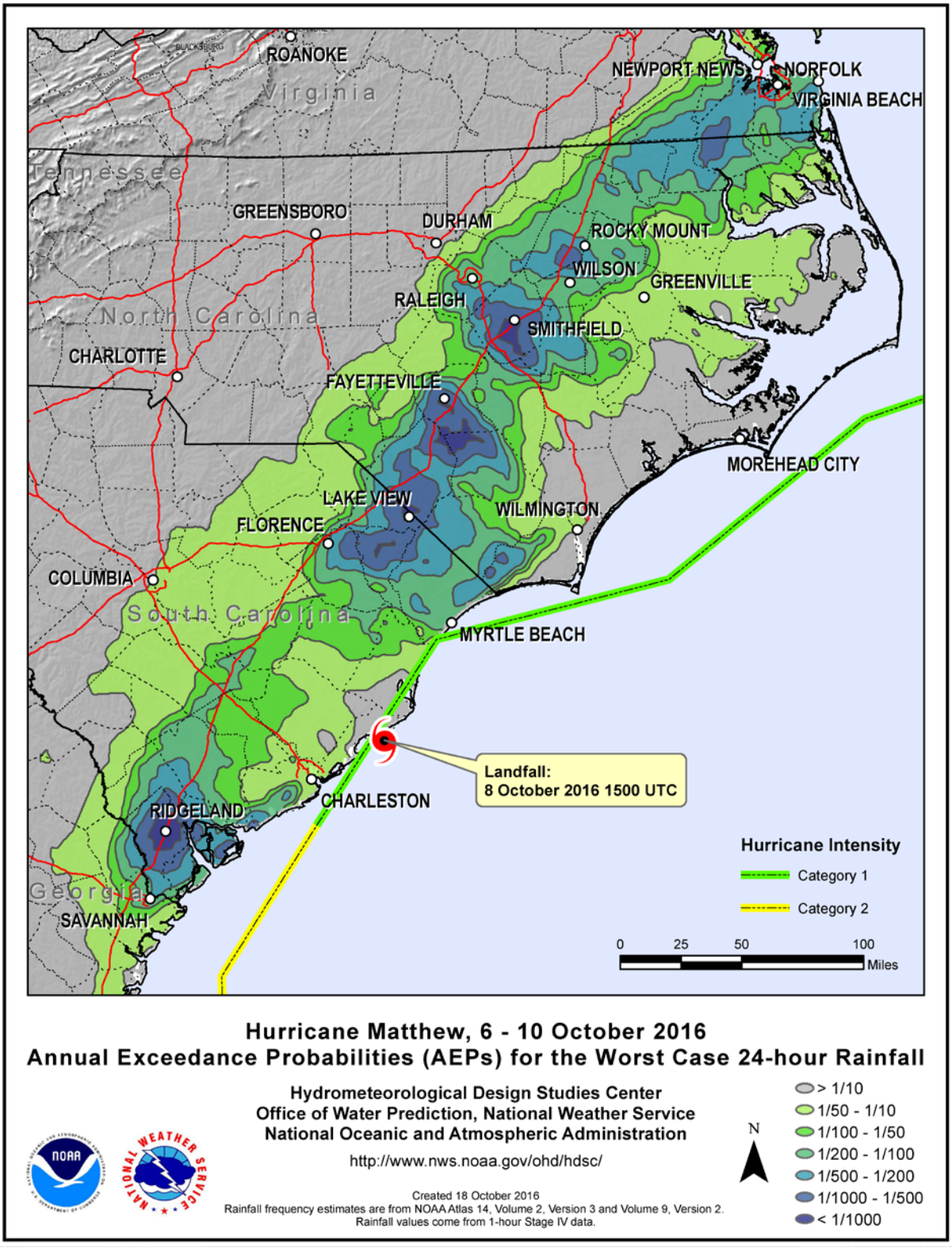

Figure 6.9. Annual exceedance probabilities of worst-case 24-h rainfall from Hurricane Matthew. (Source: NWS 2016)

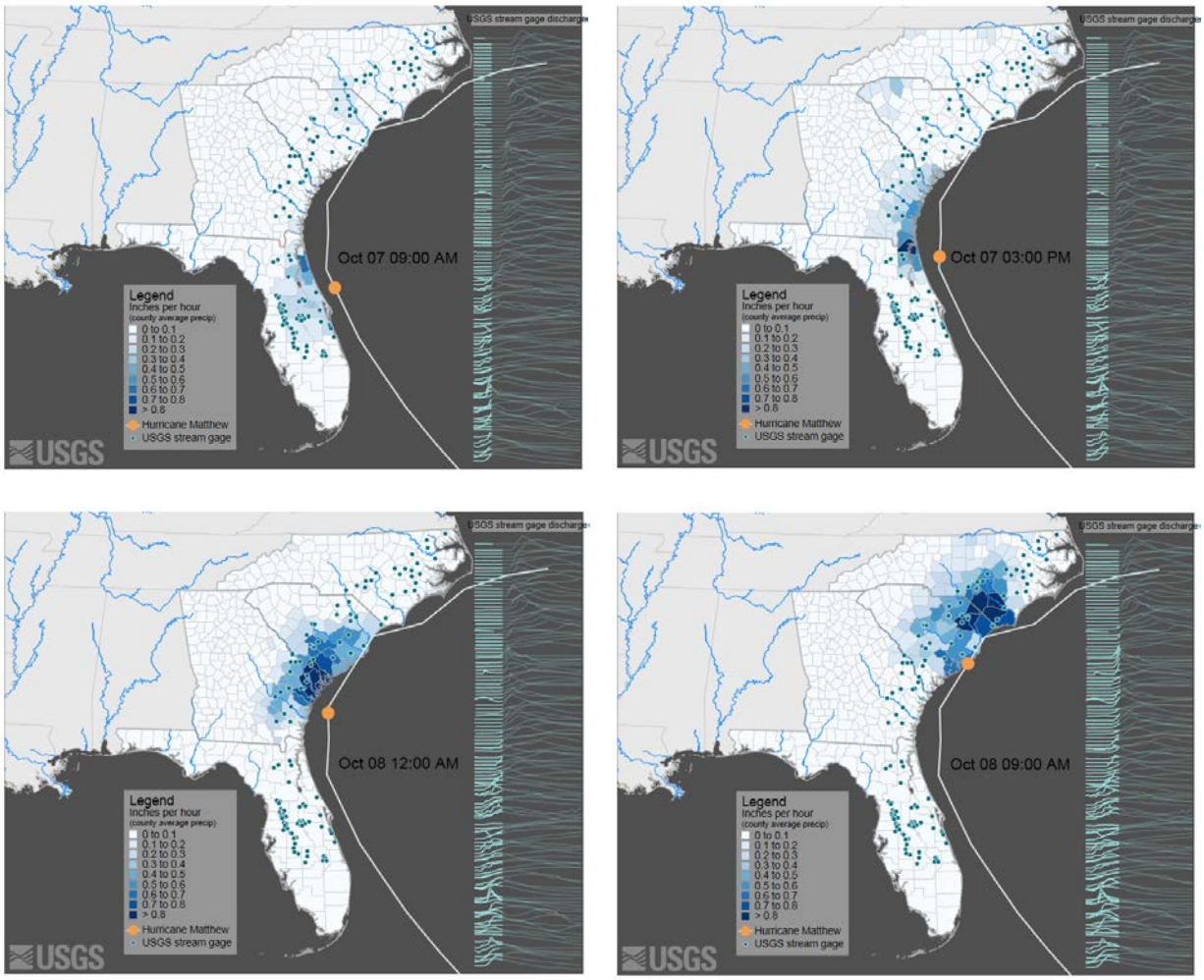

Figure 6.10. Precipitation intensity and streamflow during the progression of Hurricane Matthew. October 7, 2016 at 9:00 am (upper left) and 3:00 pm (upper right) and October 8, 2016 at 12:00 am (lower left) and 9:00am (lower right). (Source: USGS 2016a)

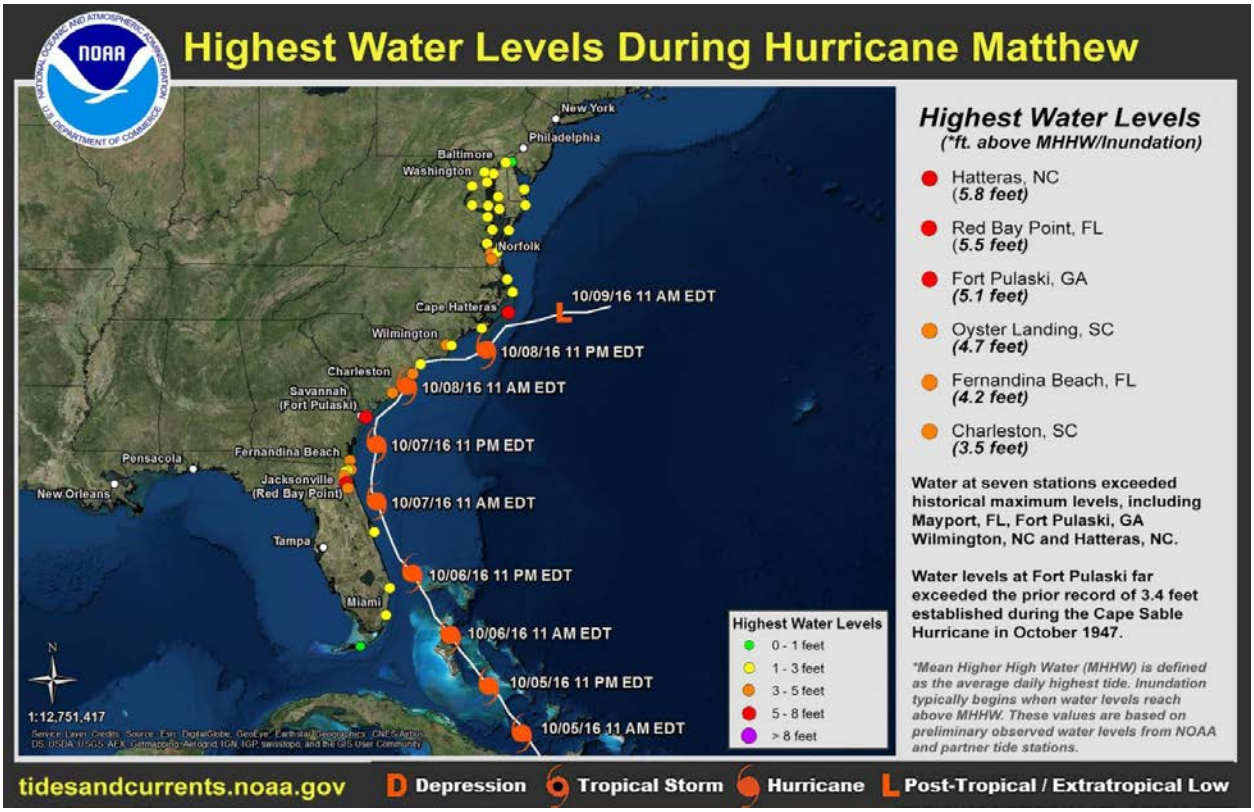

Figure 6.11. Storm surge recorded during Hurricane Matthew. (Source: NOAA 2016a)

Neuse River at Kinston, North Carolina (70 mi southeast of Raleigh, North Carolina; Figure 6.12) exceeded its historical peak stage of 27.7 ft previously recorded during Hurricane Floyd on September 22, 1999, to reach a stage of 28.3 ft on October 14, 2016 (Figure 6.13). On other nearby streams and rivers, peak stages approached the historical peak stage recorded during Hurricane Floyd.

Musser et al. (2017) analyzed 24 streamflow gauges after Hurricane Matthew-generated floods. They reported that new gauge height records were set at 14 of the 24 gauges. At five gauges (all unregulated), the peak discharges during October 2016 were estimated to have AEPs less than 0.002. At another nine gauges (6 unregulated), AEPs for peak discharges were estimated to be between 0.002 and 0.01.

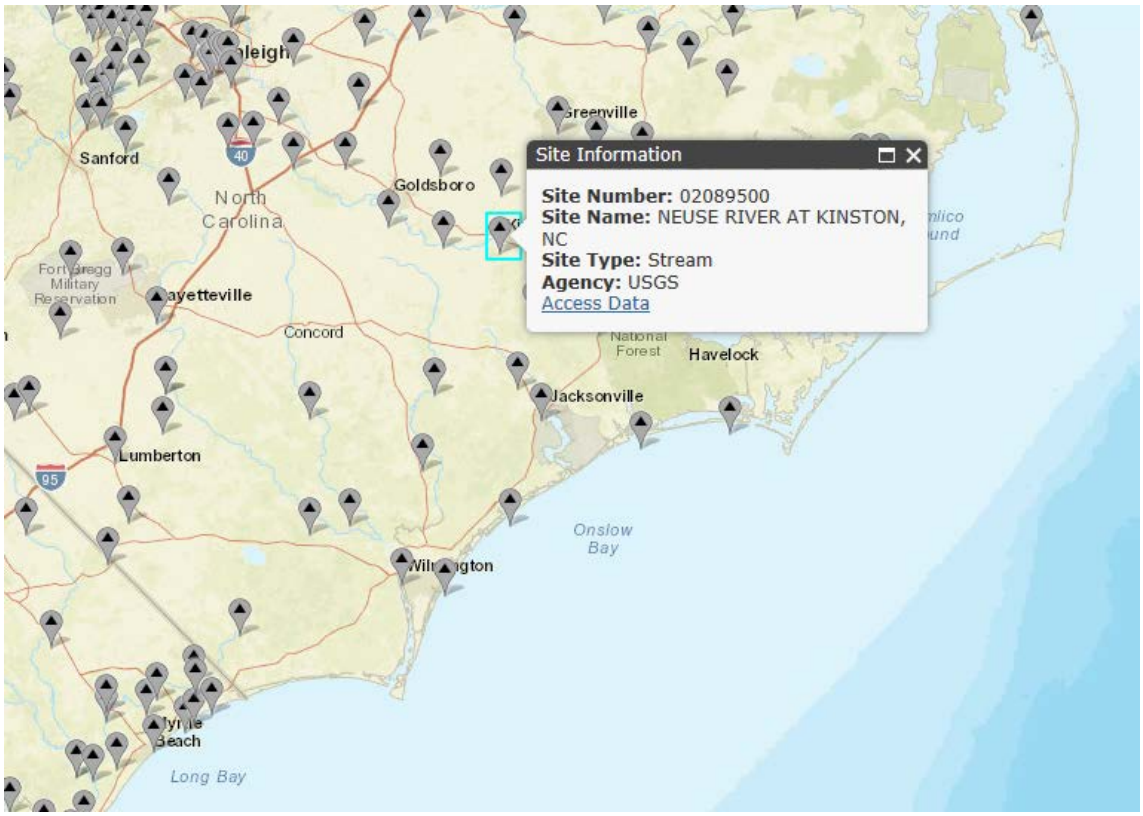

Figure 6.12. Location of Neuse River streamflow gauge at Kinston, North Carolina. (Source: USGS 2016b)

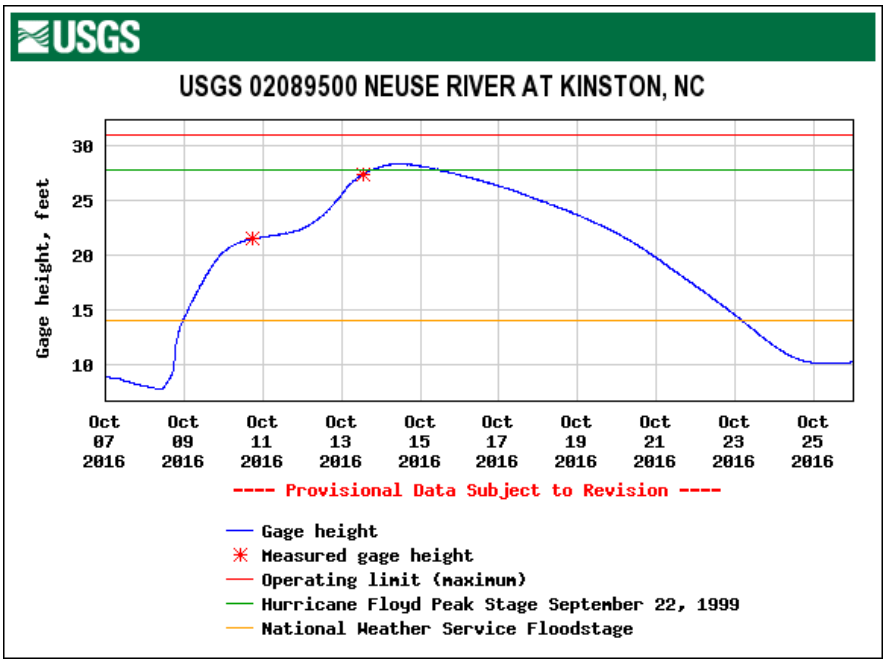

Figure 6.13. Flooding in Neuse River during Hurricane Matthew. (Source: USGS National Water Information System 2016c)

6.2 Hydrologic Cycle, Streamflow, and Floods

By the end of this century, the magnitudes of spring precipitation over the northern portions of the Southeast Region are projected to increase moderately for RCP 2.6 scenario (Figure 6.14). The other seasons do not show appreciable projected changes. For the RCP 8.5 scenario, the magnitude of winter and spring precipitation over the northern parts of the region are projected to increase significantly, and summer precipitation over the southern portion of the region is projected to decrease significantly; fall precipitation over the Florida peninsula is projected to moderately increase.

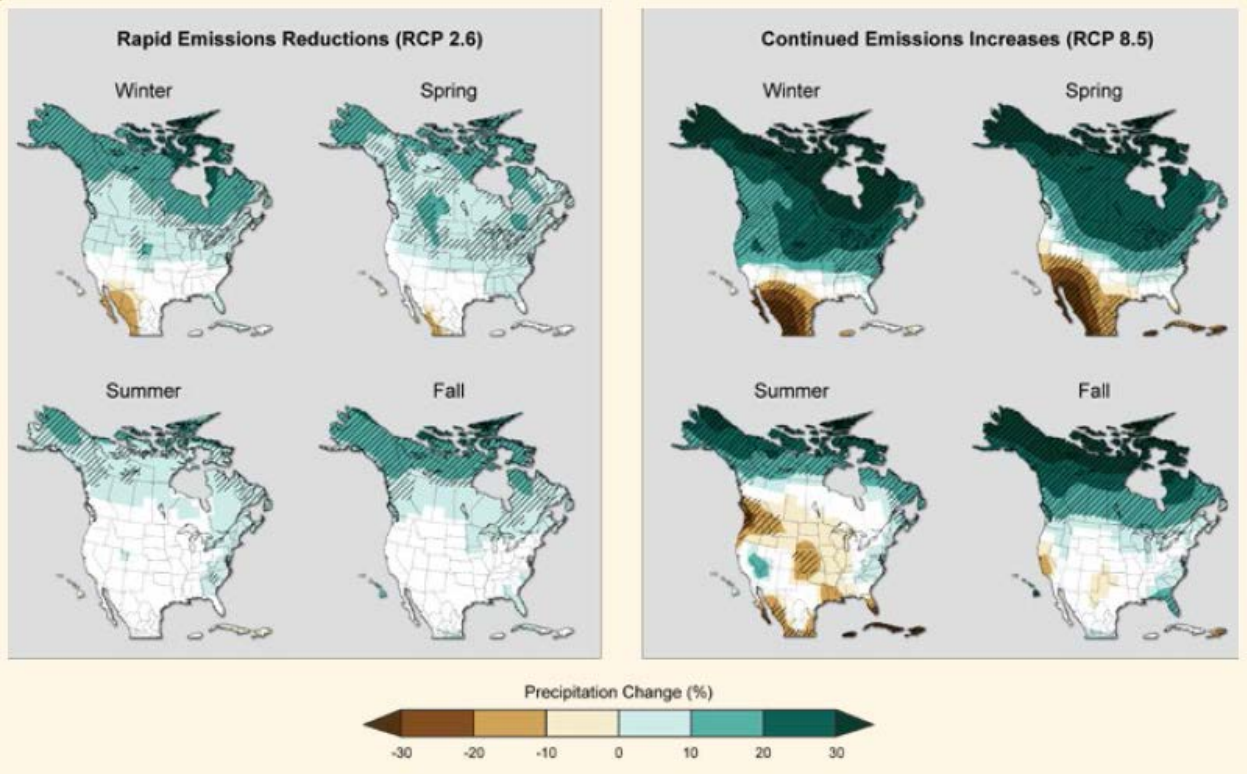

Figure 6.14. Projected changes in mean precipitation for four seasons from CMIP5 models using two emission scenarios corresponding to a climate forcing of 2.6 Wm^{-2} and 8.5 Wm^{-2} by the end of the 21st century. (Source: Melillo et al. 2014)

Changes in extreme precipitation event frequency have been examined by USGCRP (2017) for 2-day duration and 5-year return events. In the Southeast Region, the frequency of extreme precipitation is projected to increase by more than double the historical frequency under the RCP8.5 scenario by the end of the 21st century (Figure 6.15). Besides frequency, extreme precipitation intensity based on the 20-year return period daily precipitation amount is also projected to increase. For RCP8.5, this amounts to a 20 percent increase over the Southeast Region by the late century (see Figure 3.8).

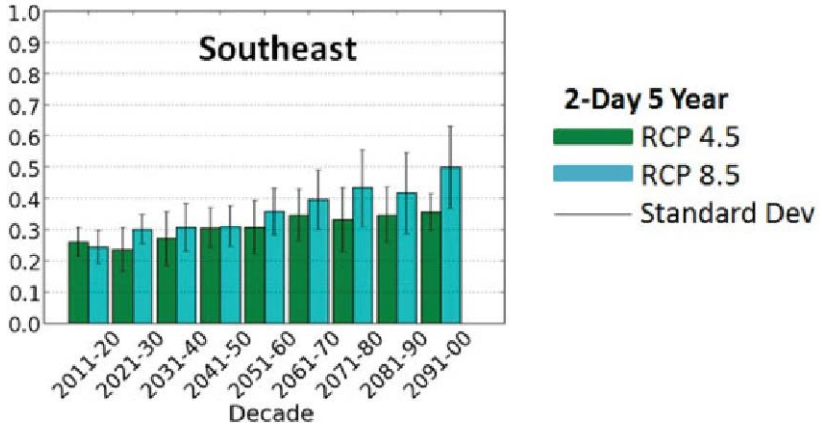

Figure 6.15. Extreme precipitation event frequency for RCP4.5 (green) and RCP8.5 (blue) for 2-day duration and 5-year return events for the Southeast Region. Calculations are for 2006–2100; however, decadal anomalies begin in 2011. Error bars are ±1 standard deviation. (Source: USGCRP 2017)

With the modest increase in mean precipitation (Figure 6.16), evapotranspiration (ET) in a warmer climate will likely outpace the precipitation increases, leading to drier soil.

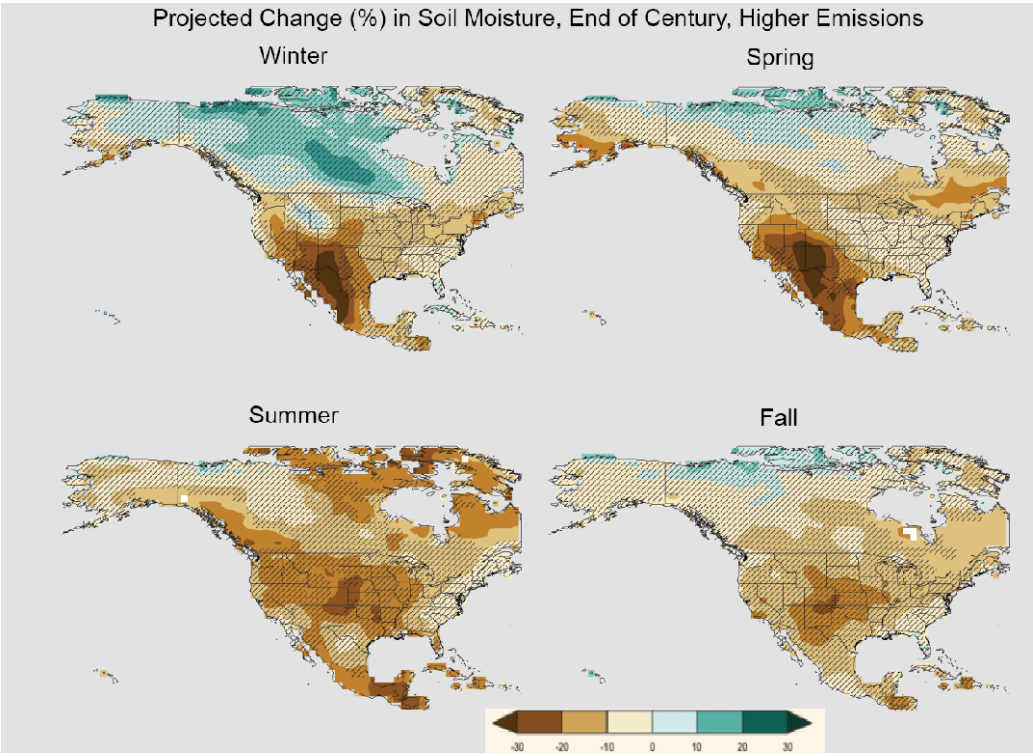

Figure 6.16. Projected end of the 21st century weighted CMIP5 multimodel average percent changes in near surface seasonal soil moisture under the RCP8.5 scenario. Stippling indicates that changes are assessed to be large compared to natural variations. Hashing indicates that changes are assessed to be small compared to natural variations. Blank regions (if any) are where projections are assessed to be inconclusive. (Source: USGCRP 2017)

In the Southeast Region, soil moisture is projected to decrease by up to 20 percent in some regions during summer in the RCP8.5 scenario by the end of the century (Figure 6.17). Compared to other regions, especially the southwestern United States, the changes in soil moisture in the Southeast Region are rather modest and not statistically significant.

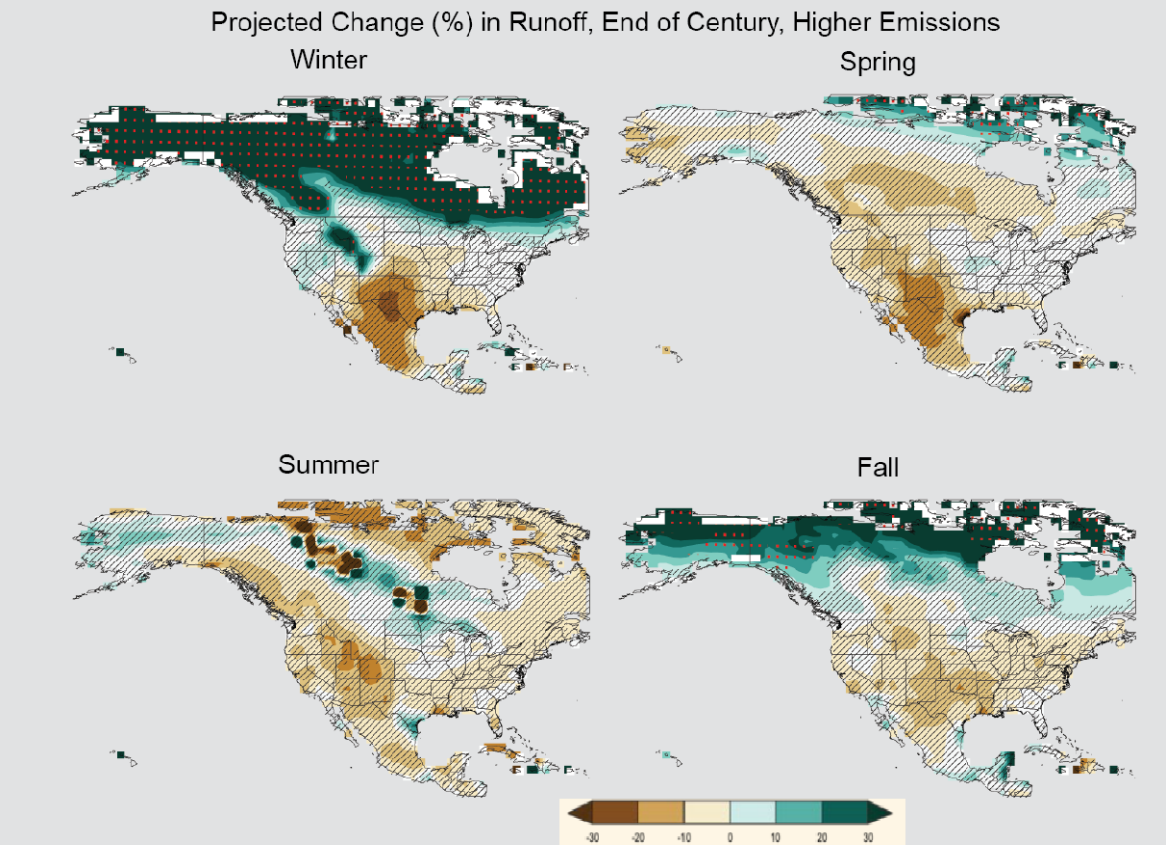

Figure 6.17. Projected end of the 21st century weighted CMIP5 multimodel average percent changes in near surface seasonal runoff under the RCP8.5 scenario. Stippling indicates that changes are assessed to be large compared to natural variations. Hashing indicates that changes are assessed to be small compared to natural variations. Blank regions (if any) are where projections are assessed to be inconclusive. (Source: USGCRP 2017)

Despite precipitation increases (even though small) and soil-moisture reduction leading to increased ET, runoff generally decreases in the Southeast Region in all seasons (Figure 6.18). However, the runoff changes are very small and not statistically significant. The largest changes in seasonal runoff in North America occurred in the mountainous western United States, Alaska, and Canada where warming increases snowmelt in fall and winter, which increases runoff in the two seasons.

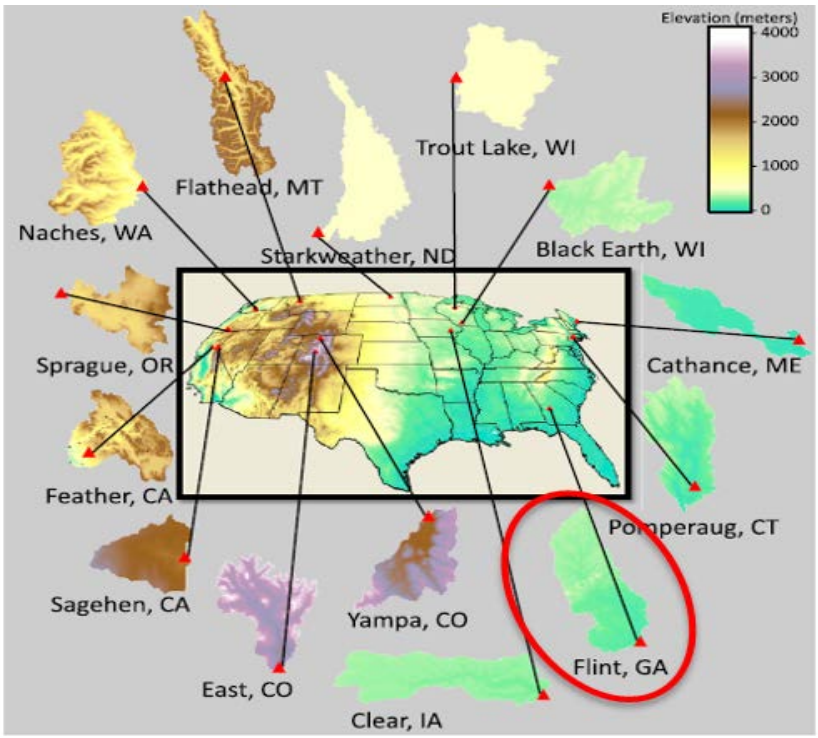

Figure 6.18. Drainage basins studied by Hay et al. (2011). The Flint River basin located in Georgia was the only one within the Southeast Region. (Source: Hay et al. 2011)

Several recent studies have attempted to assess the impacts of climate change on hydrology in the Southeast Region. Hay et al. (2011) and Viger et al. (2011) examined the potential effects of urbanization and climate change on freshwater resources in the Flint River basin located in Georgia. Hay et al. (2011) used a calibrated Precipitation-Runoff Modeling System (PRMS) model with statistically downscaled Coupled Model Intercomparison Project Phase 3 (CMIP3) GCM) scenarios to evaluate the hydrologic response of 14 drainage basins from different hydroclimatic regions across the United States (Figure 6.19).

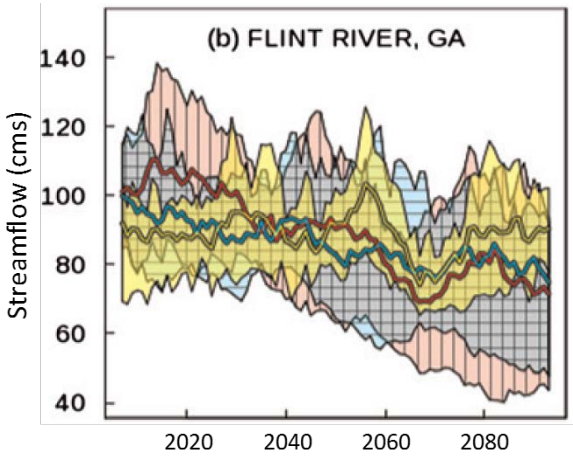

Figure 6.19. Range of 11-year moving mean daily streamflow for the Flint River basin. Red, blue, and yellow refer to emission scenarios A2, A1B, and B1, respectively. The correspondingly colored shaded areas show the maximum and minimum of simulated mean daily streamflow. (Adapted from Hays et al. 2011, Figure 10)

In the Southeast Region, they evaluated the response of the Flint River basin in Georgia. The Flint River basin is 2,900 mi^2 (7,511 km^2) in area with elevation ranging from 295 to 938 ft (90 to 286 m). The PRMS model was calibrated to accurately reproduce mean monthly solar radiation, potential ET, and streamflow for the baseline period of 1988–1999 (Figure 4 of Hay et al. 2011). Mean monthly change factors using a 12-year moving-average window for the 2001–2099 period were computed from five GCMs and three emission scenarios for a total of 1,320 future scenarios (Hay et al. 2011). The daily precipitation and temperature inputs from the baseline were modified using the monthly change factors, with the temporal sequencing remaining unchanged. Therefore, this study evaluated changes in mean climate conditions only (Hay et al. 2011). For the Flint River basin, precipitation had a significant negative trend in two of the three emission scenarios and all three emission scenarios showed significant positive trends in temperatures and ET. Streamflow and soil moisture showed negative trends (Figure 6.6). Peak monthly streamflow, which historically occurs in March with a secondary peak in July, showed declines for all emission scenarios. However, the authors noted that there were numerous sources of uncertainties in the simulations (i.e., in the GCMs, the downscaling techniques, and the hydrologic model itself) (Hay et al. 2011).

Viger et al. (2011) evaluated the effects of climate change and urbanization on the Flint River basin using the same model used by Hay et al. (2011). The future trend of land cover was estimated using the USGS landcover data with process-based and statistical extrapolation techniques (Viger et al. 2011). The authors noted that the estimated future landcover estimates underestimated the low and overestimated the high levels of imperviousness. Projected urbanization for 2006 to 2050 was obtained from the estimated trend reported by Viger et al. (2011). Climate change factors for 2001–2045 (12-year moving windows) were

obtained from Hay et al. (2011). Using the same five GCMs and three emission scenarios used by Hay et al. (2011) in combination with the 45 moving windows, the authors performed 675 PRMS simulations (Viger et al. 2011). Using these simulations, Viger et al. (2011) evaluated three configurations: effects of changes in urbanization, effects of changes in climate under constant urbanization, and effects of changes in urbanization and climate. For the first configuration, Viger et al. (2011) used PRMS simulations that used the baseline (1988–1999) climate input and 45 alternative urbanization scenarios. The results indicated that mean annual streamflow increased slightly with a corresponding increase in the surface runoff component of the water balance with ET and groundwater and subsurface flow decreasing. The authors evaluated these trends to be significant (Viger et al. 2011).

For the second configuration, Viger et al. (2011) used essentially the same approach as that of Hay et al. (2011) and reported that all GCM simulations showed increases in temperatures and highly variable precipitation projections, both positive and negative, but not statistically significant. The mean annual streamflow showed a decrease for all scenarios and two were statistically significant (Figure 6.20).

For the third configuration, Viger et al. (2011) reported that mean annual streamflow decreases for two of the three emission scenarios although none of the changes were statistically significant. Mean annual surface runoff increased for all scenarios, and the changes were statistically significant. Mean annual subsurface flow decreased for all scenarios and two were statistically significant. Mean annual groundwater flow decreased for all scenarios and one was statistically significant. The authors concluded that the impact of climate change and urbanization taken together is less clear because of corresponding offsetting changes in runoff and groundwater flows (Viger et al. 2011; Figure 6.21). The authors also noted that the large degree of uncertainty in GCM-projected precipitation also contributes to interpreting trends in streamflow (Viger et al. 2011).

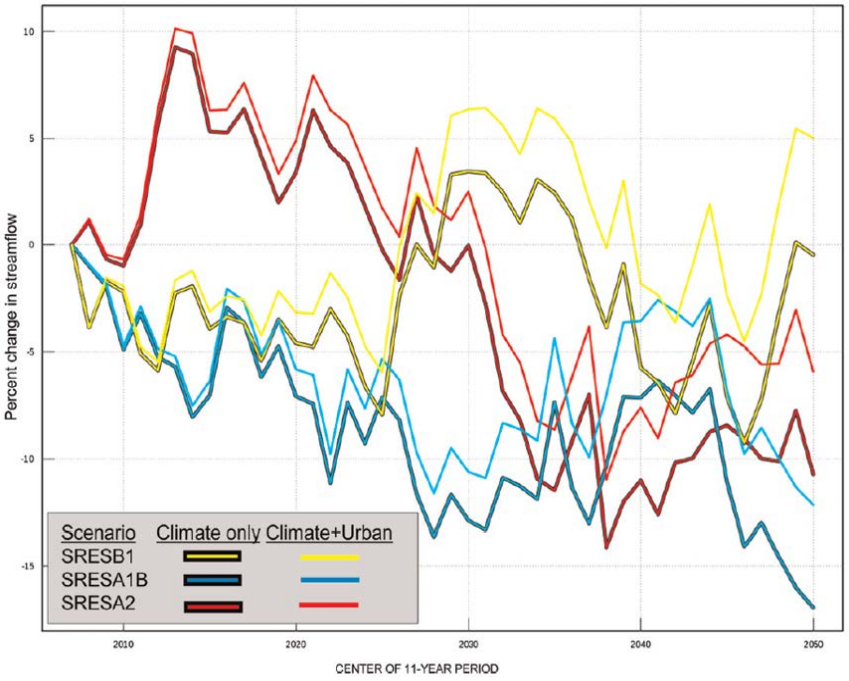

Figure 6.20. Changes in 11-year moving mean daily streamflow for climate-only and climate and urbanization changes. (Adapted from Viger et al. 2011, Figure 11)

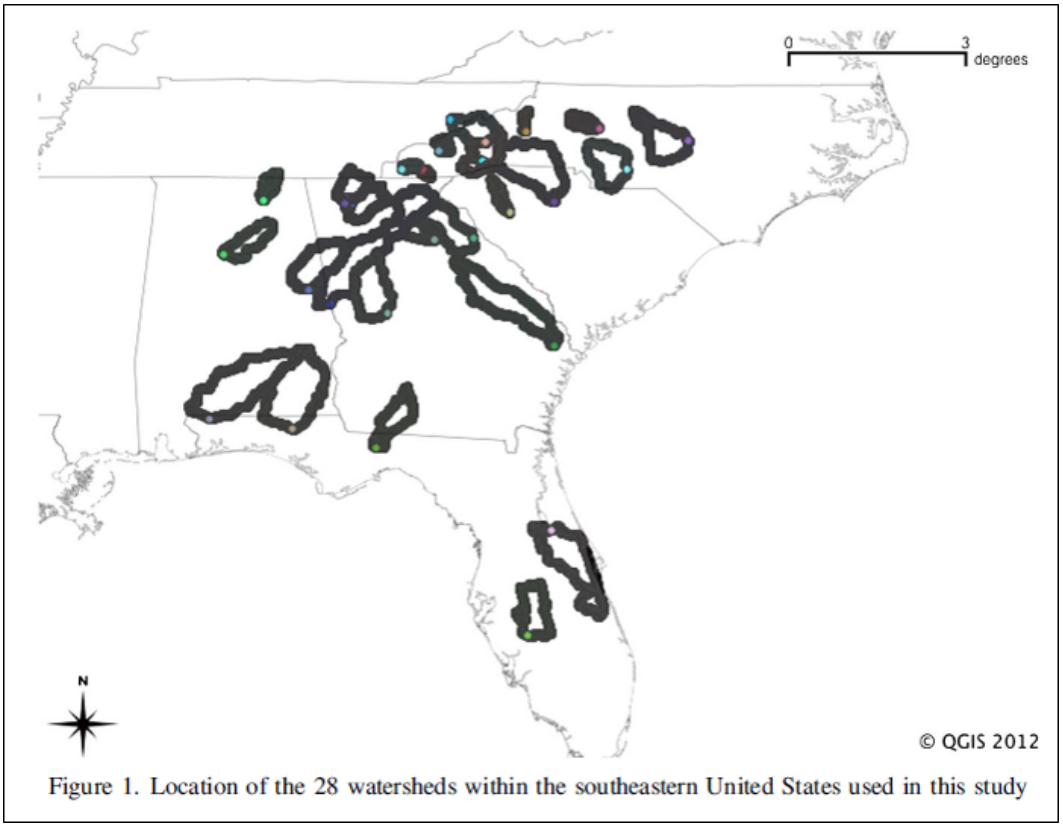

Figure 1. Location of the 28 watersheds within the southeastern United States used in this study

Figure 6.21. Southeastern U.S. watersheds studied by Bastola (2013). (Adapted from Bastola and Misra [2014], Figure 1)

Bastola (2013) assessed the impacts of climate change on 28 southeastern U.S. watersheds that have minimal human intervention, using CMIP3 and CMIP5 outputs (Figure 6.22). Three CMIP3 scenarios (A1B, A2, and B1) and four CMIP5 scenarios (RCP2.6, RCP4.5, RCP6.0, and RCP8.5) were used (Bastola 2013). The author used monthly temperature and precipitation data from 1961 to 2100 for 17 CMIP3 GCMs and 22 CMIP5 GCMs (Bastola 2013). All model outputs were regridded at 2.5° × 2.5° resolution. Bastola (2013) used three 2.5° × 2.5° grid cells to estimate monthly change factors for precipitation and temperature for three 20-year periods—the 2020s (2011–2030), 2050s (2041–2060), and 2070s (2061–2080). The change factors showed considerable variation among GCMs using the same emission scenarios. All models showed increases in future temperatures (Figure 1 of Bastola 2013) but disagreed on magnitude and change in precipitation (Figure 2 of Bastola 2013). A total of 100 daily future climate scenarios were generated using the Weather Generators model by sampling the distribution of change factors of temperature and precipitation; potential ET was estimated using Hargreaves' method (Bastola 2013) (Figure 6.22). The author used three hydrologic models: the HYdrologic MODel (Boyle 2001), Nedbør-Afstrømnings Model (Madsen 2000), and TANK (Sugawara 1995) with calibrated model parameters for the 28 watersheds from Bastola and Misra (2013). Spring (March-April-May) and summer (June-July-August) streamflow decreased for the 2070s for the CMIP3 scenarios for all watersheds; fall (September-October-November) streamflow increased for all but three small watersheds in North Carolina (Bastola 2013). CMIP5 scenarios showed an increase in streamflow for all seasons except for the spring streamflow under high-end emission scenarios (Bastola 2013). The author concluded that uncertainty in streamflow prediction remains high, even when approaching mean streamflow, and attributed some of this uncertainty to both the GCMs and the hydrologic models, the uncertainty in the latter partly arising from variability in the wetness index, or the ratio of precipitation to potential ET (Bastola 2013).

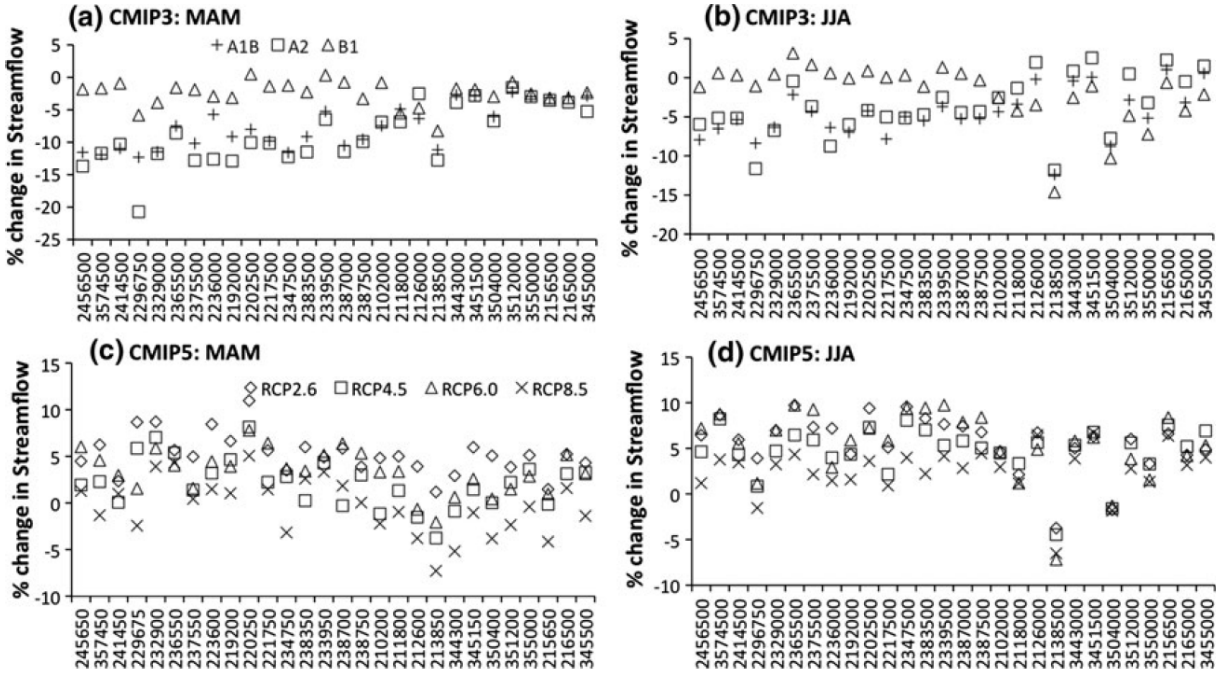

Figure 6.22. Percent change in sprint (MAM) and summer (JJA) streamflow for CMIP3 scenarios (top panels) and CMIP5 scenarios (bottom panel). The numbers on the horizontal axes are watershed IDs. (Adapted from Bastola 2013)

Sun et al. (2015) examined the effects of urbanization and climate change on streamflow in the Upper Neuse River basin in North Carolina that is expected to undergo rapid urbanization in the next 25 years. The A1B emission scenario from CMIP3 was used with two GCM outputs (Sun et al. 2015). Historical climate data for 1961–2010 were derived from the Precipitation Elevation Regression on Independent Slopes Model (PRISM; Daly et al. 2008). The U.S. Department of Agriculture's Water-Supply Stress Index (WaSSI) model was used to simulate six scenarios: two historic climate scenarios with baseline (2006) land use and 2005 population and 50 percent of forests converted to urban land use with 2050 A1B population, and two GCM model scenarios with the above two land use and population scenarios (Sun et al. 2015). The two GCMs represented an increase in precipitation and potential ET and a decrease in precipitation and increase in potential ET, respectively (Sun et al. 2015). Two hydrologic variables were evaluated for the six alternative scenarios—water yield from the Upper Neuse River basin (essentially streamflow) and water-supply stress that accounts for increased water use with growing population (Sun et al. 2015). The authors reported that streamflow increased 8 percent from baseline when 50 percent of forests were converted to urban land use. Using the first GCM scenario, because increases in precipitation and ET were comparable, the streamflow did not change significantly. However, streamflow decreased significantly, by 25 percent, for the second GCM scenario. Under urbanization, streamflow increased moderately but did not fully offset streamflow reduction of the second climate scenario (Sun et al. 2015). WaSSI was estimated to be 0.287 (28.7 percent withdrawal) and decreased under the urbanization only scenario resulting from the increase in streamflow. Under both GCM scenarios with baseline land use but increased population, WaSSI increased to 0.3 and 0.458, respectively. Increased urbanization reduced the WaSSI but not significantly (Sun et al. 2015).

6.3 Flooding in the Southeast Region – The NRC Context

- Depending on future emissions scenarios, seasonal precipitation shows moderate to significant decreases in magnitude.
- Very heavy precipitation events are projected to increase in frequency.
- Annual maximum precipitation is expected to increase in magnitude.
- Urbanization and changing land use may result in changes in runoff.

As stated above, many hydrometeorologic parameters that influence floods are not directly addressed in the NCAs. Some of the studies summarized above have attempted to investigate the impacts of climate change on runoff characteristics in the Southeast Region. However, most of these studies used mean streamflow indicators (i.e., mean annual, seasonal, or monthly flows). Floods of interest to the NRC, particularly for safety analysis and review, include those that occur at significantly shorter timescales (hours to days) and almost always are in the tails of the distribution, away from the mean. Therefore, direct conclusions regarding shorter-duration, lower-frequency floods of interest to NRC are difficult to draw. In addition, uncertainties arising from GCM differences, uncertainties in hydrologic models, uncertainties in socioeconomic responses, and uncertainties in water management can further complicate assessment of future floods.

Nevertheless, certain conclusions can be made that will give the NRC greater insights into flood analyses and their review. First, a site-specific analysis should be performed to assess the impacts of climate change on the behavior of floods. If frequency analyses are used, explicit accounting for non-stationarity in precipitation, land use, and/or flood data should be employed to ensure attribution of causative factors. A change in the mean behavior of floods can also reflect a change in the behavior in the tails. It is clear that the practical resolution of GCMs is going to remain incompatible with the need for a local-to-

regional-scale flood assessment. Therefore, further investigations, which may include exploring dynamical downscaling and nesting of hydrological models, are needed to couple the outputs of GCMs to hydrologic models.

Second, significant uncertainty in predictions of hydrologic models (both aleatory and epistemic) will exist for the foreseeable future and can directly affect estimates of flood magnitues under altered climate scenarios. A clear framework for enumerating and attributing the sources of these uncertainties, explicitly accounting for these uncertainties in flood estimation approaches, and propagating the uncertainties throughout flood analyses should be used. This framework will assist the NRC in investing resources to improve the parts of a flood assessment where uncertainties can be reduced given newer data sets and additional information. Given that climate change research, hydrologic understanding including newer data sets, and water-management practices are expected to continually evolve, a periodic refinement of site-specific flood assessments should be made.

Third, a site-specific flood-protection and mitigation assessment will be very useful from a safety perspective. It is noted that NRC current practice for permit and license application reviews relies on site-specific hydrologic engineering assessments that include both floods caused by multiple mechanisms relevant for the site and low-water issues. The site-specific flood assessment, including quantification of associated uncertainties, can facilitate clear articulation of risk faced by a plant and provide useful information for risk-informed licensing decisions.

6.4 Low Flows in the Southeast Region – The NRC Context

- Streamflow is expected to decline.
- Urbanization and population growth may increase stress on water supplies.

As stated above, many hydrometeorologic parameters that influence low flows are not directly addressed in the NCAs. Some of the studies summarized above have attempted to investigate the impacts of climate change on runoff characteristics in the Southeast Region. However, most of these studies used mean streamflow indicators (i.e., mean annual, seasonal, or monthly flows). These metrics are useful to the NRC in the review of water use and environmental impacts of plants. Additional low-flow metrics that are useful to the NRC include persistence and frequency of low flows, both seasonally and in the context of multi-year low-flow events, and are not directly addressed in current studies.

Site-specific assessments may be needed to assess the characteristics of low-flow metrics under climate change scenarios. Some large-scale atmospheric patterns (e.g., the Bermuda/Azores High) affect low-flow events in the Southeast Region. Regional and local characteristics, including streamflow generation, urbanization and population growth, and water-management practices, would influence low flows at spatiotemporal scales of interest to NRC licensing. Dynamically downscaled GCM outputs, nested climate and hydrologic modeling, and inclusion of water-management practices in low-flow assessments would be needed, with particular focus on seasonal to interannual persistence of low flows, to support NRC licensing.

As stated before, uncertainties in all aspects of climate hydrology assessments are expected to exist at significant levels for the foreseeable future. Given these uncertainties, decision-making would benefit from a framework for enumerating and attributing the sources of these uncertainties, explicitly accounting for these uncertainties in hydrologic estimation approaches and propagating the uncertainties throughout hydrologic analyses. This framework will assist the NRC in investing resources to improve the parts of

low-flow assessment where uncertainties can be reduced given newer data sets and additional information. A periodic refinement of site-specific low-flow assessments can assist plants in mitigating the effects of sustained low-flow events on energy production and the environment.

6.5 Summary and Discussion

The NCA has provided useful information about projected changes in precipitation, runoff, and soil moisture from climate models. To bridge between climate projections that are typically made at a grid resolution between 50 and 200 km and hydrologic information needed to assess climate change impacts on water resources, some hydrologic modeling studies provide projections of hydrologic parameters such as streamflow, snowpack, and soil moisture in small river basins. Overall, warming in the future can lead to changes in precipitation, runoff, and soil moisture in the Southeast Region. More specifically, increases in extreme precipitation have implications for floods. Besides warming, urbanization and land use change could also affect the hydrologic characteristics through changes in both water demand and water supply. In general, previous studies examined mean changes rather than hydrologic extremes, and were not performed at the site level; thus, future studies are needed to assess hydrologic changes in the Southeast Region at spatial and temporal scales more relevant to NRC needs.

Projections of future changes in flooding are often generated using offline hydrologic models driven by climate model outputs, rather than by analyzing the changes in ET, soil moisture, snowpack, and runoff directly simulated by the climate models. With offline modeling, hydrologic simulations can be performed at higher spatial resolutions than afforded by global climate models, and this is deemed important because hydrologic processes are strongly influenced by surface heterogeneity, such as that associated with topography, soil, and vegetation. In addition, the climate model outputs could be bias-corrected and spatially downscaled based on observations to provide more realistic atmospheric forcing for the hydrologic models to simulate the hydrologic regimes of the present climate. However, it is noteworthy to mention that Milly and Dunne (2016) cautioned against the use of offline analyses of climate model outputs for estimation of hydrologic changes driven by climate change. They noted that the Penman-Monteith equation that is often used to calculate potential ET (PET) using inputs from climate model outputs severely overpredicts the changes in non-water-stressed ET computed in climate models. The overprediction is partly due to the neglect of the stomatal conductance reductions as carbon dioxide concentrations increase in the future. Hence, the use of the Penman-Monteith method in offline modeling could lead to an overprediction of drying in offline calculation of aridity and low-flow indices and offline hydrologic modeling of runoff. While Milly and Dunne (2016) recommended the direct examination of climate model simulated variables to evaluate drying trends and hydrologic changes in the future, biases and uncertainties in climate models have implications when assessing hydrologic changes, so key challenges remain.

Berghuijs et al. (2016) studied the flood-generating mechanisms using observed data from over 400 catchments in the United States. Their analysis suggested that in the Southeast Region, flooding is primarily caused by (1) the single largest precipitation excess event (i.e., precipitation in excess of the soil-moisture storage capacity) or (2) the single largest precipitation event independent of the pre-event antecedent soil-moisture storage. In the former mechanism, antecedent soil-moisture storage is the primary control of runoff generation in flood events; while in the latter, runoff generation associated with floods can be infiltrated by excess overland flow, preferential subsurface flow, saturation excess overland flow, and fill and spill flow for soil with very small storage capacities. These flood-generating mechanisms have important implications for what processes must be modeled accurately to simulate the present and future hydrologic conditions. For example, for areas where the single largest precipitation event is important for flood generation, the inability of the climate models to simulate the precipitation characteristics, including frequency and intensity, could present challenges for assessing flood risk. Due to the relatively coarse spatial resolution, global models have the tendency to produce more drizzles or light rain and not enough intense precipitation (Stephens et al. 2010).

In general, the climate research community has not focused on evaluating trends and impacts of meteorological (and by extension, hydrologic) events of exceedance probabilities that are of interest to the NRC for permitting and licensing. The assessment of trends and impact at annual exceedance probablilities of interest to NRC also is limited by the fact that current climate models have significantly larger uncertainties for these events, therefore limiting the usefulness of predictions that may have large uncertainties. Moreover, uncertainties in climate model predictions are carried through and combined with uncertainties in hydrologic and hydraulic modeling approaches employed in hydrologic engineering assessments including PFHAs. Therefore, a consistent framework for enumerating, attributing, and incorporating these uncertainties, both in climate models and in hydrologic engineering assessments, should be used in site-specific PFHAs for permitting and licensing to clearly articulate the confidence associated with predictions at low annual exceedance probabilities.

7.0 Status of Climate Modeling and Federal Agency Activities

The USGCRP has a legal mandate to conduct an NCA every 4 years.[1] The third national climate assessment, NCA3, was released in May 2014 (Melillo et al. 2014). The fourth assessment, NCA4, was published in 2017 and 2018 (USGCRP 2017, 2018). This NRC Climate Change Annual Report has incorporated significant information from the NCAs. More specifically, USGCRP (2017) provide an update of the physical climate science presented in NCA3, including updated climate science findings and projections important to the authors of NCA4.

While NCA4 uses climate projections largely from CMIP5 that contributed to IPCC AR5, the CMIP6 experimental protocols have been finalized and summarized in the *Geoscientific Model Development* Special Issue on "Coupled Model Intercomparison Project Phase 6 (CMIP6) Experimental Design and Organization."[2] This special issue consists of 27 peer-reviewed papers that provide an overview of the CMIP6 experimental design and organization and more detailed descriptions of model intercomparison projects on specific topics that contribute to CMIP6. The IPCC Working Group I on the Physical Basis of Climate Change has initiated scoping nomination and other activities.[3] At the same time, several IPCC special reports are under development, including the "Special Report on Climate Change, Desertification, Land Degradation, Sustainable Land Management, Food Security, and Greenhouse Gas Fluxes in Terrestrial Ecosystems" and "Special Report on 1.5°C." In the United States, a set of low warming target simulations has been completed using the Community Earth System Model, including targets of 1.5°C, 2.0°C, and overshoot 1.5°C by 2100.[4]

The U.S. Climate Modeling Summit held the second annual meeting of the six U.S. climate modeling centers during March 9–10, 2016.[5] The purpose of the summit was to improve the coordination and communication of national climate modeling goals and objectives. Representatives from the U.S. "CMIP-class" climate model development centers and from operational climate-prediction programs participated. Specifically, two representatives—one lead and one additional delegate—from each of the following groups were invited to participate in the summit: GFDL CM/ESM, Climate Forecast System, Goddard Institute for Space Studies (GIS Model E), Goddard Earth Observing System (GEOS-5), Community Earth System Model, and Accelerated Climate Model for Energy. The meeting was coordinated by the U.S. Global Change Research Program Interagency Group on Integrative Modeling (IGIM). The next Summit held in June 2017 focused on model intercomparison projects and subseasonal-to-seasonal and decadal predictions. The IGIM also organized a workshop on "IA-IAV-ESM: Toward Multi-Model Frameworks Addressing Multi-Sector Dynamics, Risks, and Resiliency"6 to develop concepts for a modeling framework or architecture to couple impacts, adaptation, and vulnerability (IAV) models; integrated assessment (IA) models; and climate, Earth system, hydrology, land use, demography, and other models.

In April 2016, the U,S, Department of Defense released the report, *Regional Sea-Level Scenarios for Coastal Risk Management: Managing the Uncertainty of Future Sea-Level Change and Extreme Water Levels for DoD Coastal Sites Worldwide*[7] (Hall et al. 2016). The report was developed by a multi-agency team of researchers and includes an accompanying online database to provide regionalized sea-level and

[1] http://www.globalchange.gov/what-we-do/assessment
[2] http://www.geosci-model-dev.net/special_issue590.html
[3] http://wg1.ipcc.ch/AR6/AR6.html
[4] Model outputs are available at https://www.earthsystemgrid.org/dataset/ucar.cgd.ccsm4.lowwarming.html
[5] https://climatemodeling.science.energy.gov/sites/default/files/IGIM_CMS_agenda%20_5916.pdf
[6] http://www.globalchange.gov/about/iwgs/igim-resources#IA-IAV-ESM%20Workshop
[7] www.serdp-estcp.org

extreme water-level scenarios for three future time horizons (2035, 2065, and 2100) for 1774 military sites worldwide. Decision-makers can use these scenarios for relative vulnerability or impact assessments at the site level or across several installations or military services.

The U.S. Army Corps of Engineers (USACE) Civil Works recently published the Engineering and Construction Bulletin (ECB) No. 2016-25, "Guidance for Incorporating Climate Change Impacts to Inland Hydrology in Civil Works Studies, Designs, and Projects" (USACE 2016). The ECB recognizes that in some geographical locations and for some impacts that are relevant to the USACE, climate change may be shifting, not only the climatological baseline, but also the natural variability about that baseline (USACE 2016). The ECB noted that projections of climate change and impacts at local scales can be highly uncertain and proposed a qualitative assessment that may assist in future project modifications and consideration of alternatives (USACE 2016). The ECB requires the qualitative analysis to be performed for all hydrologic studies at inland watersheds at the time of its issuance. Figure 7.1 is the flow chart included in ECB No. 2016-25 and lays out the elements of the qualitative analysis.

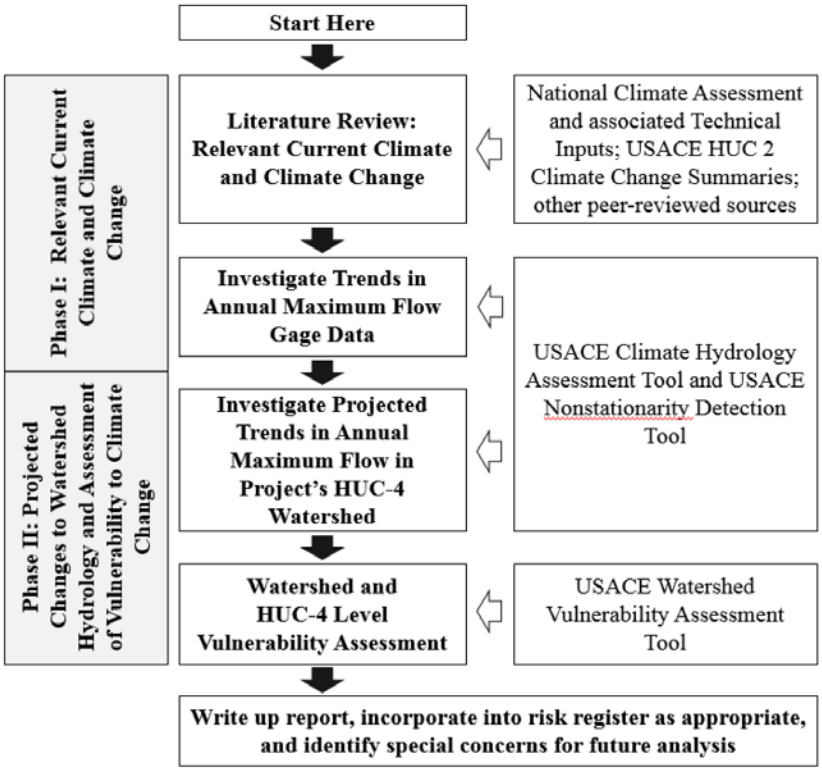

Figure 7.1. Flow chart for qualitative assessment of the impacts of climate change in hydrologic analyses. (Source: USACE 2016)

USACE has also developed a web-based qualitative Climate Hydrology Assessment Tool available publicly at http://corpsclimate.us/ptcih.cfm (USACE 2016). However, USACE cautions users if the tool that the climate hydrology output may be limited in precision, may not adequately represent watershed complexities including snowmelt and regulation, and may only be suitable for watershed-scale decisions (USACE 2016). Examples of the qualitative assessment are included in the ECB (USACE 2016).

At the time of the publication of ECB No. 2016-25, USACE did not require qualitative assessment of climate change impacts on probable maximum flood because substantial research to investigate effects of climate change on a probable maximum flood does not exist yet (USACE 2016).

The USACE also has a "Responses to Climate Change Program" to understand the potential impacts of climate change to natural and human-made systems (USACE 2017). As part of this program, the USACE is preparing 21 regional climate syntheses. These regions are at the scale of a two-digit Hydrologic Unit Code across the continental United States, Alaska, Hawaii, and Puerto Rico (Figure 7.2). The regional syntheses summarize observed and projected climate and hydrological patterns as reported in national and regional reports and peer-reviewed literature. The syntheses for Regions 3, 5, 6, 8, and 11 were published in January 2015, and those of Regions 2 and 12 in May 2015. The syntheses assess the vulnerability of each region to USACE business lines, including navigation, flood risk management, water supply, ecosystem restoration, hydropower, recreation, emergency management, regulatory mission, and military programs against several climate variables including increased ambient temperatures, increased maximum temperatures, increased storm intensity and frequency, and SLR.

In the regional climate syntheses, based on information from a literature review, the USACE summarized the observed and projected changes in climate for the NCA3 Southeast Region (Table 7.1).

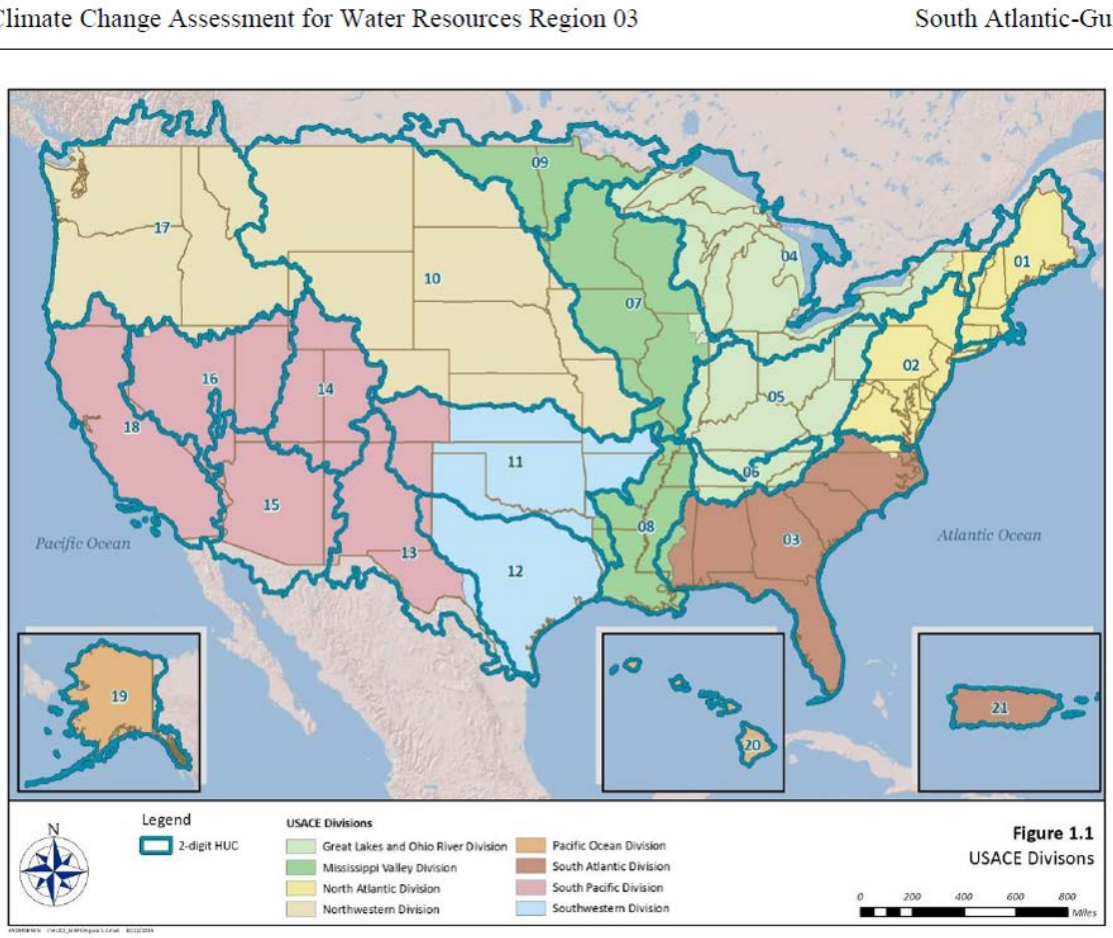

Figure 7.2. Regions used in the USACE Responses to Climate Change Program. The NCA3 Southeast Region consists of the complete USACE Region 3 and parts of Regions 2, 5, 6, 8, 11, and 12. (Source: USACE 2015).

Table 7.1. Summary of USACE conclusions from a literature review performed for the 2-Digit Hydrologic Unit Codes (HUC) comprising the NCA3 Southeast Region

2-Digit HUC	Temperature		Precipitation		Streamflow	
	Observed	**Projected**	**Observed**	**Projected**	**Observed**	**Projected**
02 Mid-Atlantic Region	Annual average temperatures have warmed over the past century, particularly early in the century and in the past 3-4 decades. The mid-Atlantic region appears to be outside of the "warming hole." There is an increasing trend in number of extreme heat days and a decreasing trend in number of extreme cold days.	There is a strong consensus in literature that temperatures in the future would continue rising through the next century.	Over the past century, an upward trend exists in annual total precipitation as well as the frequency and magnitude of storm events.	There is a reasonable consensus in the literature that total annual precipitation as well as the frequency and magnitude of extreme storm events will increase. However, the the extent of these increases is uncertain.	No significant trends in historical streamflow was identified. The apparent paradox that no change in streamflow was identified although precipitation has increased could be attributed to seasonal differences in timing of precipitation and streamflow changes.	There is moderate consensus in literature that peak flows will increases through the 21st century and low flows will decrease. Studies also indicate decreased snowpack and earlier snowmelt.
05 Ohio Region	There is general consensus in the literature that the northern part of the Ohio Region exhibits a century-long warming trend and the southern part exhibits a cooling trend. The geographic extent of the cooling and warming zones are uncertain.	There is a strong consensus in the literature that average and extreme temperatures will increase. However, the amount of increase varies among studies. There may also be considerable spatial variation.	Although there is no clear consensus, multiple studies have identified increasing annual total precipitation and frequency of storms. One study showed that rainfall may have been concentrated in larger storms in the latter half of the 20th century.	Multiple studies project increasing precipitation. However, uncertainty exists regarding the magnitude and spatial distribution of future changes in average and extreme precipitation.	More studies indicated an increasing trend in streamflow over the past 60 years than studies that indicated the opposite.	There is significant variation in projected streamflow across studies.

2-Digit HUC	Temperature		Precipitation		Streamflow	
	Observed	**Projected**	**Observed**	**Projected**	**Observed**	**Projected**
06 Tennessee Region	There is low consensus in the literature that there is a possible warming trend, particularly since 1970, in the Tennessee Region.	There is strong consensus in the literature that projected temperatures show an increasing trend over the next century.	There is no clear consensus in literature; however, multiple studies point to a mild increasing trend in annual total precipitation amount, frequency of storms, and year-to-year variability in precipitation amount.	There is strong consensus in the literature that projected intensity and frequency of extreme storms will increase and there is low consensus that total annual precipitation will change in the Tennessee Region.	No significant trends have been identified in streamflow data for second half of the 20th century.	Projected streamflow in the Tennessee Region shows variability across studies.
08 Lower Mississippi River Region	No significant trend exists in observed mean air temperature but extreme minimum air temperature may be increasing.	There is strong consensus in the literature that projected temperatures show an increasing trend over the next century.	Although clear consensus does not exist, multiple studies have identified a mild upward trend in precipitation.	There is little consensus in literature that projected precipitation in the Lower Mississippi Region show any trend.	Although clear consensus does not exist, multiple studies have identified a mild upward trend in mean streamflow.	Although clear consensus does not exist, multiple studies have identified a mild downward trend in streamflow.
11 Arkansas, White and Red Rivers Region	General consensus exists that mean temperature in the Arkansas, White and Red Rivers Region shows a mild upward trend. However, this trend is spatially variable within the region. While maximum temperatures have remained the same, a slight increase in frequency of minimum temperature was found.	There is strong consensus in the literature that projected mean temperatures show a moderate upward trend and projected maximum temperatures show a significant upward trend.	General consensus exists that average precipitaton and frequency of extreme precipitation show mild upward trends.	General consensus exists that there is no trend in projected annual precipitation. However, there is consensus that projected frequency of extreme precipitation events and the number of consecutive dry days will increase,	General consensus exists that average streamflow shows an upward trend.	Limited consensus exists that there is a downward trend in projected streamflow in portions of the Arkansas, White and Red Rivers Region with the projected trends varying with GCM selection.
12 Texas-Gulf Region	There is low consensus that observed mean temperature in the Texas-Gulf Region shows a slight decreasing trend. A few studies indicate that extreme temperature may show an upward trend.	There is strong consensus in the literature that projected temperatures show an increasing trend over the next century.	General consensus exists that annual precipitaton and frequency of extreme precipitation shows mild increases.	There is little consensus in literature that projected total precipitation in the Texas-Gulf Region show any trend. There is moderate consensus that risk of droughts and the intensity of storm events will increase in the future.	Although clear consensus does not exist, multiple studies have identified a mild upward trend in mean streamflow.	A few studies show that streamflow through the next century will mildly decrease.

8.0 References

Agee E, J Larson, S Childs, and A Marmo. 2016. Spatial redistribution of U.S. tornado activity between 1954 and 2013. *J. Appl. Meteor. Climatol*. 55, 1681–1697, doi: 10.1175/JAMC-D-15-0342.1.

AMAP. 2017. *Snow, Water, Ice and Permafrost. Summary for Policy-makers*. Arctic Monitoring and Asssessment Programme (AMAP), Oslo, Norway, 20pp.

Ashley S. 2007. Spatial and temporal analysis of tornado fatalities in the United States: 1880–2005. Wea. Forecast. 22, 1214-1228, doi: 10.1175/2007WAF2007004.1.

Balaguru K, DR Judi, and LR Leung. 2016. Future hurricane storm surge risk for the U.S. Gulf and Florida coasts based on projections of thermodynamic air-sea potential intensity. *Clim. Change* doi:10.1007/s10584-016-1728-8.

Balaguru K, GR Foltz, and LR Leung. 2018. Increasing magnitude of hurricane rapid intensification in the central and eastern tropical Atlantic. Geophysical Research Letters, 45, doi:10.1029/2018GL077597.

Barnes EA and LM Polvani. 2015. CMIP5 projections of arctic amplification, of the North American/North Atlantic circulation, and of their relationship. *J Clim.* 28 (13), 5254–5271, doi:10.1175/JCLI-D-14-00589.1.

Bastola S. 2013. Hydrologic impacts of future climate change on Southeast US watersheds. *Reg. Environ. Change*, 13, S1, S131-S139, doi: 10.1007/s10113-013-0454-2.

Bastola S and V Misra. 2013. Evaluation of dynamically downscaled reanalysis precipitation data for hydrological application. *Hydrol Process*. doi:10.1002/hyp.9734.

Bengtsson L, K Hodges, and N Keenlyside. 2009. Will extratropical storms intensify in a warmer climate? *J. Clim*. 22, 2276–301.

Berghuijs WR, RA Woods, CJ Hutton, and M Sivapalan. 2016. Dominant flood generating mechanisms across the United States. *Geophys. Res. Lett*. 43, 4382–4390, doi: 10.1002/2016GL06807.

Boyle D. 2001. *Multicriteria calibration of hydrological models*. PhD dissertation. Department of Hydrology and Water Resources, University of Arizona, Tucson, Arizona.

Breaker BK, KM Watson, PA Ensminger, JB Storm, and CE Rose. 2016. *Characterization of peak streamflows and flood inundation of selected areas in Louisiana, Texas, Arkansas, and Mississippi from flood of March 2016*. U.S. Geological Survey Scientific Investigations Report 2016–5162, 33 p. https://doi.org/10.3133/sir20165162.

Brooks HE. 2013. Severe thunderstorms and climate change. *Atmos. Res*. 123, 129–38. doi:10.1016/j.atmosres.2012.04.002.

Brooks HE, JW Lee, and JP Craven. 2003. The spatial distribution of severe thunderstorm and tornado environments from global reanalysis data. *Atmos. Res*. 67–68, 73-94, doi:10.1016/S0169-8095(03)00045-0.

Brooks HE, AR Anderson, K Riemann, I Ebbers, and H Flachs. 2007. Climatological aspects of convective parameters from the NCAR/NCEP reanalysis. *Atmos. Res*. 83, 294–305.

Brooks HE, GW Carbin, and PT Marsh. 2014. Increased variability of tornado occurrence in the United States. *Science*, 346 (6207), 349-352, doi:10.1126/science.1257460.

Burkett VR, AG Suarez, M Bindi, C Conde, R Mukerji, MJ Prather, AL St. Clair, and GW Yohe. 2014. Point of departure. In: Climate Change 2014: Impacts, Adaptation, and Vulnerability. Part A: Global and Sectoral Aspects. Contribution of Working Group II to the Fifth Assessment Report of the Intergovernmental Panel on Climate Change [Field, C.B., V.R. Barros, D.J. Dokken, K.J. Mach, M.D. Mastrandrea, T.E. Bilir, M. Chatterjee, K.L. Ebi, Y.O. Estrada, R.C. Genova, B. Girma, E.S. Kissel, A.N. Levy, S. MacCracken, P.R. Mastrandrea, and L.L. White (eds.)]. Cambridge University Press, Cambridge, United Kingdom and New York, NY, USA, pp. 169-194.Camargo SJ. 2013. Global and Regional Aspects of Tropical Cyclone Activity in the CMIP5 Models. *J. Clim.* 26, 9880–9902. doi: 10.1175/JCLI-D-12-00549.1.

Camargo SJ, and SE Zebiak. 2002. Improving the detection and tracking of tropical cyclones in atmospheric general circulation models. *Wea. Forecasting* 17, 1152–1162.

Chang EKM, C Zheng, P Lanigan, AMW Yau, and JD Neelin. 2015. Significant modulation of variability and projected change in California winter precipitation by extratropical cyclone activity. *Geophys. Res. Lett*. 42 (14), 5983-5991, doi:10.1002/2015GL064424.

Church JA and NJ White. 2011 Sea-level rise from the late 19th to the early 21st century. *Surveys in Geophysics*, 32, 585-602. http://dx.doi.org/10.1007/s10712-011-9119-1.

Colle BA, Z Zhang, K Lombardo, P Liu, E Chang, and M Zhang. 2013. Historical evaluation and future prediction in Eastern North America and western Atlantic extratropical cyclones in the CMIP5 models during the cool season. *J. Clim*. 26, 6882–903.

Colle BA, JF Booth, and EKM Chang. 2015. A review of historical and future changes of extratropical cyclones and associated impacts along the US east coast. *Curr. Clim. Change Rep*. 1, 125–143, doi: 10.1007/s40641-015-0013-7.

Daly C, M Halbleib, JI Smith, WP Gibson, MK Doggett, GH Taylor, J Curtis, and PP Pasteris. 2008. Physiographically sensitive mapping of climatological temperature and precipitation across the conterminous United States. *Int. J. Climatol*. 28, 2031–2064, doi: 10.1002/joc.1688.

DeConto RM and D Pollard. 2016. Contribution of Antarctica to past and future sea-level rise. *Nature*, 531, 591–597, doi:10.1038/nature17145.

Di Liberto T. 2016. https://www.climate.gov/news-features/event-tracker/maya-express-behind-gulf-coast-soaking.

Diffenbaugh NS and M Ashfaq. 2010. Intensification of hot extremes in the United States. *Geophys. Res. Lett*. 37(15), doi: 10.1029/2010GL043888.

Diffenbaugh NS, M Scherer, and RJ Trapp. 2013. Robust increases in severe thunderstorm environments in response to greenhouse forcing. *Proc. Natl. Acad. Sci. (USA)* 101, 16,361–16,366, doi: 10.1073/pnas.1307758110.

Emanuel KA. 2005. Increasing destructiveness of tropical cyclones over the past 30 years. *Nature* 436, 686–688.

Emanuel KA. 2007. Environmental factors affecting tropical cyclone power dissipation. *J. Clim*. 20, 5497–5509.

Emanuel KA. 2013. Downscaling CMIP5 climate models shows increased tropical cyclone activity over the 21st century. *Proc. National Acad. Sci*. 110(30), 12219–12224.

Emanuel KA. 2017. Assessing the present and future probability of Hurricane Harvey's rainfall. *Proc. Nat. Acad. Sci.* doi:10.1073/pnas.1716222114.

Francis JA and SJ Vavrus. 2012. Evidence linking Arctic amplification to extreme weather in mid-latitudes. *Geophys. Res. Lett.* 39, L06801, doi:10.1029/2012GL051000.

Gao Y, JS Fu, JB Drake, Y Liu, and J-F Lamarque. 2012. Projected changes of extreme weather events in the eastern United States based on a high resolution climate modeling system. *Environ. Res. Lett*. 7, 044025, doi: 10.1088/1748-0326/7/4/044025.

Gregory JM and JA Lowe. 2000. Predictions of global and regional sea-level rise using AOGCMs with and without flux adjustment. *Geophys. Res. Lett*. 27, 3069–3072, doi: 10.1029/1999GL011228.

Haarsma RJ, M Roberts, PL Vidale, CA Senior, A Bellucci, Q Bao, P Chang, S Corti, NS Fučkar, V Guemas, J von Hardenberg, W Hazeleger, C Kodama, T Koenigk, LR Leung, J Lu, J.-J Luo, J Mao, M Mizielinski, R Mizuta, P Nobre, M Satoh, E Scoccimarro, T Semmler, J Small, and J.-S von Storch. 2016. High-resolution model intercomparison project (HighResMIP v1.0) for CMIP6. *Geosci. Mod. Dev*. 9, 4185–4208, doi: 10.5194/gmd-9-4185-2016.

Hall JA, S Gill, J Obeysekera, W Sweet, K Knuuti, and J Marburger. 2016. *Regional Sea Level Scenarios for Coastal Risk Management: Managing the Uncertainty of Future Sea Level Change and Extreme Water Levels for Department of Defense Coastal Sites Worldwide*. 224 pp. U.S. Department of Defense, Strategic Environmental Research and Development Program, Alexandria, Virginia.

Hay LE, SL Markstrom, and C Ward-Garrison. 2011. Watershed-scale response to climate change through the twenty-first century for selected basins across the United States. *Earth Interactions* 15(20), doi: 10.1175/2010EI379.1.

Hoogewind KA, ME Baldwin, and RJ Trapp. 2017. Climate change and hazardous convective weather in the United States: Insights from high-resolution dynamical downscaling. *J. Clim*. submitted.

Ingram K, K Dow, L Carter, and J Anderson (eds.). 2013. *Climate of the Southeast United States: Variability, change, impacts, and vulnerability*. Washington D.C.: Island Press.

Jackson LC, R Kahana, T Graham, MA Ringer, T Woollings, JV Mecking, and RA Wood. 2015. Global and European climate impacts of a slowdown of the AMOC in a high resolution GCM. *Clim. Dyn*. 45, 3299-3316. http://dx.doi.org/10.1007/s00382-015-2540-2.

Kalnay E and Coauthors. 1996: The NCEP/NCAR 40-Year Reanalysis Project. *Bull. Amer. Meteor. Soc.* 77, 437–471.

Kendon EJ, NM Roberts, HJ Fowler, MJ Roberts, SC Chan, and CA Senior. 2014. Heavier summer downpours with climate change revealed by weather forecast resolution model. *Nat. Clim. Change* 4, 570–6.

Knight DB and RE Davis. 2009. Contribution of tropical cyclones to extreme rainfall events in the southeastern United States. *J. Geophys. Res*. 114, D23102, doi:10.1029/2009JD012511

Knutson TR, JJ Sirutis, GA Vecchi, S Garner, M Zhao, HS Kim, M Bender, RE Tuleya, IM Held, and G Villarini. 2013. Dynamical downscaling projections of twenty-first-century Atlantic hurricane activity: CMIP3 and CMIP5 model-based scenarios. *J. Clim.* 26, 6591–6617.

Knutti R, and J Sedláček. 2012: Robustness and uncertainties in the new CMIP5 climate model projections. *Nature Climate Change* 3, 369-373, doi: 10.1038/NCLIMATE1716.

Kopp RE, RM Horton, CM Little, JX Mitrovica, M Oppenheimer, and DJ Rasmussen. 2014. Probabilistic 21st and 22nd century sea-level projections at a global network of tide gauge sites. *Earth Future* 2, 383–406. doi:10.1002/2014EF000239.

Kopp RE, CC Hay, CM Little, and JX Mitrovica. 2015. Geographic variability of sea-level change. *Current Climate Change Reports*, 1, 192-204. http://dx.doi.org/10.7282/T37W6F4P.

Kossin JP, KA Emanuel, and GA Vecchi. 2014. The poleward migration of the location of tropical cyclone maximum intensity. *Nature* 509 (7500), 349-352, doi:10.1038/nature13278.

Kumar S, J Kinter III, PA Dirmeyer, Z Pan, and J Adams. 2013. Multidecadal climate variability and the ‘‘warming hole’’ in North America: Results from CMIP5 twentieth- and twenty-first-century climate simulations. *J. Clim*. 26, 3511-3527, doi: 10.1175/JCLI-D-12-00535.1.

Kunkel KE, A Billot, JG Dobson et al. 2013a. *Regional Climate Trends and Scenarios for the U.S. National Climate Assessment. Part 2. Climate of the Southeast U.S. NOAA Technical Report NESDIS 142-2*. 94pp.

Kunkel KE, D Arndt, H Brooks et al. 2013b. Monitoring and understanding trends in extreme storms: State of knowledge. *Bull. Amer. Meteor. Soc*. 94, 499-514, doi: 10.1175/BAMS-D-11-00262.1.

Landsea CW et al. 2004. The Atlantic Hurricane Database Re-Analysis Project: Documentation for 1851–1910 alterations and additions to the HURDAT database. *Hurricanes and Typhoons: Past, Present, and Future*, RJ Murnane and KB Liu (eds.), Columbia University Press, 177–221.

Levermann A, PU Clark, B Marzeion, GA Milne, D Pollard, V Radic, and A Robinson. 2013. The multimillennial sea-level commitment of global warming. *Proc. Natl. Acad. Sci. (USA)* 110, 13745–13750, doi: 10.1073/pnas.1219414110.

Li W, L Li, R Fu, and Y Deng. 2011. Changes to the North Atlantic subtropical high and its role in the intensification of summer rainfall variability in the southeastern United States. *J. Clim*. 24, 1499–1506, doi: 10.1175/2010JCLI3829.1.

Li L, W Li, and Y Kushnir. 2012. Variations of the North Atlantic subtropical high western ridge and its implication to southeastern US summer precipitation. *Clim. Dyn*. 39, 1401–1412, doi: 10.1007/s00382-011-1214-y.

Little CM, RM Horton, RE Kopp, M Oppenheimer, GA Vecchi, and G Villarini. 2015. Joint projections of US east coast sea level and storm surge. *Nature Climate Change*, doi: 10.1038/nclimate2801.

Lu J, GA Vecchi, and T Reichler. 2007. Expansion of the Hadley cell under global warming. *Geophys. Res. Lett.* 34, L06805, doi:10.1029/2006GL028443.

Madsen H. 2000. Automatic calibration of a conceptual rainfall–runoff model using multiple objectives. *J. Hydrol*. 235, 276–288.

Melillo JM, TC Richmond, and GW Yohe (eds.). 2014. *Climate Change Impacts in the United States: The Third National Climate Assessment*. U.S. Global Change Research Program, 841 pp. doi:10.7930/J0Z31WJ2.

Mengel A, A Levermann, K Frieler, A Robinson, B Marzeion, and R Winkelmann. 2016. Future sea level rise constrained by observations and long-term commitment. *Proc. Natl. Acad. Sci. U.S.A.* 113, 2597.

Merrifield MA, ST Merrifield, and GT Mitchum. 2009. An anomalous recent acceleration of global sea level rise. *J. Clim*. 22, 5772–5781, doi: 10.1175/2009JCLI2985.1.

Milly PCD and KA Dunne. 2016. Potential evapotranspiration and continental drying. *Nature Climate Change*, doi: 10.1038/nclimate3046.

Misra V, L Moeller, LB Stefanova, SC Chan, JJ O'Brien, TJ Smith, et al. 2011. The influence of the Atlantic warm pool on the Florida panhandle sea breeze. *J. Geophys. Res.* 116, doi: 10.1029/2010JD015367.

IPCC 2000. *Special Report on Emissions Scenarios: A Special Report of Working Group III of the Intergovernmental Panel on Climate Change*. Nakićenović N, R Swart, eds., Cambridge Press, ISBN 0-521-80081-1.

Musser JW, KM Watson, and AJ Gotvald. 2017. *Characterization of peak streamflows and flood inundation at selected areas in North Carolina following Hurricane Matthew*, October 2016 (ver. 2.0, August 2017). U.S. Geological Survey Open-File Report 2017–1047, 24 p., https://doi.org/10.3133/ofr20171047.

National Academy of Sciences, Engineering, and Medicine. 2016. *Attribution of Extreme Weather Events in the Context of Climate Change*. Washington, D.C.: The National Academies Press. doi: 10.17226/21852.

NRC (U.S. Nuclear Regulatory Commission). 2018. Information Digest, 2018-2019. NUREG-1350, Volume 30. Accessed May 15, 2019 at https://www.nrc.gov/reading-rm/doc-collections/nuregs/staff/sr1350/.

NRC (U.S. Nuclear Regulatory Commission). 2016. Guidance for Activities Related to Near-Term Task Force Recommendation 2.1, Flooding Hazard Reevaluation; Focused Evaluation and Integrated Assessment. Interim Staff Guidance JLD-ISG-2016-01. Available at https://www.nrc.gov/docs/ML1609/ML16090A140.pdf.

NCEI (National Centers for Environmental Information). 2016a. *Comparative Climatic Data For the United States Through 2015*. NOAA NCEI, Ashville, North Carolina. Available at http://www1.ncdc.noaa.gov/pub/data/ccd-data/CCD-2015.pdf.

NCEI (National Centers for Environmental Information). 2016b. *U.S. Climate Atlas*. Available at http://www.ncdc.noaa.gov/climateatlas/.

NOAA (National Oceanic and Atmospheric Administration). 2016a. Highest Storm Water Levels – Highest Water Levels During Hurricane Matthew. Tides and Currents, NOAA National Ocean Service. Available at https://www.tidesandcurrents.noaa.gov/quicklook_highest_storm.html. Accessed on November 2, 2016.

NOAA (National Oceanic and Atmospheric Administration). 2016b. Hurricane Matthew - October 8-9, 2016. Available at http://www.weather.gov/mhx/MatthewSummary. Accessed on November 2, 2016.

NOAA (National Oceanic and Atmospheric Administration). 2016c. "Maya Express" behind Gulf Coast soaking. Available at https://www.climate.gov/news-features/event-tracker/maya-express-behind-gulf-coast-soaking. Accessed on November 2, 2016.

NOAA (National Oceanic and Atmospheric Administration). 2016d. Louisiana Flood of 2016 resulted from '1,000-year' rain in 2 days. Available at http://www.nola.com/weather/index.ssf/2016/08/louisiana_flood_of_2016_result.html. Accessed on November 2, 2016.

NWS (National Weather Service). 2016. http://www.weather.gov/mhx/MatthewSummary.

NWS (National Weather Service). 2017. October 2016 Hurricane Matthew – Service Assessment. U.S. Department of Commerce National Oceanic and Attmospheric Administration, Silver Spring, Maryland. Available at https://www.weather.gov/media/publications/assessments/HurricaneMatthew8-17.pdf.

Oppenheimer M and RB Alley. 2016. How high will the seas rise? *Science* 354, 1375–1376.

Pal JS and EAB Eltahir. 2015. Future temperature in southwest Asia projected to exceed a threshold for human adaptability. *Nature Climate Change* 6, 197–200, doi: 10.1038/nclimate2833.

Pierce DW, DR Cayan, and BL Thrasher. 2014. Statistical downscaling using Localized Constructed Analogs (LOCA). *J. Hydrometeor*. 15, 2558–2585, doi: 10.1175/JHM-D-14-0082.1.

Prein AF, W Langhans, G Fosser, A Ferrone, N Ban, K Goergen, M Keller, M Tolle, O Gutjahr, F Feser, E Brisson, S Kollet, J Schmidli, NPM van Lipzig, and LR Leung. 2015. A review on regional convection permitting climate modeling: Demonstrations, prospects, and challenges. *Rev. Geophys*. doi: 10.1002/2014RG000475.

Prein AF, RM Rasmussen, K Ikeda, C Liu, MP Clark, and GJ Holland. 2017. The future intensification of hourly precipitation extremes. *Nature Climate Change* 7, 48–52, doi: 10.1038/nclimate3168.

Rahmstorf S, JE Box, G Feulner, ME Mann, A Robinson, S Rutherford, and EJ Schaffernicht. 2015. Exceptional twentieth-century slowdown in Atlantic Ocean overturning circulation. *Nature Climate Change* 5, 475-480, doi: 10.1038/nclimate2554.

Risser MD and MF Wehner. 2017. Attributable human-induced changes in the likelihood and magnitude of the observed extreme precipitation during Hurricane Harvey. *Geophys. Res. Lett.* 44(24), 12,457-412,464.

Schleifstein 2016: http://www.nola.com/weather/index.ssf/2016/08/louisiana_flood_of_2016_result.html.

Seeley JT and DM Romps. 2015. The effect of global warming on severe thunderstorms in the United States. *J. Clim*. doi:10.1175/JCLI-D-14-00382.1.

Sheffield J, AP Barrett, B Colle, D Nelun Fernado, R Fu, KL Geil, Q Hu, J Kinter, S Kumar, B Langenbrunner, K Lombardo, LN Long, E Maloney, A Mariotti, JE Meyerson, KC Mo, JD Neelin, S Nigam, Z Pan, T Ren, A Ruiz-Barradas, YL Serra, A Seth, JM Thibeault, JC Stroeve, Z Yang, and L Yin. 2013. North American climate in CMIP5 experiments. Part I: evaluation of historical simulations of continental and regional climatology. *J. Clim*. 26, 9209–9245, doi: 10.1175/JCLI-D-12-00592.1.

Sherwood SC and M Huber. 2010. An adaptability limit to climate change due to heat stress. *Proc. Natl. Acad. Sci.* 107(21), 9552–9555, doi: 10.1073/pnas.0913352107.

SRCC (Southeast Regional Climate Center). 2016. Multi-sensor precipitation estimates, October 4–10, 2016, Hurricane Matthew storm total rainfall. Available at http://www.sercc.com/Hurricane_Matthew_MPE_Map.png.

Stephens GL, T L'Ecuyer, R Forbes, A Gettleman, J-C Golaz, A Bodas-Salcedo, K Suzuki, P Gabriel, and J Haynes. 2010. Dreary state of precipitation in global models. J. Geophys. Res. 115, D24211, doi:10.1029/2010JD014532.

Sugawara M. 1995. Tank model. In: Singh VP (ed.). *Computer models of watershed hydrology*. Water Resources Publications, Littleton, Colorado, pp 165–214.

Sun MT, G Sun, C Liu, JA Moore Myers and SG McNulty. 2015. Future water budgets and water supply stress under climate change and urbanization in the Upper Neuse River Basin, North Carolina, USA. *Amer. J. Environ. Sci*. 11(4), 175–185, doi: 10.3844/ajessp.2015.175.185.

Sweet, W., J. Park, J. Marra, C. Zervas, and S. Gill, 2014: Sea Level Rise and Nuisance Flood Frequency Changes around the United States. *NOAA Technical Report NOS CO-OPS 073.* National Oceanic and Atmospheric Administration, National Ocean Service, Silver Spring, MD. 58 pp. http://tidesandcurrents.noaa.gov/publications/NOAA_Technical_Report_NOS_COOPS_073.pdf.

Taylor KE, RJ Stouffer, and GA Meehl. 2012 An overview of CMIP5 and the experiment design. *Bull. Am. Meteorol. Soc*. 93, 485-495.

Tippett MK, AH Sobel, and SJ Camargo. 2012. Association of U.S. tornado occurrence with monthly environmental parameters. *Geophys. Res. Lett*. 39, doi:10.1029/2011GL050368.

Tippett MK, C Lepore, and JE Cohen. 2016. More tornadoes in the most extreme U.S. tornado outbreaks. Science, 354, 1419-1423. [doi: 10.1126/science.aah7393.

Trapp RJ and KA Hoogewind. 2016. The realization of extreme tornadic storm events under future anthropogenic climate change. J. Clim. 29, doi: 10.1175/JCLI-15-0623.1.

Trapp RJ and KA Hoogewind. 2018. Exploring a possible connection between U.S. tornado activity and Arctic sea ice. *NPJ Climate and Atmospheric Science* 1:14, doi:10.1038/s41612-018-0025-9.

USACE (U.S. Army Corps of Engineers). 2015. *Recent US Climate Change and Hydrology Literature Applicable to US Army Corps of Engineers Missions – South Atlantic-Gulf Region 03*. Civil Works Technical Report, CWTS 2015-03, USACE, Washington, D.C. Accessed February 1, 2017 at http://corpsclimate.us/docs/rccvarreports/USACE_REGION_03_Climate_Change_Report_CWTS-2015-03_Hi.pdf.

USACE (U.S. Army Corps of Engineers). 2016. *Engineering and Construction Bulletin, No. 2016-25, Guidance for Incorporating Climate Change Impacts to Inland Hydrology in Civil Works Studies, Designs, and Projects*. Corps of Engineers Civil Works, Washington, D.C.

USACE (U.S. Army Corps of Engineers). 2017. *Responses to Climate Change*. Available at http://corpsclimate.us/index.cfm.

USGCRP (U.S. Global Change Research Program). 2017. *Climate Science Special Report: Fourth National Climate Assessment, Volume I.* [Wuebbles, D.J., D.W. Fahey, K.A. Hibbard, D.J. Dokken, B.C. Stewart, and T.K. Maycock (eds.)]. U.S. Global Change Research Program, Washington, DC, USA, 470 pp., doi: 10.7930/J0J964J6.

USGCRP (U.S. Global Change Research Program). 2018. Impacts, Risks, and Adaptation in the United States: Fourth National Climate Assessment, Volume II [Reidmiller, D.R., C.W. Avery, D.R. Easterling, K.E. Kunkel, K.L.M. Lewis, T.K. Maycock, and B.C. Stewart (eds.)]. U.S. Global Change Research Program, Washington, DC, USA, 1515 pp. doi: 10.7930/NCA4.2018.

USGS (U.S. Geological Survey). 2016a. Hurricane Matthew's Water Footprint. Available at https://owi.usgs.gov/vizlab/hurricane-matthew/. Accessed on November 2, 2016.

USGS (U.S. Geological Survey). 2016b. National Water Information System: Mapper. Available at https://maps.waterdata.usgs.gov/mapper/index.html. Accessed on November 2, 2016.

USGS National Water Information System. 2016a. USGS 07378000 Comite River near Comite, LA and USGS 07380200 Amite River near French Settlement, LA. Available at https://waterdata.usgs.gov/nwis/uv/?referred_module=sw. Accessed on November 1, 2016.

USGS National Water Information System. 2016b. USGS 07349250 Lake Bistineau near Ringgold, LA and USGS 02492000 Bogue Chitto River near Bush, LA. Available at https://waterdata.usgs.gov/nwis/uv/?referred_module=sw. Accessed on November 2, 2016.

USGS National Water Information System. 2016c. USGS 02089500 Neuse River at Kinston, NC. Available at https://waterdata.usgs.gov/nwis/uv/?referred_module=sw. Accessed on November 2, 2016.

van der Wiel K, SB Kapnick, GJ van Oldenborgh, K Whan, S Philip, GA Vecchi, RK Singh, J Arrighi, H Cullen. 2016. Rapid attribution of the August 2016 1 flood-inducing extreme precipitation in south Louisiana to climate change. *Hydrol. Earth Syst. Sci. Discuss*. doi:10.5194/hess-2016-448.

van Oldenborgh GJ, K van der Wiel, A Sebastian, R Singh, J Arrighi, F Otto, et al. 2017. Attribution of extreme rainfall from Hurricane Harvey, August 2017. *Environmental Research Letters* 12(12).

Viger RJ, LE Hay, SL Markstrom, JW Jones, and GR Buell. 2011. Hydrologic effects of urbanization and climate change on the Flint River Basin, Georgia. *Earth Interactions* 15, 20, doi: 10.1175/2010EI379.1.

Villarini G, and GA Vecchi. 2012: Twenty-first-century projections of North Atlantic tropical storms from CMIP5 models. *Nat. Climate Change* 2, 604–607.

Villarini G, and GA Vecchi. 2013. Projected increases in North Atlantic tropical cyclone intensity from CMIP5 models. *J. Clim*. 26, 3231–3240, doi: 10.1175/JCLI-D-12-00441.1.

Vose RS et al. 2014. Monitoring and understanding changes in extremes: Extratropical storms, winds, and waves. *Bull. Amer. Meteor. Soc*. 95(3), 377–386, doi:10.1175/BAMS-D-12-00162.1.

Wang S-Y, L Zhao, and RR Gillies. 2016: Synoptic and quantitative attributions of the extreme precipitation leading to the August 2016 Louisiana flood. *Geophys. Res. Lett*. 43, 11,805–11,814, doi:10.1002/2016GL071460.

Wang, SY, L Zhao, JH Yoon, P Klotzbach, and RR Gillies. 2018. Quantitative attribution of climate effects on Hurricane Harvey's extreme rainfall in Texas. *Environmental Research Letters* 13(5).

Wang XL, Y Feng, GP Compo, VR Swail, FW Zwiers, RJ Allan, and PD Sardeshmukh. 2013. Trends and low frequency variability of extra-tropical cyclone activity in the ensemble of the Twentieth Century Reanalysis. Climate Dyn. 40, 2775–2800, doi:10.1007/S00382-012-1450-9.

Watson, KM, JB Storm, BK Breaker, and CE Rose. 2017. *Characterization of peak streamflows and flood inundation of selected areas in Louisiana from the August 2016 flood*. U.S. Geological Survey Scientific Investigations Report 2017–5005, 26 p., https://doi.org/10.3133/sir20175005.

Yang H, G Lohmann, W Wei, M Dima, M Ionita, and J Liu. 2016. Intensification and poleward shift of subtropical western boundary currents in a warming climate. *J. Geophys. Res. Oceans* 121, 4928–4945, doi: 10.1002/2015JC011513.

Yin J and PB Goddard. 2013. Oceanic control of sea level rise patterns along the East Coast of the United States. *Geophys. Res. Lett*. 40, 5514–5520, doi: 10.1002/2013GL0579.

Pacific Northwest
NATIONAL LABORATORY

U.S. DEPARTMENT OF
ENERGY